FUNCTIONALIZATION OF NANOCARBONS OF DIFFERENT DIMENSIONALITIES AND STUDY THE PHYSICAL PROPERTIES OF THEIR NANOCOMPOSITES WITH THE THERMOSETTING POLYMER

A THESIS SUBMITTED TO THE

CENTRAL DEPARTMENT OF CHEMISTRY

INSTITUTE OF SCIENCE AND TECHNOLOGY

TRIBHUVAN UNIVERSITY

NEPAL

FOR THE AWARD OF

DOCTOR OF PHILOSOPHY

IN CHEMISTRY

BY

SONAM TAMANG

OCTOBER 2023

FUNCTIONALIZATION OF NANOCARBONS OF DIFFERENT DIMENSIONALITIES AND STUDY THE PHYSICAL PROPERTIES OF THEIR NANOCOMPOSITES WITH THE THERMOSETTING POLYMER

A THESIS SUBMITTED TO THE

CENTRAL DEPARTMENT OF CHEMISTRY

INSTITUTE OF SCIENCE AND TECHNOLOGY

TRIBHUVAN UNIVERSITY

NEPAL

FOR THE AWARD OF

DOCTOR OF PHILOSOPHY

IN CHEMISTRY

BY

SONAM TAMANG

OCTOBER 2023

DECLARATION

The thesis entitled **"Functionalization of nanocarbons of different dimensionalities and study the physical properties of their nanocomposites with the thermosetting polymer"** which is being submitted to the Central Department of Chemistry, Institute of Science and Technology (IOST), Tribhuvan University, Nepal for the award of the degree of Doctor of Philosophy (Ph.D.), is a research work carried out by me under the supervision of Assoc. Prof. Dr. Sabita Shrestha of the Central Department of Chemistry, Tribhuvan University and co-supervised by Prof. Dr. Rameshwar Adhikari of Central Department of Chemistry, Tribhuvan University.

This research work is original and has not been submitted earlier in part or full in this or any other form to any university or institute, here or elsewhere for the award of any degree.

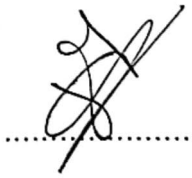

.....

Sonam Tamang

RECOMMENDATION

This is to recommend that **Sonam Tamang** has carried out research entitled **"Functionalization of nanocarbons of different dimensionalities and study the physical properties of their nanocomposites with the thermosetting polymer"** for the award of Doctor of Philosophy (Ph.D.) in **Chemistry** under our supervision. To our knowledge, this work has not been submitted for any other degree.

She has fulfilled all the requirements laid down by the Institute of Science and Technology (IOST), Tribhuvan University, Kirtipur for the submission of the thesis for the award of Ph.D. degree.

.....

Dr. Sabita Shrestha

Supervisor

(Associate Professor)

Central Department of Chemistry

Tribhuvan University

Kirtipur, Kathmandu, Nepal

.....

Dr. Rameshwar Adhikari

Co-Supervisor

(Professor)

Central Department of Chemistry

Tribhuvan University

Kirtipur, Kathmandu, Nepal

October 2023

त्रिभुवन विश्वविद्यालय
TRIBHUVAN UNIVERSITY
विज्ञान तथा प्रविधि अध्ययन संस्थान
Institute of Science and Technology
रसायन शास्त्र केन्द्रीय विभाग
CENTRAL DEPARTMENT OF CHEMISTRY
कीर्तिपुर, काठमाडौं, नेपाल
Kirtipur, Kathmandu, NEPAL

पत्र संख्या:
Ref. No.:

LETTER OF APPROVAL

Date: 24/05/2024

On the recommendation of **Assoc. Prof. Dr. Sabita Shrestha and Prof. Dr. Rameshwar Adhikari,** this Ph.D. thesis submitted by **Ms. Sonam Tamang** entitled **"Functionalization of nanocarbons of different dimensionalities and study the physical properties of their nanocomposites with the thermosetting polymer"** is forwarded by Central Department Research Committee (CDRC) to the Dean, IOST, T.U..

.....

Dr. Jagadeesh Bhattarai
Professor
Head
Central Department of Chemistry
Tribhuvan University
Kirtipur, Kathmandu
Nepal

Tel.: 977-1-4332034, Fax No.: +977-1-4330537, http://www.cdctu.edu.np e-mail: head@cdc.tu.edu.np

ACKNOWLEDGEMENTS

I would like to express my profound appreciation to my supervisors, Assoc. Prof. Dr. Sabita Shrestha and Prof. Dr. Rameshwar Adhikari, for their invaluable guidance, unwavering motivation, and consistent support throughout my Ph.D. research. Their expert advice, encouragement, and dedication have been instrumental in shaping my academic journey and ensuring the successful completion of my studies. I am deeply grateful for their mentorship and the significant impact they have had on both my professional and personal development.

I am thankful to Prof. Dr. Jagadeesh Bhattarai, Head, Prof. Dr. Ram Chandra Basnyat and Prof. Dr. Megh Raj Pokharel, former Heads of Central Department of Chemistry, Tribhuvan University, Kathmandu for their kind cooperation in carrying out the research. I am extremely grateful to the University of Applied Science, Institut für Polymerwerkstoffe (IPW), Polymer Service GmbH, Merseburg, and Bethge Foundation, Halle, Germany, particularly Prof. Goerg H. Michler, Dr. Ralf Lach, Prof. Dr. Beate Langer, and Dr. Andre Wutzler for providing funding for the research stay in Germany as well as for supervision of my research as a part of collaboration agreement between Nepal Polymer Institute (NPI) and the IPW.

I would like to thank Ms. Anu Surendran for guiding me in the laboratory work, and Prof. Dr. Sabu Thomas and his team, for providing funding, laboratory facility, and sample characterization. I am indeed grateful to Prof. Dr. Maruyama Takahiro, Dr. Kamal Prasad Sharma, Meijo University, Nagoya, Japan and their whole team for microscopic investigations of the sample. My sincere thank goes to the Sakura Science Program and Japan Science and Technology for providing funding to stay in Japan. I also thank to Nepal Academy of Science and Technology (NAST), Khumaltar, Lalitpur for providing Ph.D. fellowship. My sincere gratitude goes to Nepal Polymer Institute (NPI) for providing me assistance for the collaborative stay during my research work and also to the Research Centre for Applied Science and Technology (RECAST) and Central Department of Biotechnology, Tribhuvan University for providing me with laboratory facilities. I would also like to thank Dr. Jyoti Giri, Dr. Kedar Nath Dhakal, Dr. Rajesh Pandit, Dr. Netra Lal Bhandari, Dr. Sharmila Pradhan, Dr. Shanta Bhattarai, Dr. Santosh Khanal, Dr. Pramod Aryal, Mr.

Bidit Lamsal, Dr. Hari Sharan Adhikari, Dr. Komal Malla, Dr. Suresh Kumar Dhungel, Assist. Prof. Yub Narayan Thapa and our team for their guidance and support. Last but not least, I am truly indebted to my late grandfather, father and all my family members.

Sonam Tamang

October 2023

ABSTRACT

The epoxy/nanocarbon (EP/NCs) nanocomposites were prepared by incorporating NCs of different dimensionalities (such as multiwalled carbon nanotubes; MWCNTs (1D), graphite nanoplatelets; GnP (2D) and nanodiamond; ND (0D), aiming at enhancing their physical and electrical properties thus making them useful in various applications. The NCs were functionalized to a different extent and added to the EP matrix. The functionalization of NCs was confirmed by spectroscopic, thermal and diffraction techniques. The prepared nanocomposites were further characterized by different spectroscopic, thermal and microscopic methods. The electrical and surface wetting properties of those materials were discussed in correlation to their morphologies. The chemical modifications of the NCs were confirmed by Fourier transform infrared (FTIR) spectroscopy and Raman spectroscopy showing different oxygen containing functional and increased intensity ratio of D and G band value indicating a high degree of graphitization. The increase in interlayer distance was observed after the acid treatment and the thermal degradation of the acid-treated nanocarbons occurred at lower temperatures also evidencing their successful functionalization. The structural and morphological analysis of the nanocomposites confirmed that there was an effective dispersion between the NCs and epoxy (EP) matrix. In addition to this the hydroxyl functional group was also observed in the case of the acid-treated samples of CNTs, microscopic investigations displayed the brittle nature of the neat epoxy and the addition of nanocarbons on epoxy prevented cracks from propagating, increased the area of the fractured surface and provided a high resistance to fracture. The well-dispersed and cluster-free dispersion of CNTs in the EP/pCNT nanocomposite was observed and the pull-out of the CNTs was also witnessed in the epoxy nanocomposites with pristine CNTs. The thermal stability of EP/NCs composites containing separately pristine and acid-treated nanocarbons was improved slightly in the range of 5-13 °C. The resistivity of EP/pCNT nanocomposites was found to be decreased as high as about 40 times compared to acid-treated nanocomposites. The higher resistivity of Ep/mCNT was attributed to the shortening of CNT length thereby altering its aspect ratio on acid treatment. On the contrary, acid-treated graphite showed as high as about 35 times decrease in

resistivity than that of the pristine graphite because of the well dispersion of graphite particles on the EP matrix. However, in terms of surface wetting properties surface modification of NCs enhances hydrophilicity and wettability of EP/NCs nanocomposites

Keywords: *Nanocarbon, Functionalization, Morphology, Resistivity, Wettability*

शोध सार

प्रस्तुत अनुसन्धान कार्यमा मुलत: विभिन्न आयामिकतायुक्त नानोकार्बनहरु (जस्तै एक आयामिक कार्बन नानोट्यूब, द्वैआयामिक ग्राफाइट नानोप्लेटलेट तथा सुन्यआयामिक नानोडायमंड) लाई एपोक्सी रेजिन नामक थर्मोसेटिङ् पोलिमरसँग बिभिन्न अनुपातमा मिलाएर नानोकम्पोजिटका नमुनाहरु तयार गरि तिनिहरुको भौतिक एवं विद्युतीय लक्षणहरु जस्ता व्यवहारोपयोगी गुणहरुको अध्ययन प्रसतुत गरिएको छ। यसका लागि प्रत्येक नानोकार्बनको सतहमा उपयुक्त विधिद्वारा विभिन्न परिमाणमा रासायनिक क्रियाशिलताको उद्भब गराई त्यासलाई एपोक्सी रेजिन भित्र समानरुपले घुलाइएको थियो। नानोकार्बनको सतहमा आरोपित रासायनिक क्रियाशिलताको पुष्टिका खातिर प्रकाशपटिय (Spectroscopy), तापिय (Thermal) तथा विवर्तन (Diffraction) विधिहरूको सहयोग लिइएको थियो। अनुसन्धान कार्यका दौरान तयार पारिएका नानोकम्पोजिटहरूका विभिन्न गुणहरूको अवलोकनार्थ पनि प्रकाशपटिय, तापिय, विवर्तन तथा सुक्ष्मदर्शक यन्त्रिय विधिहरूको प्रयोग गरिएको थियो। साथै आन्तरिक शुक्ष्म वनोटको आधारमा ति बस्तुहरुका विद्युतीय एवं सतह संबन्धित गुणहरूको व्याख्या गरिएको थियो। नानोकार्बनहरुको सतहमा रासायानिक परिवर्तन भए नभएको फोरिएर ट्रान्स्फर्म ईन्फ्रारेड (FTIR) तथा रमण स्पेक्ट्रोस्कोपीद्वारा निधो गरिएको थियो। त्यसवाट क्रमशः नानोकणिकाको सतहमा विभिन्न अक्सिजनयुक्त प्रतिक्रियात्मक समुहहरु जोडीएका तथा डि (D) र जी (G) ब्याण्डको तिव्रताको अनुपात (जसलाई नानोकणिकाको ग्राफाईटमा रुपान्तरण भएको सुचकको रुपमा लिइन्छ) पनि केही हदसम्म बढेको पाईयो । अम्लसंगको संसर्गपछि नानोकणिकाका आपसि तहहरु विचको दूरीमा वृद्धि भएको तथा तिनिहरुको उच्च तापक्रममा तताउंदा तौल ह्रास हुने तापमानमा पनि गिरावट आएकोवाट ति कणको सतहमा प्रतिक्रियात्माक समुहहरु जोड्ने कार्य सफल भएको निक्यौंल गरिएको थियो। नानोकम्पोजिटहरूको संरचनात्मक र रुपात्मक विश्लेषण गर्दा एपोक्सि रेजिन थर्मोसेटीङ्ग पोलिमर र नानोकणिकाहरु बीच प्रभावकारी अन्तरवन्धन (intertwine) भएको पुष्टी भयो । यसका साथै नानोकणिकाहरुको अम्लसंग प्रतिकृया गरेपस्चात तिनिहरुको सतहमा हाइड्रोक्सिल समूहहरु पनि जोडीएका तथा सुक्ष्मदर्शक यन्त्रद्वारा गरिएको अध्ययनले विसुध्द एपोक्सि रेजिनले ब्रिटल प्रकृति देखाए पनि नानोकार्वन पोलिमरसंग मिसाए पश्चात यिनीहरुले यान्त्रिक वलद्वारा उत्पन्न हुन सक्ने शुक्ष्मदरार (Microcrack) लाई रोक्ने तथा शक्ति शोषक सतहको क्षेत्रफल बढाएर उक्त पदार्थको तात्कालिक बिघटनलाई प्रतिरोध गर्ने क्षमतालाई समेत बढाएको पाईयो। एक आयामिक नानोकार्वन, कार्बन नानोट्यूब, को पोलिमरको भित्रि आयतनसम्म राम्रोसंग फैलावट भएको तथ्य त्यसको एपोक्सि रेजिनसंगको मिश्रणको शुक्ष्म अध्ययनमा राम्रोसँग देख्न पाईन्छ। साथै शुद्ध अवस्था र अम्लसँग प्रतिक्रिया पस्चात प्राप्त भएको नानोकार्वन प्रयोग गरी तयार गरिएका नानोकम्पोजिटहरूको थर्मल स्थिरतामा ५-१३ °C तापक्रमले वृद्धि भएको पाइयो। शुद्ध नानोकार्बन प्रयोग गरी बनाइएको नानोकम्पोजिटहरूको विद्युतीय प्रतिरोधात्मकता अम्लसँग प्रतिक्रिया पश्चात प्राप्त भएको भन्दा लगभग ४० गुणाले कम भएको पाइयो। प्राप्त नतिजाहरुको विश्लेषणबाट यो निस्कर्षमा पुगिन्छ कि नानोकार्वनको अम्लसँग प्रतिक्रिया गराउँदा यीनिहरुको वनोटलाई खन्डित भई

आस्पेक्ट अनुपात परिवर्तन हुन्छ र कम्पोजिटको विद्युतीय गुणमा नकारात्मक असर गर्दछ। यसको विपरीत अम्लसँग प्रतिक्रिया गरेका द्वैआयामिक नानोकार्वन (जस्तै ग्राफाइट नानोप्लेटलेट) एपोक्सि रेजिनसंग राम्रोसँग फैलिएर बनेको हुनाले नानोकम्पोजिटको विद्युतीय प्रतिरोधात्मकता शुद्ध अवस्थाको नानोकार्वन भएको नानोकम्पोजिटको तुलनामा लगभग ३५ गुणाले कम भएको देखियो। नानोकम्पोजिटहरूले आफ्नो सतहमा जलाकर्षण गर्ने गुणहरुलाई केलाउने क्रममा भने रासायानिक रुपमा परिमार्जीत तीनै प्रकारका सूक्ष्म कणहरुले सकारात्मक भूमिका खेलेको पाईयो।

कुञ्जिपदावली: *नानोकार्बन, रासायानिक क्रियाशिलता, संरचनात्मक विश्लेषण, प्रतिरोधात्मकता, जलाकर्षण क्षमता*

LIST OF ACRONYMS AND ABBREVIATIONS

EP	: Pure Epoxy Resin
MWCNTs	: Multi Walled Carbon Nanotubes
SWCNTs	: Single Walled Carbon Nanotubes
DWCNT	: Double Walled Carbon Nanotube
CNT	: Carbon Nanotubes
GnP	: Graphite Nano-Platelets
ND	: Nanodiamond
DGEBA	: Diglycidyl Ether of Bisphenol A
FTIR	: Fourier Transform Infrared Spectroscopy
TGA	: Thermogravimetric Analysis
DTG	: Derivative Thermogravimetry
XRD	: X-ray Diffraction
DSC	: Differential Scanning Calorimetry
SEM	: Scanning Electron Microscopy
XPS	: X-ray Photoelectron Spectroscopy
FE-SEM	: Field Emission Scanning Electron Microscopy
DMA	: Dynamic Mechanical Analysis
DND	: Detonation Nanodiamond
CVD	: Chemical Vapor Deposition
NG	: Natural Graphite
SG	: Synthetic Graphite
CND	: Carboxylic Nanodiamond
OND	: Oxidized Nanodiamond
pCNT	: Pristine Carbon Nanotubes

mCNT	: Modified Carbon Nanotubes
pGnP	: Pristine Graphite-Nanoplatelets
mGnP	: Modified Graphite-Nanoplatelets
pND	: Pristine Nanodiamond
mND	: Modified Nanodiamond
PPA	: Phenylphosphonate
PEEK	: Poly(Ether-Ether-Ketone)
g	: Gram
mL	: Millilitre
mg	: Milligram
cm	: Centimetre
mm	: Millimetre
nm	: Nanometre
MPa	: Mega Pascal
wt.	: Weight
UV	: Ultra Violet
I_D	: Intensity of D Band
I_G	: Intensity of G Band
R	: Intensity Ratio
D	: D Band in Raman Spectra
G	: G Band in Raman Spectra

LIST OF SYMBOLS

º	: Degree
ºC	: Degree Celsius
Ω	: Ohm
%	: Percentage
Θ	: Theta
δ	: Resistivity
Λ	: Lambda
B	: Beta
D	: Interlayer Distance
N	: Numerical Value
a.u.	: Arbitrary Unit
>	: Greater Than
D	: Average Crystallite Size
I	: Current
V	: Voltage
R	: Resistance
σ	: Conductivity
eV	: Electron Volts
S/cm	: Siemens/cm
wt. %	: Weight Percentage
$Wm^{-1}K^{-1}$	: Watt per meter per kelvin

LIST OF TABLES

LIST OF FIGURES

TABLE OF CONTENTS

CHAPTER 1

1. INTRODUCTION

1.1 General Introduction to Nanocarbons

Carbon, the most versatile element possesses different outstanding properties due to this, they are used for various purposes. By taking into account the arrangement of carbon atoms, there are two types of carbon materials in nature. They are crystalline and amorphous. Crystalline carbon possesses fixed geometrical shapes and regular arrangements of atoms in their structure. Further crystalline carbon is classified into four types as shown in Figure 1; three-dimensional (3D) nanostructure in the form of diamond or carbon sponge, two-dimensional (2D) nanostructure in the form of graphene, a one-dimensional (1D) nanostructure in the form of carbon nanotube and carbon nanofiber, a zero-dimensional (0D) in the form of fullerene and carbon dot.

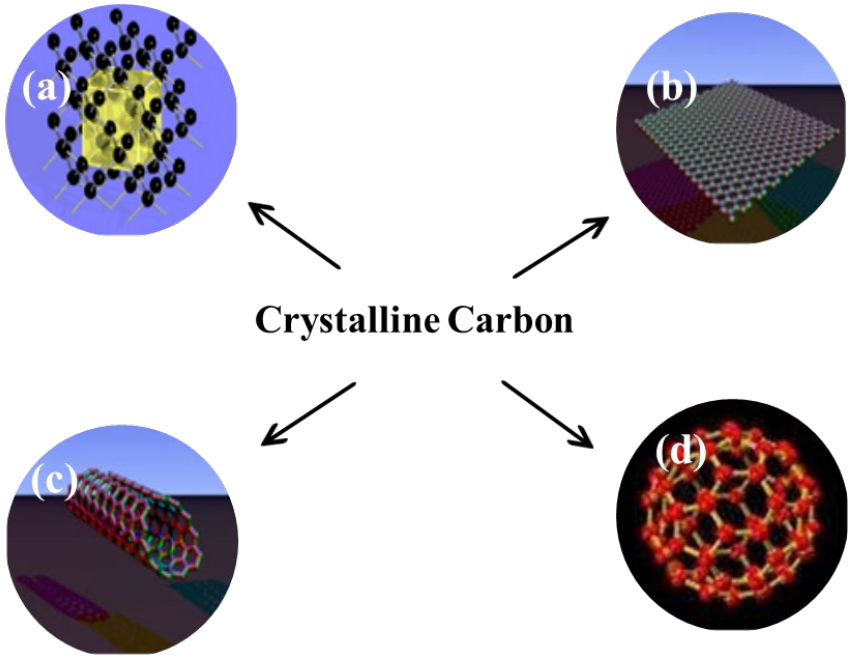

Figure 1: Different forms of crystalline carbon (a) Diamond (b) Graphene (c) Carbon nanotube (d) Fullerene (Dhawane *et al*., 2018)

Amorphous carbon is a carbon material without long-range crystalline order. Examples of amorphous carbons are coke, charcoal, carbon black, etc. shown in Figure 2.

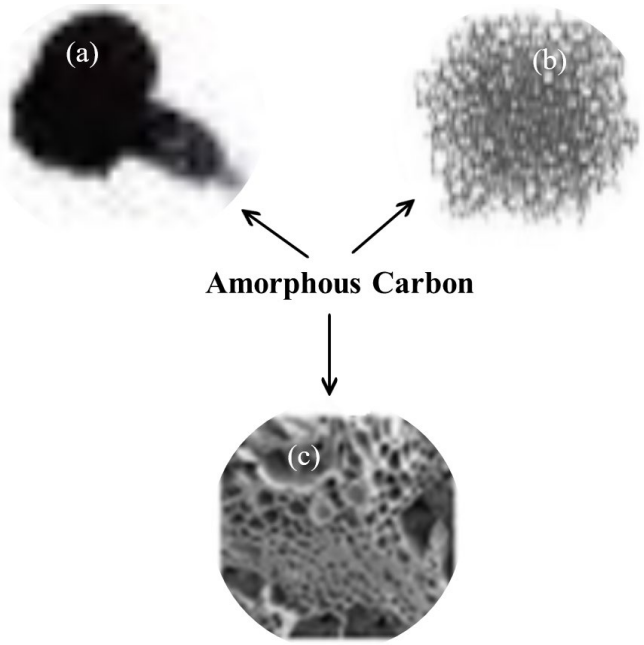

Figure 2: Different forms of amorphous carbon (a) carbon black (b) coke (c) charcoal (Dhawane *et al*., 2018)

In this research work, three different types of carbon materials were taken, namely carbon nanotubes, graphite, and nanodiamond. A brief introduction to these materials is given below.

1.1.1 Carbon nanotubes

Carbon nanotubes were first reported by Iijima in 1991 when he discovered multi-walled carbon nanotubes (MWNTs) in carbon soot made by an arc-discharge method (Iijima, 1991). About two years later, he observed single-walled nanotubes (SWNTs) (Iijima & Ichihashi, 1993). Since then, nanotubes have gained worldwide attention. A significant amount of work has been done in the past decade to reveal the unique structural, electrical, mechanical, electromechanical, and chemical properties of carbon.

Carbon nanotubes are one-dimensional materials with a small diameter of (1-100 nm) and a long length, resulting in a high aspect ratio (Sun & Chen, 2009). They are made of rolled single sheets of graphene which are a single layer of graphite-structured carbon atoms forming six-membered rings of carbon atoms with sp^2 hybridization (Kausar *et al*., 2017; Smart *et al*., 2006). They have high mechanical and electrical properties, good thermal and chemical stability, low density, high expansion coefficient, or a large specific surface area, so they are considered interesting

reinforcing materials for nanocomposite materials (Kausar *et al*., 2017; Mittal *et al*., 2015). Carbon nanotubes are classified into three types based on their number of walls. These are Single-walled carbon nanotubes (SWCNTs), double- walled carbon nanotubes (DWCNTs), and multi-walled carbon nanotubes (MWCNTs). SWCNTs are single graphene sheets rolled into cylinders, DWCNTs are graphene sheets with a double layer, and MWCNTs are graphene sheets with multiple concentric cylinders. The structures of different forms of carbon nanotubes are given in Figure 3 (Rahmam *et al*., 2014).

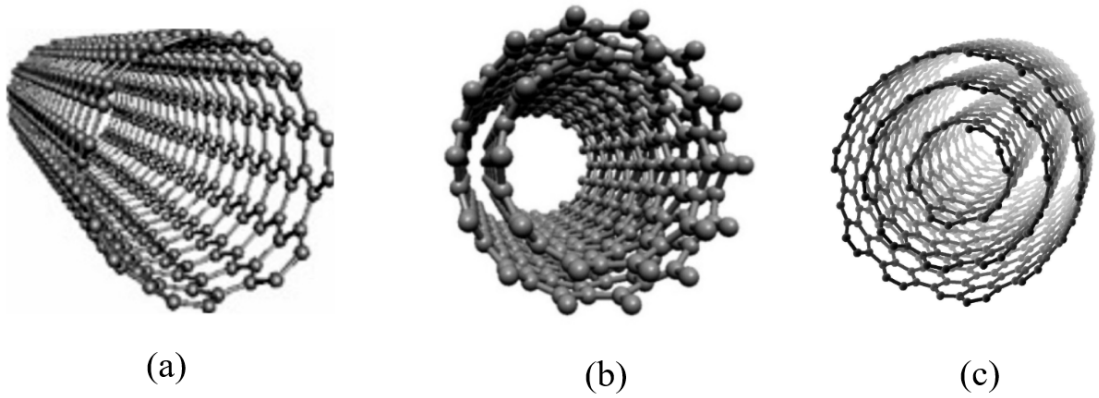

Figure 3: Structures of (a) single-walled carbon nanotubes (SWCNTs) (b) double-walled carbon nanotubes (DWCNTs) (c) multi-walled carbon nanotubes (MWCNTs) (Chemi *et al.*, 2018; Goze-Bac, 2008; Saleh & Koller, 2019)

Carbon in the form of graphite was discovered in 1779. It is a three-dimensional layered structure. The carbon atoms are covalently bonded around each carbon atom, and its layers are bound by much weaker Van der Waals forces (Kaushik *et al*., 2010).

Each carbon atom releases a pair of an electron that moves freely along the plane, which is responsible for its electrical and thermal conductivity. Graphite has sp^2 carbon bonding hybridization states. It is anisotropic. Due to its anisotropic nature, it is used as a good lubricant and pencil material. Carbon layers are stacked in a hexagonal pattern and are connected by a weak Van der Walls force. Graphite undergoes chemical reactions because of its anisotropic nature, allowing the reactant to be incorporated between the graphene layers, ultimately forming compounds known as intercalated compounds. Graphite intercalated compounds are more electrically conductive than graphite (Chung, 2002).

Graphene sheets are both thermally and electrically conductive due to the overall

distribution of π orbitals (electrons). It exhibits a two-dimensional (2D) order (Sengupta *et al.*, 2011). The structures of graphite and graphene are given in Figure 4.

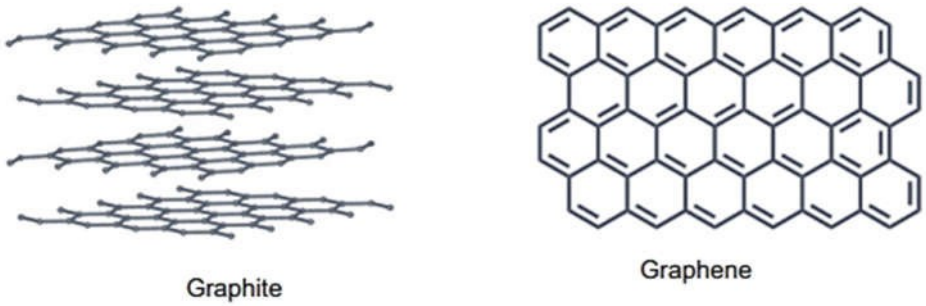

Figure 4: Structure of graphite and graphene (Bai *et al.*, 2019)

Graphene is a two-dimensional carbon nanomaterial consisting of single-layer atoms arranged in a honeycomb lattice with sp^2 hybridization (Mbayachi *et al.*, 2021). Graphite has a layered two-dimensional structure of graphene. The carbon atoms are covalently bonded around each carbon atom, and the layers are bonded by Van der Waals forces. Each carbon atom releases a pair of electrons that move freely along the plane, which is responsible for its electrical and thermal conductivity (Yao *et al.*, 2020).

Graphite is popular among all the conductive fillers because of its high electrical conductivity, variety of shapes and sizes, and ease of obtaining using a conventional process (Cunningham *et al.*, 2007; Hwang *et al.*, 2008).

The use of graphite materials is popular in many fields, including the chemical industry, petroleum refining, and energy conversion, because of its high electrical and thermal conductivity, and corrosion resistance (Yao *et al.*, 2020).

1.1.2 Nanodiamond

Zero-dimensional carbonaceous material, also known as nanodiamond, nanocrystalline particle, and diamond (Mochalin & Gogotsi, 2015) has dimensions between 1 and 100 nm. Nanodiamond has three-layered structures composed of sp^3 diamond and sp^2 graphitic bonds (Koumoulos *et al.*, 2015). The surface layer is made up of sp^2 carbon with a variety of polar functional groups, the central part has a sp^3 nanodiamond core and the intermediate layer is made up of diamond-type carbon (Kausar, 2018). It's superior thermal, mechanical, and multifunctional

properties, as well as improved interaction with the matrix, improved dispersion, biocompatibility, non-toxicity, tailorable surface chemistry, and structural integrity, make it a promising reinforcing material for the fabrication of nanocomposites (Kausar, 2019; Koumoulos *et al*., 2015).

Nanodiamond was first synthesized in the 1960s by Soviet scientists. It has complex structures consisting of a diamond core and an amorphous carbon shell (Zhang *et al*., 2018). They are less toxic than other carbon nanoparticles (Byrne, 2009; Schrand *et al*., 2007). The sp^3 phase of nanodiamonds is crystalline, and the remaining sp^2 fraction is a mixture of amorphous carbon and olefinic molecules (Ferrari & Robertson, 2004; Krueger & Lang, 2012). The structure of nanodiamond is given in Figure 5.

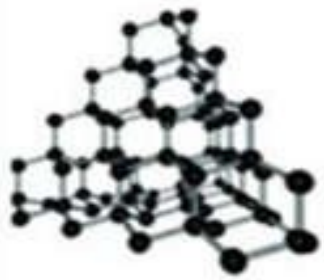

Figure 5: Structure of nanodiamond (Xinchun Chen & Li, 2020)

Nanodiamonds have been used in many fields, like tribology and lubrication (Chou &Lee, 2010; Lee *et al*., 2017; Shirani *et al*., 2019), drug delivery (Chauhan *et al*., 2020; Giammarco *et al*., 2016; Kaur & Badea, 2013; Mochalin *et al*., 2013), bioimaging (Prabhakar & Rosenholm, 2019; Torelli *et al*., 2019), biosensors (Huang *et al*., 2004), energy storage (Gu *et al*., 2013; Wang & Cui, 2019), catalysis (Basso *et al*., 2020; Bogatyreva *et al*., 2004; Hunge *et al*., 2021; Moosa *et al*., 2014; Zhou *et al*., 2017) and photodevices (Qin, Yang, Lv, Li, Chen, *et al*., 2021). Nanodiamonds tend to aggregate. These aggregations of nanodiamond particles can be removed by various techniques like dry milling, ultrasonic treatments (Krueger *et al*., 2008), and surface graphitization (Liang *et al*., 2011).

1.2 Thermosetting Epoxy Resin

Thermosets are polymers that, when heated or when a curing agent is added, form three-dimensional, robust, stiff structures of a strongly cross-linked network. Thermosets are mostly applied in the building and construction industries, while they

can also be used in transportation, adhesives, and electronic devices. Additionally, they are employed in advanced applications including the military and aerospace industries (AlMaadeed *et al*., 2020). Polyesters, epoxies, polyurethanes, and silicones are typical thermosets. In thermoset polymers, the linkages are covalent and naturally cross-linked (Markets, 2007). A few of them are chemically stable in most solvents, optically clear, gas-impermeable, and photo-resistive (Li *et al*., 2021).

Epoxy resins are organic polymer compounds with a low molecular weight having more than one epoxide group. They are more successful than other thermoset polymers due to their versatility and exceptional properties including excellent specific strength, high adhesion with many substrates, good mechanical strength, superior thermal properties, dimensional stability, low cost, availability in abundance and low shrinkage rate during curing. These attributes allow epoxy resins to be used in a wide range of applications (Kausar *et al.*, 2016; Mittal *et al.*, 2016; Saba *et al.*, 2016; Singh *et al.*, 2019; Zhao & Abu-Omar, 2017). They are widely applied in the field of paints and coatings (Zhou *et al*., 2020), adhesives (Kocaman *et al*., 2020), aerospace industries, electronics materials, and biomedical systems (Wang *et al*., 2014). Several curing agents, such as amines, are used to cure them to create solid, cross-linked structures. (Khatiwada, 2020; Januszewski *et al*., 2021). Owing to these astounding properties, epoxy resin of bisphenol A is used in this work prepared by reacting epichlorohydrin with bisphenol A in the presence of a basic catalyst (Jin *et al*., 2015). The structure of epoxy resin is given in Figure 6.

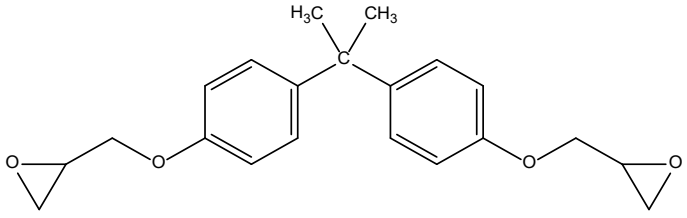

Figure 6: Structures of epoxy resin (DGEBA)

1.3 Nanocarbons-Based Polymer Nanocomposites

Nanocarbons/polymer nanocomposites are polymer materials with the reinforcement of nanosized particles in a polymer matrix to enhance their mechanical, thermal, and electrical properties. The polymer nanocomposites comprise two components: reinforcement filler and the polymer matrix. In the nanocarbons/polymer

nanocomposites, nanocarbons like carbon nanotube, graphite, nanodiamond, fullerene, nanoclay, and carbon fibre act as reinforcement fillers, and classes of polymers like thermoplastic and thermoset are used as the polymer matrix. These types of composites have extraordinary properties and are widely used in engineering applications, including aerospace, aviation, industries, military, marine, and so on (Friedrich, 1986; Rahman *et al*., 2011).

Because of their excellent physical properties, they are used as fillers in reinforced polymer nanocomposites. Thus, formed nanocomposites have superior mechanical properties, thermal stability, thermal conductivity, and tribological properties. Nanodiamond/polymer nanocomposites are widely used as sensors, optical computing and quantum calculations, electrical energy storage, wastewater treatment, and bioapplications. They are also used in the aviation, automobile, and petrochemical industries (Zhang *et al*., 2018).

Nanodiamond/polymer nanocomposites are used in the manufacture of aircraft, automobiles, ships, medicine, chemical and petrochemical industries, and in protective and antifriction coatings (Dolmatov, 2001; Post *et al*., 2002).

Graphite/epoxy nanocomposites are also well known for their good conductivity, higher modulus, and tensile strength. The oxidation of graphite causes the change of sp^2-hybridized states of graphite into a disordered structure of sp^2 and sp^3 carbon due to covalent bonding with oxygen functionalities. The attachments of functional groups increase the hydrophilicity, change the conductivity and allow the intercalation of molecules between graphene. All these properties of graphite oxide make it popular for use in various applications like electrode materials, water purification systems, and precursor materials for the synthesis of graphene (Boukhvalov *et al*., 2012; Dimiev *et al*., 2012; Gao *et al*., 2009, 2011; J. Kim *et al*., 2012; Loh *et al*., 2010; Zhu *et al*., 2010). The significant impact on the adhesion, distribution, and reinforcement effects in the polymer/CNT composites after surface modification of the CNT is well reported in the literature (Adhikari & Michler, 2009).

To get the best performance out of polymer nanocomposites, a good mix of nanocarbons and polymers is required. When the nanocarbon is homogeneously dispersed in the solvent, the mixing is appropriate. Therefore, before mixing the nanocarbons with the polymer, they must be functionalized. It has been difficult to

prepare nanocarbon-reinforced polymer nanocomposites because it is difficult to get well-dispersed nanocarbons in a polymer matrix, which reduces their performance. As a result, multi-walled carbon nanotubes, graphite, and nanodiamonds, which are functionalized nanocarbons of different dimensions, are well dispersed in the polymer matrix, enhancing its numerous properties.

1.4 Rationale of Study and Research Questions

The functionalization of nanocarbons and their nanocomposites with the epoxy matrix with a focus on mechanical and electrical properties has been documented in the aforementioned different literatures. However, a comparative investigation of nanocomposites with various nanocarbon dimensional compositions, concentrating on their structural, thermal, morphological, electrical, and surface-wetting characteristics, has not been fully explored. As a result, the structural properties of nanocarbon/polymer nanocomposites of various dimensions have been associated in this study, including correlation between the morphological, structural, thermal, electrical, and surface wetting properties of the nanocarbon/polymer nanocomposites.

1.5 Research Questions

1. How does the functionalization of nanocarbons differ depending on the dimensionality of nanocarbons?

2. How does chemical functionalization alter the structural properties of nanocarbons?

3. How are the physical properties of composites affected by the introduction of nanocarbons?

4. Does a correlation exist between filler dimensionality and the physical properties of polymer nanocomposites?

1.6 Objectives

The aim of the present study is the functionalization of nanocarbons of different dimensionalities and to study the physical properties of their nanocomposites with the epoxy resin thermosetting polymer.

The specific objectives of the work are as follows:

1. Functionalization of multi-walled carbon nanotubes, graphite nanoplatelets, and

nanodiamonds

2. Preparation of polymer nanocomposite of the nanocarbon with DGEBA-based thermosetting plastic, the epoxy resin

3. Characterization of prepared polymer nanocomposite in terms of structural, thermal and morphological study

4. Study of electrical and surface properties of polymer nanocomposites

CHAPTER 2

2. LITERATURE REVIEW

2.1 Preparation of Different Forms of Nanocarbons

Carbon nanotubes (CNTs), graphites (GPs), and nanodiamonds (NDs) can be synthesized by mainly three different techniques: chemical vapour deposition method, laser ablation method, and electric arc discharge method see Figure 7 (Dervishi *et al*., 2009; Kamal *et al*., 2020; Qin, Yang, Lv, Li, Liu, *et al*., 2021).

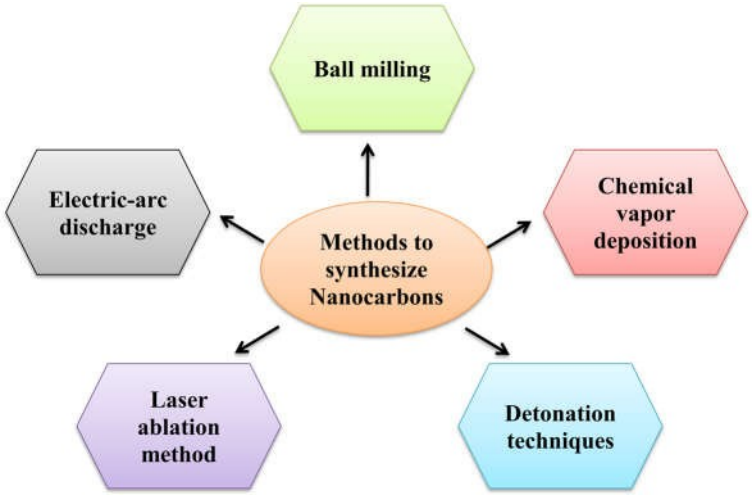

Figure 7: Schematic diagram of different methods for synthesizing nanocarbons

(a) Electric-arc discharge

The MWCNTs can be commonly prepared by striking an arc between graphite electrodes in an inert atmosphere (Ar or He). This process also produces carbon soot containing fullerene. The carbon arc provides a convenient and traditional tool for generating the high temperature needed to vaporize carbon atoms into plasma (>3000 ^{o}C). The yield of CNTs depends on the stability of the plasma formed between the electrodes, the current density, inert gas pressure, and cooling of the electrodes and chamber. Among the various inert gases, helium gives the best result, due to its high ionization potential. After evacuating the chamber with a vacuum pump, an appropriate ambient gas (He or Ar) is introduced at the desired pressure (about 500 torrs) and the direct current arc voltage is applied (20-25 V) between the two graphitic rods (separated by 1mm distance). When the electrodes are made to strike each other, it produces an electric arc. The energy that is produced in the arc gets transferred to

the anode, ionizing the carbon atoms of the pure graphite anode, producing C^+ ions, and forming plasma. When these positively charged carbon ions approach the cathode, they are reduced, deposited, and grow as carbon nanotubes on the cathode. There are different experimental conditions for the synthesis of SWCNTs, DWCNTs, and MWCNTs (Dervishi *et al*., 2009).

b) Laser ablation method

It is a physical vapour deposition technique in which a piece of graphite target is vapourised by laser irradiation at high temperatures in an inert atmosphere. MWCNTs were found when a pure graphitic target was used. A graphitic target is placed in the middle of a long quartz tube mounted in a temperature-controlled furnace. The laser vaporization produces carbon species, which are swept away by the flowing gas from the high-temperature zone and deposited on a conical, water-cooled copper collector. The quality and yield of the products have been found to depend on the reaction temperature. The best quality is obtained at a reaction temperature of 1200 ^oC. At low temperatures, the structure quality deteriorates and the CNTs begin to exhibit numerous defects.

As soon as small quantities (few % or less) of transition metals (Ni, Co) playing the role of catalyst are incorporated into the graphite pellet, the products yielded undergo significant modification, and SWCNTs are formed instead of MWCNTs. The yield of SWCNTs strongly depends on the type of metal catalyst used and is seen to increase with furnace temperature. A high yield of about 50 % conversion of transition metal/graphite composite rods to SWCNTs was reported in the condensing vapour in a heated flow tube operating at 1200 ^oC.

Unfortunately, the process requires high-purity graphite rods, and high laser powers, and produces fewer MWCNTs per day than the arc discharge approach does. As a result, the laser technique is not commercially viable (Dervishi *et al*., 2009).

(c) Chemical vapour deposition method

Chemical vapour deposition (CVD) is a popular method for thin film depositions. This method is very different from the arc discharge and laser vaporization methods for CNT production. Arc discharge and laser vaporization can be classified as high temperature (>3000 K) and short time (micro to the millisecond) reaction techniques,

whereas catalytic CVD is a medium temperature (500-1000 ºC) and long-time reaction (minutes to an hr) technique. The main technological disadvantages of arc discharge and laser vaporization are that CNTs are produced and can stand alone. The CNTs do not grow on a patterned substrate. A major advantage of CVD is that the CNTs can be used directly without further purification unless the catalyst particles are required to be removed. The CVD synthesis schematic diagram is displayed in Figure 8.

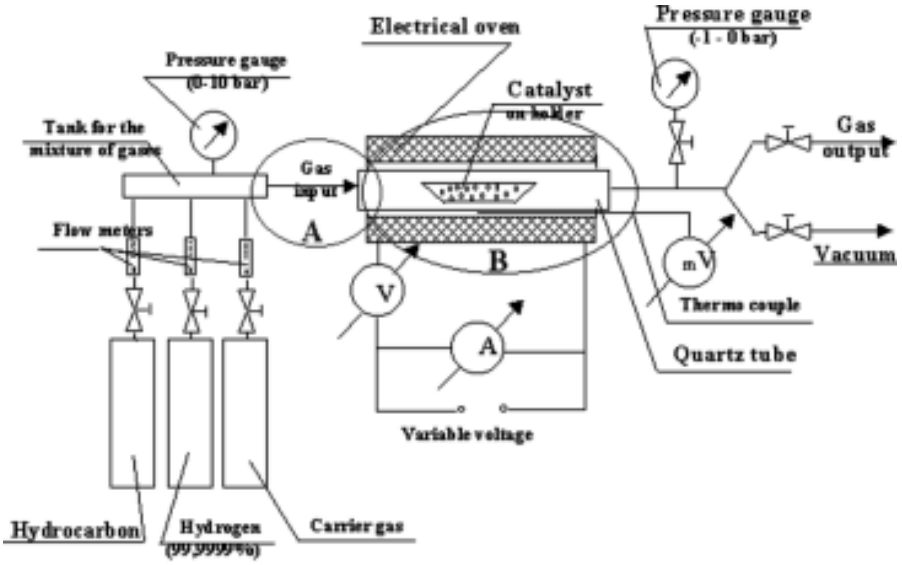

Figure 8: Schematic diagram of CVD for the synthesis of nanotubes (Dervishi *et al.*, 2009)

The synthesis of carbon nanotubes by the thermal CVD method uses hydrocarbon gas as a carbon source. In this method, a quartz tube is placed inside a furnace maintained at a temperature of 500-900 ºC. A substrate-coated crucible with nanoparticles is placed inside the quartz tube, which is filled with argon gas and then the hydrocarbon gas is pumped into the tube where it undergoes a pyrolysis reaction and forms vaporized carbon atoms. These carbon atoms were bonded to the substrate, joining each other with the Van der Waals force of attraction, which eventually grows as multi-walled carbon nanotubes on the substrate.

Different CVD methods are reported. They are thermal chemical vapour deposition, plasma-enhanced chemical vapour deposition, and catalytic pyrolysis of hydrocarbons.

Besides the above techniques, there are other methods reported for the synthesis of CNTs, such as different solution-based techniques, diffusion fusion synthesis,

electrolysis using graphite electrodes immersed in molten ionic salts, ball milling of graphite, heat treatment of polymers, etc. (Pham *et al*., 2017).

Additionally, nanodiamonds can be synthesized by

(a) Detonation techniques

The detonation technique has been widely used in the preparation of nanodiamonds due to its advantages of easy operation, simple equipment fast reaction, and low synthetic cost. The gun spray process used in detonation techniques is shown in Figure 9.

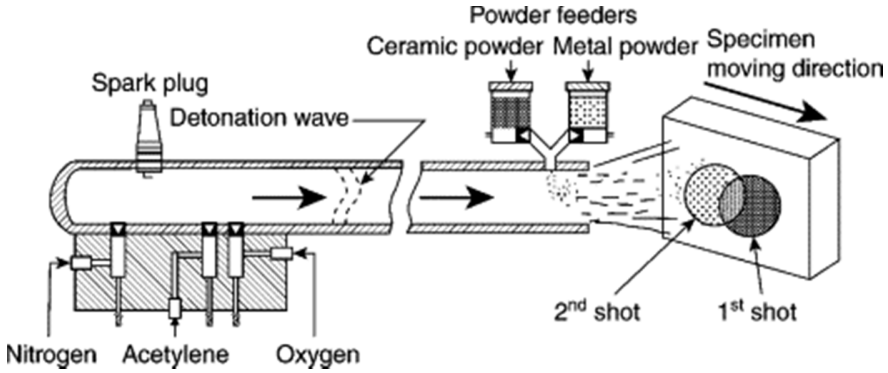

Figure 9: Schematic representation of showing gun spray process (Ke *et al.*, 2011)

(b) High pressure and high temperature

In this method, nanodiamonds were synthesized from graphite with metal catalysts in a large volume. The pressure and temperature of 5-6 GPa and 1300-1500 ^{o}C were maintained in the system. From this method, high-quality and nanosized diamonds can be synthesized. NDs synthesized from this method contain no metal impurities and are highly biocompatible, which makes them suitable for medical applications. Thus synthesized NDs have high toughness, wear resistance, and thermal stability, making them applicable in abrasives, cutting, and polishing tools.

(c) Ball milling

It is the method that uses the rotation and vibration of a ball mill to make the balls strongly impact, grind, and agitate the raw materials to crush the samples into nanoscale particles. Ball milling techniques are used to create NDs, which are useful for bioimaging and drug administration because of their small size and high fluorescence defects (Qin *et al*., 2021).

2.2 Nanocarbons Functionalization

2.2.1 General methods of functionalization

(a) Covalent functionalization

Carbon nanotubes have more reactive end caps than side walls. It also contains defect sites like pentagon-heptagon, sp^3 hybridized effects, and vacancies in the nanotube lattice (Hirsch, 2002; Sinnott, 2002).

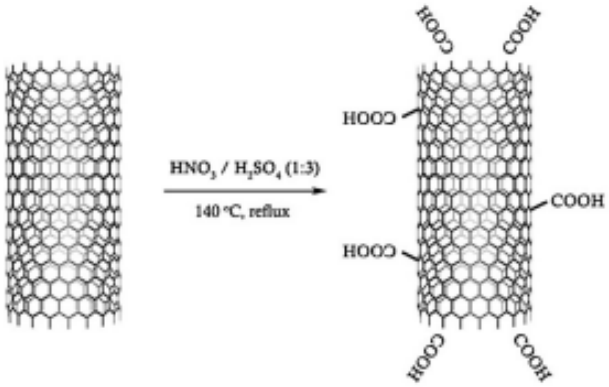

Figure 10: Schematic representation of covalent sidewall functionalization of nanotube (Bikiaris *et al.*, 2008)

In direct covalent sidewall functionalization, the change of hybridization from sp^2 to sp^3 takesplace with a simultaneous loss of the p-conjugation system on the graphene layer. In another method, namely defect functionalization of CNTs, defects are supplemented by oxidative damage to the nanotube framework by strong acids, which leave holes functionalized with oxygenated functional groups. When CNT is treated with strong acids such as HNO_3, H_2SO_4, or mixtures of these acids, oxygenated functional groups such as -COOH, -OH, and -C=O are added as shown in Figure 10 (Chen *et al.*, 1998).

Due to the attachment of these functional groups during covalent functionalization (Hirsch & Vostrowsky, 2005; Le *et al.*, 2013), the solubility and dispersion are enhanced in a variety of solvents including water, dimethyl formamide, ethyl alcohol, 1,3-dimethyl-2-imidazolinone, dimethyl sulfoxide, and chloroform (Guo *et al.*, 2017).

(b) Non-covalent functionalization

Non-covalent functionalization does not destroy the conjugated system of CNT sidewalls. CNTs are mostly functionalized by aromatic compounds, surfactants, and

polymers through stacking or hydrophobic interactions in non-covalent functionalization (Jeon *et al*., 2011). The graphitic structure and original properties of CNTs after modification remain the same as before (Cao *et al*., 2020; Meng *et al*., 2009).

(c) Direct sidewall functionalization

In direct sidewall functionalization, there is a change of carbon atoms from sp^2 to sp^3. The cycloaddition and electrophilic or nucleophilic attack on the aromatic rings resulted in the loss of conjugation by carbon atoms (Meng *et al*., 2009; Syrgiannis *et al*., 2020).

The various methods for sidewall functionalization, in which the carboxylic acid groups are covalently bonded to the sidewall of a single SWNT, were described by Darabi *et al*. (2012).

(d) Endohedral Functionalization

In endohedral functionalization, the inner cavity of the tubes is explored in terms of various reactions that do not happen outside the tubes (Pichler *et al*., 2003; Setaro, 2017).

CNTs behave like other organic molecules by encapsulating molecules or atoms within their central concave space through a variety of synthetic methods (De Juan & Pérez, 2013; Khlobystov *et al*., 2005).

2.2.2 Functionalization of carbon nanotubes (CNTs)

Ahmed *et al.* (2013) studied the functionalization of multi-walled carbon nanotubes (MWCNTs) treated with oil olive and nitric acid (65 %). They have functionalized the surface of MWCNTs. The acid-modified MWCNTs were characterized by fourier transform infrared spectroscopy (FTIR), X-ray diffraction (XRD), and scanning electron microscope (SEM). The existence of the carboxyl group was confirmed by the FTIR, whereas the occurrence of surface modification was confirmed by SEM. Finally, they were successful in obtaining well dispersed MWCNTs which can be used in various applications.

Mohl *et al.* (2007) have chemically modified the multi-walled carbon nanotubes (MWCNTs) to impart a specific desired property. The functionalization of MWCNTs

is carried out using HNO_3 and $KMnO_4$; afterwards, amine-containing groups were introduced. They have successfully explored a covalent strategy for the functionalization of multi-walled carbon nanotubes.

Multi-walled carbon nanotubes (MWCNTs) were modified and functionalized *via* Fischer esterification by Abuilaiwi *et al.* (2010). MWCNTs were treated with nitric acid to remove the catalyst and introduce carboxylic groups to the surface of MWCNTs. After that, functional groups were successfully covalently attached to the MWCNTs surface *via* amidation or esterification. The functionalized MWCNTs were then characterized by FTIR, thermogravimetric analysis (TGA), and differential scanning calorimetry (DSC). The TGA data has confirmed the presence of functional groups attached to the surface of MWCNTs and their corresponding degradation with increasing temperature in an inert atmosphere.

Abdullah & Zulkepli (2015) treated the multi-walled carbon nanotubes (MWCNTs) with concentrated nitric acid. After functionalization, the treated MWCNTs were analysed by FTIR and XRD. From the XRD, the percent of crystallinity was determined. When pristine MWCNTs were treated for 12 hrs and then fluorinated with nitric acid for another 12 hrs, the crystallinity increased from 66 wt. % to 80 wt. %. The FTIR spectra in Figure 11. shows the attachment of the carboxyl functional group after 12 hrs of treatment and 12 hrs of reflux of MWCNTs with nitric acid have shown the presenceof only a hydroxyl group on its surface.

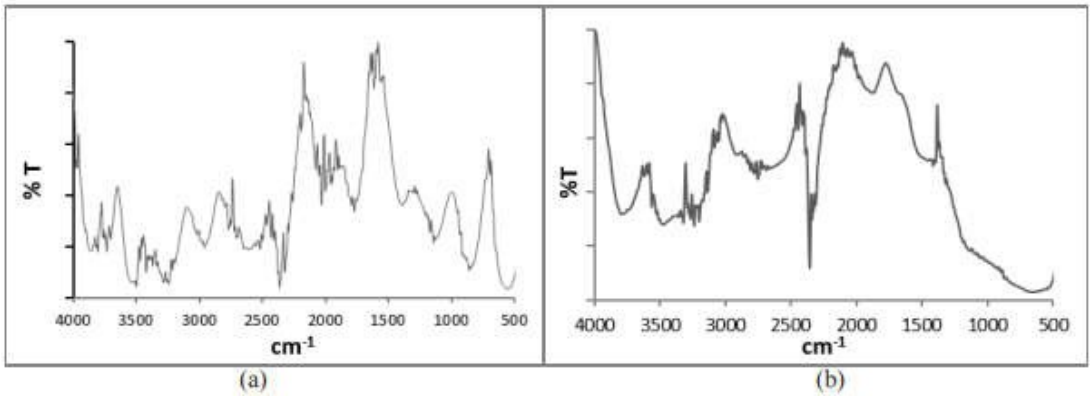

Figure 11: FTIR spectra of (a) MWCNTs treated with HNO3 for 12 hrs (b) MWCNTs treated with additional 12 hrs (M. P. Abdullah & Zulkepli, 2015)

Ahmad *et al*. (2013) investigated the purification and functionalization of commercial multi-walled carbon nanotubes MWCNTs. MWCNTs were treated with

conc. HNO_3 for 2 hrs. After that, the MWCNTs were washed with deionized water till neutral. The thermal decomposition procedure was studied by thermogravimetric analysis; on the other side chemical shift in MWCNTs is determined by Raman spectroscopy. Raman spectra revealed that the D and G band positions had shifted in oxidized Baytube and vice versa in oxidized Skyspring MWCNTs. From the TGA analysis, it was confirmed that the metal catalyst of the oxidized baytube sample has been eliminated compared to the oxidized Skyspring sample. Both measurement techniques confirmed that Baytube MWCNTs were more stable compared to Skyspring MWCNTs.

The functionalization of MWCNTs is carried out by sonication in mildly acidic conditions. A mixture of nitric acid and sulfuric acid in a ratio of 1:3 is used to functionalize MWCNTs. The functionalized MWCNTs were characterized by FTIR and field emission scanning microscopy (FESEM) to determine the chemical bond present and investigate the surface morphology. FTIR shows the attachments of different oxygen-containing functional groups. The use of low concentrations of acid and low temperature reduces the defect sites on functionalized MWCNTs. Along with this, in both pristine and functionalized MWCNTs same worm-like bundling structures were observed (Fatin *et al.*, 2014).

To evaluate their impact on the structural integrity of multi-walled carbon nanotubes (MWCNTs), the as-received MWCNTs were treated with a non-oxidative acid and a basic treatment. SEM and TGA analyses showed that the nitric acid-treated MWCNTs under reflux conditions suffered the highest degree of degradation. There was a complete removal of amorphous carbon and metal oxide impurities, but there was no disturbance in structural integrity, which is confirmed by thermogravimetric analysis (Datsyuk *et al.*, 2008).

A mixture of sulfuric acid and nitric acid (3: 1) was used to oxidize multi-walled carbon nanotubes for 1, 2, and 4 hrs respectively. The oxidized MWCNTs were characterized by FTIR, X-ray photoelectron spectroscopy (XPS), TGA, and Raman spectroscopy to determine the degree of oxidation. FTIR, TGA, and XPS confirmed that the attachment of functional groups depends on the treatment time and the better dispersibility of MWCNTs was obtained in water having a higher oxidation degree (Liu *et al.*, 2018).

MWCNTs were surface modified by treating with HCl, H_2SO_4/H_2O_2, HNO_3, and H_2O_2/NH_4OH under standard conditions. The higher conductivity was seen in the case of the mixture of H_2O_2/NH_4OH nanocomposites because of the milder impact of the mixture of H_2O_2/NH_4OH on the conductive shells of nanotubes and the effective removal of poorly conducting amorphous carbon (Špitalský *et al.*, 2009).

2.2.3 Functionalization of graphite (GP)

The inertness and robust crystallinity of graphite restrict the range of its uses in a variety of fields. Thus, it is proposed that the surface functionalization of graphite is the initial step in developing new physical and chemical qualities including solubility and dispersibility to enhance its properties as shown in Figure 12 (Aliyeva *et al.*, 2019).

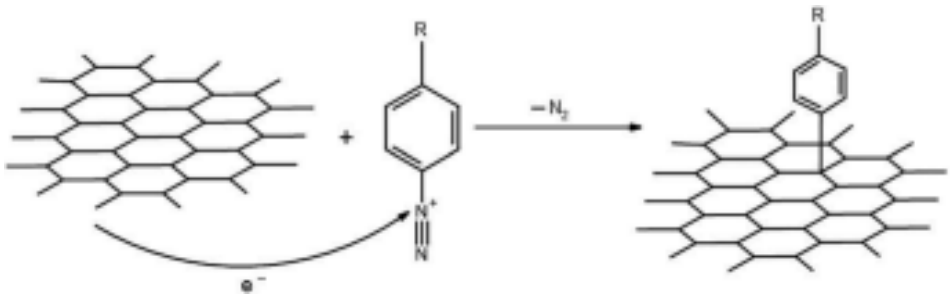

Figure 12: Schematic representation of functionalization of graphite surface *via* diazonium chemistry (Aliyeva *et al.*, 2019)

The surface functionalization of graphite was carried out by contact and remote photocatalytic oxidation methods. The photo-catalytically oxidized graphite (POG) was studied by Raman spectroscopy, which confirmed the transformation of sp^2-hybridized carbon to oxygenated sp^3-hybridized states. XPS was used to study carbon-oxygen bonding at the graphite surface after oxidation. The C=O peak was observed at the POG surface after photocatalytic graphite oxidation, indicating oxygen functional groups shown in Figure 13. The C-C peak at 284.5 eV was broadened due to graphite surface functionalization causing sp^2-sp^3 transformations (Ostyn *et al.*, 2021).

The oxidation of graphite was investigated where the oxidation process of graphite was studied by oxidation experiment and density functional theory. After that, the characterization of the unhydrolyzed oxidized graphite was carried out using nuclear magnetic resonance, thermogravimetric analysis, and X-ray photoelectron

spectroscopy techniques.

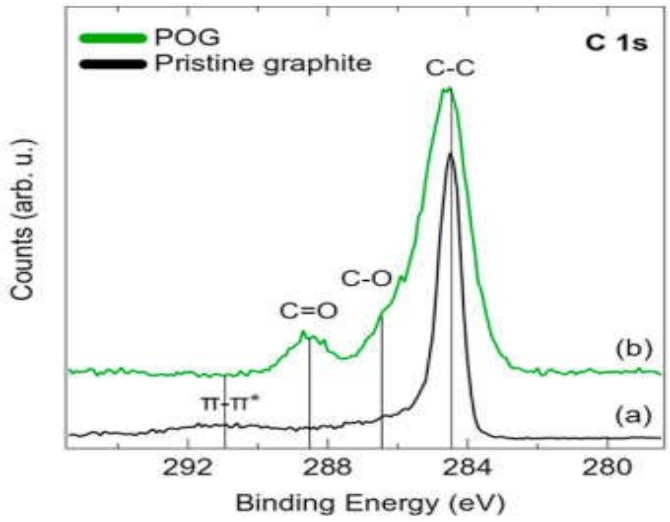

Figure 13: XPS spectra showing covalent oxygen bonding after TiO_2 photocatalytic oxidation. (a) Pristine graphite and (b) POG prepared by contact mode under 70 vol% O_2 and 1.8 vol% H_2O vapour for 120 hrs at 70 °C

It reveals that the attached functional groups are mainly hydroxyl and epoxide groups as well as monosulphate. The density functional theory is used to calculate Gibb's free energy of the oxidized microdomains (Selva *et al*., 2020).

Alam *et al.* (2017) evaluated the plasma treatment method and wet chemistry for their efficacy and efficiency in the surface modification of carbon-based nanoparticles. They concluded that using plasma techniques to change carbon nanoparticles is an efficient, non-destructive, and more ecologically friendly strategy after comparing the two methods.

2.2.4 Functionalization of nanodiamond (ND)

Polypropylene (PP) membranes were mixed with ND at concentrations ranging from 0.25 to 1 wt. % to enhance the antifouling capabilities. The attachment of the carboxyl group was confirmed by Fourier transform infrared spectroscopy analysis. The carboxylated ND was examined using FESEM, contact angle, and tensile tests after being incorporated into polypropylene membranes. The research found that at the same concentration of unmodified and carboxylated ND nanoparticles, PP/ND-COOH membranes had higher hydrophilicity, pure water flux, and tensile strength than PP/ND membranes. The 0.75 wt. % PP/ND-COOH membrane demonstrated better antifouling properties than other membranes when fouling mechanisms were

examined (Hoseinpour *et al.*, 2019).

Nanodiamond (ND) was initially functionalized to facilitate effective interaction between the polymer matrix and the filler ingredient. IR spectroscopy confirmed the presence of several carboxyl and hydroxyl groups linked to ND surfaces. The functionalized ND was then mixed with polyvinyl alcohol, and the nanocomposites were examined using TEM, SAXS, and DSC. The results demonstrated that there was no agglomeration and that ND particles were distributed consistently throughout the fabricated nanocomposites. The polymer's crystallinity was found to increase as the ND concentration increased, and the hardness value significantly increased when the ND wt. % decreased (Maitra *et al.*, 2009).

Nanodiamonds were functionalized using a variety of methods to achieve uniform dispersion and address the issue of ND aggregation. Nanodiamonds were introduced to epoxy resin by vacuum bagging process at three distinct loadings, 0.1, 0.3, and 0.5 wt. %, after being functionalized by ozone treatment. The functionalization of nanodiamonds was completed by dispersing the nanodiamonds in epoxy resin. The study showed that the addition of nanodiamonds enhances the epoxy's adhesion to the matrix, which is the main cause of the nanocomposite's enhanced mechanical properties. The nanocomposite crack deflection fracture mechanism is modified by the nanodiamonds, enhancing their strength. In Figure 14 the peaks around 1625 and 1790 cm^{-1} represent carbonyl functional groups (C=O) observed after as well as the peaks around 2800 and 3000 cm^{-1} for ND were removed after the ozone treatment (Zaheer *et al.*, 2018).

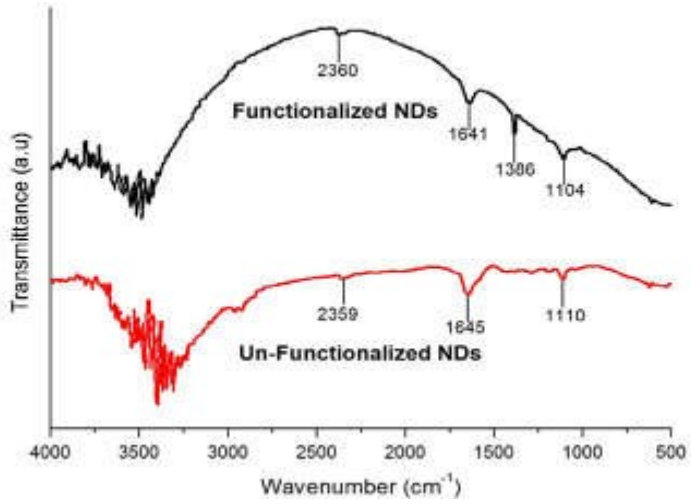

Figure 14: FTIR spectra of as-received ND and ozone-treated ND (Zaheer *et al.*, 2018)

To facilitate the interfacial molecular interaction between reinforcement and matrix, the sp^2 content of ND is minimized using the annealing procedure. According to XRD and FTIR studies, the reduction in resistivity is based on the sp^2/sp^3 carbon ratio of ND, and annealing of ND occurs at 450 °C. The characteristics of annealed EP/ND nanocomposites with low filler concentrations ranging from 0.1 wt. % to 0.5 wt. % found that the improvement of the dielectric characteristics of epoxy nanocomposites was shown to be significantly influenced by the elimination of sp^2 carbon and metal impurities. 0.3 wt. % concentrations of ND increased the thermal conductivity of EP/ND nanocomposites by 21 wt. % (0.197 W/mK) at 55 °C, and this increased as the temperature was raised. The annealed EP/ND nanocomposites show an improvement in Vickers hardness value by 107.96 wt. % (Singh & Mohanty, 2020).

PEEK poly(ether-ether-ketone) was melt blended with phenyl phosphonate modified oxidized nanodiamond (OND) or carboxylic nanodiamond (CND) to investigate the impact of surface chemistry on ND dispersion and ND/PEEK nanocomposite characteristics. The electrical conductivity of the composites does not significantly enhance when ND is introduced to PEEK. The OND dispersion in PEEK and the PEEK crystallinity do not appear to be significantly impacted by the sonication-assisted phenyl phosphonate grafting on OND. DSC confirmed that the ONDson/PEEK nanocomposites have a somewhat higher degree of crystallinity than both OND/PEEK and pure PEEK. When phenylphosphonate grafting is done on OND, it can increase composite thermal conductivity by up to 38 % when compared to pure PEEK (Wahab *et al.*, 2017).

The functionalization of ND using the microwave-assisted technique is a quick, affordable, and environmentally friendly approach. The presence of a carboxylic group on the surface of the NDs was confirmed by FTIR studies. The carboxylic nanodiamonds (C-NDs) have shown greater solubility in water, tetrahydrofuran, and dimethyl sulfoxide, and developed stable dispersions in both aqueous and organic solvents. The X-ray diffraction (XRD) analyses showed that microwave treatment had no impact on the ND's core. The carboxylation increased solubility and reduced agglomeration in both aqueous and polar organic solvents (Desai & Mitra, 2013).

The ND surface was functionalized using atom transfer radical polymerization, which

resulted in interactions between the methacrylate esters and surface functionalized ultra dispersion nanodiamond (UDD) nanoparticles, which formed UDD/polymer brushes with hydrophobic and hydrophilic properties. Today, a variety of hydrophilic UDD/polymer brush materials with controlled dispersibility and functional group reactivity are available that are created *via* acid hydrolysis (Li *et al.*, 2006).

Detonated Diamond (DND) is a strongly agglomerated substance, and deagglomeration can be accomplished by milling beads or by bead-assisted sonic disintegration, which produces stable colloids in a variety of organic solvents. The functionalized and deagglomerated DND is a potential material for use in covalently bonded composite materials as well as biological applications like labelling, drug delivery, and sensing. Additionally, surface functionalization can be done by grafting silanes and amino acids, and hydroxyl groups can be added *via* reductive surface homogenization using borane (Krueger & Boedeker, 2008).

Usually, the process of functionalizing nanodiamonds begins with nitric and/or sulfuric acid treatment. In this process, the surface graphite is removed, and the diamond surface is uniformly finished with hydrophilic oxygen-containing groups. Then, at temperatures ranging from 300 to 1000 °C, the hydrogenated and oxidized diamond surfaces were both fluorinated. Particularly for the fluorination of oxidized diamonds, the surface reaction temperature was found to be the most significant factor (Ando *et al.*, 1993).

The low-cytotoxic NDs are functionalized because they are a non-toxic substitute for inorganic nanoparticles. For the detonation of diamond agglomerates, the organic functionalization approach is discussed. Surface homogenization is accomplished through silane reduction and grafting, followed by amino acid linkage on the surface. These new functionalized diamond materials have the potential to be useful for fluorescence marker and drug delivery applications by attaching biologically active building units (Krüger *et al.*, 2006).

2.3 Preparation of Epoxy/Nanocarbons Nanocomposite (EP/NC)

Epoxy/multiwall carbon nanotube (EP/MWCNTs) nanocomposite was developed by Montazeri and his team to examine their mechanical properties using sonication. To accomplish this, the MWCNTs surfaces were first modified by a combination of acids, and only EP/MWCNTs nanocomposites were then created. The

EP/MWCNTs nanocomposites were subjected to a tensile test and an electron microscopy analysis. It was discovered that the composites containing MWCNTs that had undergone an acid treatment displayed higher Young's modulus values, indicating improved mechanical capabilities. Additionally, they discovered that the acid-treated MWCNTs were distributed uniformly throughout the epoxy matrix and had less pull-out than the untreated one (Montazeri *et al.*, 2010).

Neitzel *et al.* (2011) investigated the mechanical properties of epoxy/nanocomposites containing a higher concentration of ND. The solution casting technique, in addition to sonication, was used to produce the epoxy/nanodiamond (EP/ND) nanocomposites. The microhardness was measured using a Vicker's indenter, and the results showed a 300 % increase in hardness compared to neat EP. Additionally, it was discovered that the addition of ND particles enhanced the heat conductivity of the epoxy resin.

The schematic diagram showing different methods of preparation of nanocomposites is shown in Figure 15.

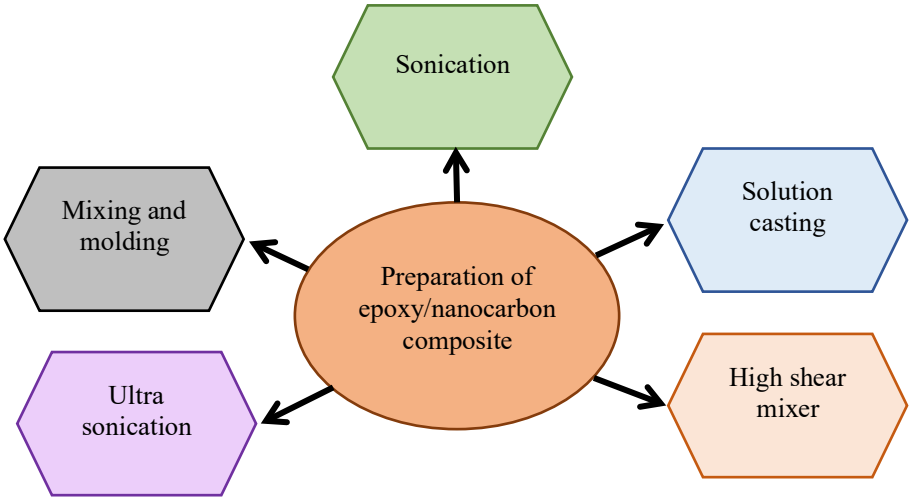

Figure 15: Schematic diagram showing different methods of preparation of epoxy/nanocarbon nanocomposites

The EP/MWCNTs nanocomposites with different weight ratios were prepared by using a shear mixer and an ultrasonication processor. The average thermal conductivities of the samples with filler concentrations of 0.2, 0.4, 0.6, and 0.8 wt. % MWCNTs were found to be approximately 0.27, 0.31, 0.36, and 0.33 $Wm^{-1}K^{-1}$. With only 0.6 wt. % of MWCNTs, the thermal conductivity was increased by around 64 % in comparison with neat EP with MWCNTs loadings of 6 wt. % (Koo & Lee, 2015).

Epoxy/graphite (EP/GP) conductive nanocomposites were prepared by mixing and

moulding techniques assisted by sonication. As a result, the prepared EP/GP composites were tested for conductivity and mechanical properties. The morphology of the fracture surface was studied using a scanning electron microscope, which showed that the white epoxy and black graphite are uniformly dispersed on the fracture surface of the nanocomposites. The 1:1 ratio of the two kinds of graphite showed the best electrical and mechanical properties, with a resistivity value of 0.0800 Ω.cm and a bending strength of 47.32 MPa (Yao *et al.*, 2020).

2.4 Properties of Epoxy/Nanocarbons Composites

2.4.1 Properties of epoxy/carbon nanotube (EP/CNT) nanocomposites

Chen *et al.* (2008) investigated the amine-treated EP/MWCNTs nanocomposites and found that they were covalently grafted into the epoxy matrix. The increment in the MWCNTs filler percentage in the composites increases its tensile and impact strength. The addition of 1.5 wt. % amine-treated MWCNTs significantly improve the tensile strength and also thermal stability of the nanocomposites.

Allaoui *et al.* (2002) reported the electrical properties of the nanocomposite with a different wt. % of nanotubes. The conductivity took place for nanotube concentration between 0.5 wt. % and 1 wt. % and was observed by an increase of nine orders of magnitude in the range of 0-4 wt. %.

The nanocomposite film contains CNTs synthesized by floating catalyst spray pyrolysis techniques. The nanocomposites comprising 59 wt. % CNT showed a high tensile strength of 1.4 GPa and a high electrical conductivity of 1.4×10^5 $S.m^{-1}$ (Chen *et al.*, 2019).

Smoleń *et al.* (2021) investigated the effect of multi-walled carbon nanotubes on the mechanical and electrical properties of EP/MWCNTs nanocomposites. They purified MWCNTs and covalently functionalized the MWCNTs to introduce functional groups on their surfaces. DC resistivity (Figure 16), tensile strength, strain, and Young's modulus with the addition of 0 to 2.5 wt. %. MWCNTs were monitored. Their study concluded the addition of functionalized MWCNTs on epoxy resin produces electrically conductive nanocomposites with a percolation threshold of 1 %.

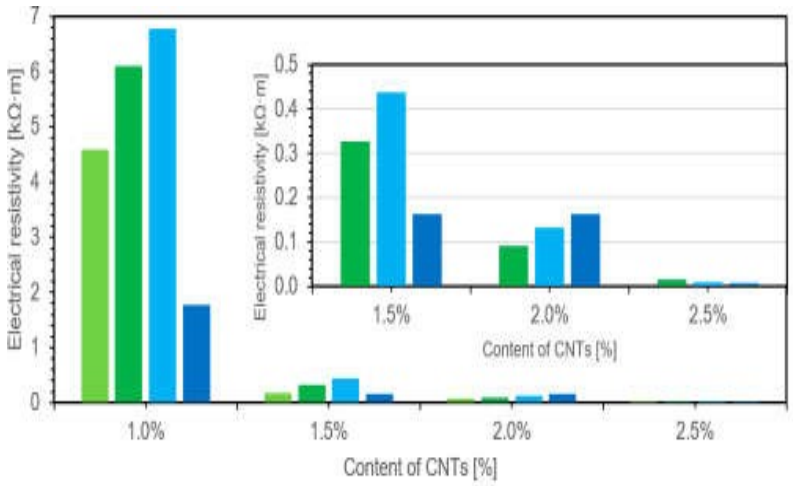

Figure 16: Plot of resistivity vs weight fraction of carbon nanotubes (Smoleń *et al.*, 2021)

Ahmad & Kumar (2012) used the epoxy matrix to produce isotropically conductive adhesives. The various wt. % of multi-walled carbon nanotubes (MWCNTs) were used to produce different concentrations. The conductivity value of 10^{-2} Scm^{-1} was obtained at a filler concentration of 0.3 wt. %. They further concluded that conductive adhesives have high electrical conductivity, and great impact strength was obtained at very low filler loadings.

Sulong *et al.* (2009) tried to improve the mechanical and electrical properties of EP/MWCNTs by increasing dispersion and interfacial bonding strength between MWCNTs and EP matrix. Chemically functionalized MWCNTs and surfactant additive MWCNTs were incorporated into the EP matrix and are investigated as a function of MWCNTs concentrations. The unbalanced polarization effect and physical structure defects due to severe conditions during the acidic treatment process made the electric conductivity dominant on surfactant additive MWCNTs over the chemically modified one. Therefore, they concluded that non-chemical methods are preferable for electrical applications.

Royan *et al.* (2013) have shown interest in the electrical and mechanical propertiesof EP/MWCNTs nanocomposites as bipolar plate applications. The conductivity and mechanical properties of acid-treated and ultraviolet-treated EP/MWCNTs nanocomposites were determined and compared. In comparison, they found that acid-treated EP/MWCNTs nanocomposites give lower electrical conductivity than the UV-treated ones. Therefore, they concluded that the dry oxidation method is preferable for the dispersion and distribution of nanomaterials in a polymer matrix in order to

achieve high electrical conductivity and good mechanical strength.

The thermal and electrical properties of the EP/SWCNT nanocomposites reinforced with purified SWCNTs were studied. Highly purified SWNTs have the potential to significantly improve the thermal conductivity of the EP/SWCNT nanocomposites on the other hand they are not favourable for electrical properties because of their inability to form an effective percolating network (Chen *et al.*, 2019).

The MWCNTs were produced using catalytic decomposition methods, and they were then subjected to chemical treatments to add various oxygen-containing functional groups. The mechanical characteristics of the EP/MWCNTs nanocomposites at 1, 2, and 3 weight percent were examined. The fracture surface analysis test and the tensile test were carried out. Because of the isotropic orientation shown in Figure 17 of MWNT in an EP matrix, their research showed that nanocomposites are brittle by nature (Breton *et al.*, 2004).

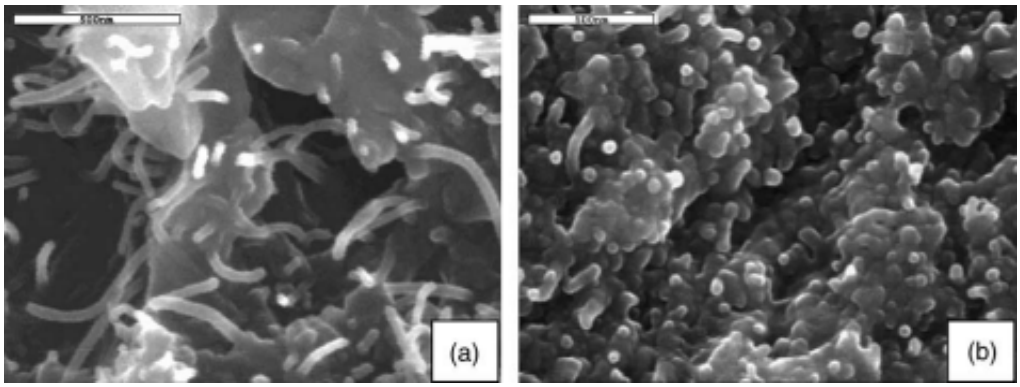

Figure 17: SEM image showing the fractured surface of (a) pristine and (b) oxidized MWCNTs of 6 wt. % (Breton *et al.*, 2004).

To develop EP/MWCNTs nanocomposites, the multi-walled carbon nanotubes (MWCNTs) were first functionalized using the diazonium salt process. The attached functional groups after chemical treatment of the nanocomposites were then determined by thermogravimetric analysis (TGA) and Fourier transform infrared spectroscopy (FTIR). Similarly, a scanning electron microscope was used to study the surface's fractography (SEM). They discovered that aromatic diamines attained higher functionalization degrees than aliphatic diamines. After MWCNTs were functionalized with diamines, fractography observations showed significant changes in the fracture mode of the reinforced nanocomposites (Moaseri *et al.*, 2019).

MWCNTs of varying diameters were used to reinforce the EP matrix, and their impact on the mechanical and fracture properties of EP/MWCNTs nanocomposites was examined. It was discovered that selecting MWCNTs of varied diameters had a direct impact on the dispersion performance. The diameter of MWCNTs, the additional amount of MWCNTs, and their dispersion all influence the reinforcing effect of MWCNTs on the EP matrix. MWCNTs-25/EP composites demonstrated a significant improvement in tensile strength, with increases in elastic modulus of 11.5 % and 8.3 % over those of neat EP, respectively, when 0.5 wt. % MWCNTs were incorporated. The best toughening result was obtained at the MWCNTs diameter of 25 nm (MWCNTs-25), which comprised 0.7 wt. % of modifiers (Xu *et al.*, 2021).

Using shear mixing and sonication, MWCNTs reinforced EP nanocomposites were produced. The fabricated specimens' mechanical, viscoelastic, thermal, and electrical characteristics were determined and evaluated. The samples with a nanotube concentration of 0.6 wt. % showed better dispersion and greater strength than those of the other specimens, according to the microscopic investigations and the measured tensile strengths. The sample with a 0.6 wt. % nanotube filler concentration had also shown higher thermal conductivity than the other. It was also discovered that the electrical conductivity improved as the concentration of nanotubes increased (Koo *et al.*, 2014).

Vajaiac *et al.* (2015) prepared EP/MWCNTs nanocomposites of different weight ratios like 0.5, 2, and 4 wt. % with functionalized MWCNTs. The presence of the strong interaction bonding between the EP matrix and filler particles was characterized by Raman spectroscopy and DSC. Mechanical examinations of nanocomposites show a general improvement in flexural strength under tensile stress and Young's modulus at low nanotube concentrations. A low mass concentration of fMWCNTs, up to 0.5 wt. % was shown to generally enhance the mechanical properties of the EP resin, with more fMWCNTs addition having a negative impact.

The EP/MWCNTs nanocomposites with functionalized MWCNTs were prepared and their nanomechanical, structural and viscoelastic properties were investigated. It was found that nanohardness was improved approximately by 22 % in storage modulus for 0.1 % of chemically modified EP/MWCNTs nanocomposites with that of the neat EP resin. In contrast to neat EP, the fractured surface of nanocomposites was noticeably

rougher, demonstrating typical brittle fracture behaviour (Ivanov *et al.*, 2014). Figure 18 demonstrated that nanohardness increased with the addition of the MWCNTs.

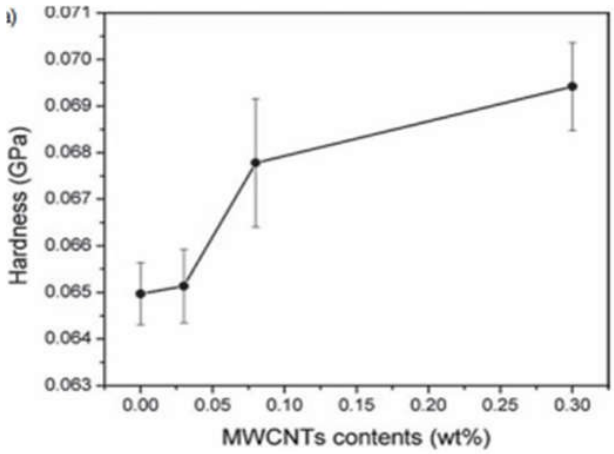

Figure 18: Plot showing hardness as a function of MWCNTs wt. % (Ivanov *et al.*, 2014)

The elastic mechanical characteristics of the EP/MWCNTs nanocomposites were investigated by Moumen and his teams using the microindentation test. It was found that EP reinforced with MWCNTs nanocomposites show outstanding mechanical properties. The elastic modulus, fracture toughness, and ability to withstand crack evolutions appear to be improved by the addition of a modest number of MWCNTs. By incorporating just 1 % MWCNTs, the stiffness of the nanocomposites modified with nanotubes was dramatically increased roughly by 3.5 % (Moumen *et al.*, 2017).

The multiwall carbon nanotubes (MWCNTs) were functionalized using a variety of techniques, including plasma treatment, chemical oxidations, ball milling, and thermal treatment, and then added to the EP matrix to form nanocomposites. It was discovered that the addition of MWCNTs with epoxy resin leads to brittle nanocomposites however the fracture strength and tensile modulus are reduced for all treatment methods. The highest value of Young's modulus was obtained for oxygen-plasma-treated MWCNTs (Breton *et al.*, 2002).

The effect of sonication and the content of the multiwall carbon nanotubes (MWCNTs) on the mechanical and electrical properties of the composites were studied. The nanocomposites were prepared with different wt. % of MWCNTs sonicated in three different outputs. The tensile test, thermal analysis, DSC test, and the microscopic test was carried out. With 75 W of sonication power output and 0.6 wt. % of MWCNTs, the greatest increase in tensile characteristics was recorded. The

glass transition temperature (T_g) of the nanocomposites examined here rises with increasing sonication power output. When compared to neat EP resin, the thermal study showed that the presence of MWCNTs raised the T_{onset} of the nanocomposites (Neto *et al.*, 2020).

Vacuum-assisted resin transfer moulding was used to construct multiwall carbon nanotube EP/MWCNTs nanocomposites, as described by Lee and his research teams. For EP resins with different weight ratios of MWCNTs, the mechanical characteristics, fracture surface morphologies, and thermal stabilities of these produced nanocomposites were investigated. The thermal analysis revealed that the increased MWCNTs concentration improved the thermal stability of nanocomposites. The tensile strength, modulus, impact strength, and thermal stability of the composite were significantly improved as a result of the successful integration of a substantial amount of MWCNTs into EP resin using the vacuum-assisted resin transfer moulding approach (Lee *et al.*, 2014).

The thermal, electrical, and morphological properties of the EP/MWCNTs nanocomposites with various filler contents of MWCNTs were studied. According to their research, adding MWCNTs to EP resin improved its glass transition temperature (T_g) and electrical properties but did not significantly alter its thermal conductivity. According to the microscopic analyses, the majority of MWCNTs were uniformly dispersed, but some of them were aggregated (Yuen *et al.*, 2007).

To fabricate EP/MWCNTs nanocomposites, MWCNTs were first functionalized by adding carboxylic acid groups (-COOH) to their surface. This was accomplished using a solution-mixing process. The EP/MWCNTs nanocomposites with 1 wt. % of MWCNTs were found to have a hardness value of 133 %. Microscopical analysis proved that nanocomposites with filler contents of 0.75 wt. % had superior dispersion and adherence. This work shows that epoxy resin has good mechanical and thermo-mechanical properties when MWCNTs are added at lower fractions (Saha & Bal, 2017).

Different mixing methods were employed to make EP/MWCNTs nanocomposites using various proportions of multi-walled carbon nanotubes (MWCNTs). Fracture toughness tests were used to describe the nanocomposites, and field emission scanning electron microscopy was employed to examine their morphology (FESEM).

It was discovered that adjusting the MWCNTs concentration and mixing methods causes a change in the mechanical characteristics of EP/MWCNTs nanocomposites. This work also showed that the MWCNTs were uniformly dispersed by the sonication method in the EP matrix, which was confirmed by microscopy (Chow & Tan, 2010).

MWCNTs were embedded into the epoxy matrix with additives to improve flame-retardant properties. To obtain better dispersion both multi-walled carbon nanotubes (MWCNTs) were fluorinated and then mixed with the EP to obtain the required blend. The structural, morphological, and thermal properties of the blend were studied by using field emission scanning electron microscopy and thermogravimetric analysis. It was concluded that the thermal stability of the EP/MWCNTs was found significantly improved on using fluorinated montmorillonite and MWCNTs as filler particles (Im *et al*., 2010).

Lau *et al.* (2003) measured the hardness and flexural properties of the EP/MWCNTs nanocomposites with different wt. % of carbon nanotubes. The nanocomposites with varying content of the MWCNTs demonstrate varied hardness values. It was also observed that the number and size of voids in the composites were higher in the case of the EP/MWCNTs nanocomposites than the neat EP. The flexural strength of a nanotube nanocomposite beam declined. The SEM fractographic pictures showed pull-outs of the nanotubes as shown in Figure 19, which indicated a weak bond between the MWCNTs and the EP matrix. As a result, the matrix's ability to transfer stress to the MWCNTs in the direction of the load was reduced thus decreasing flexural strength.

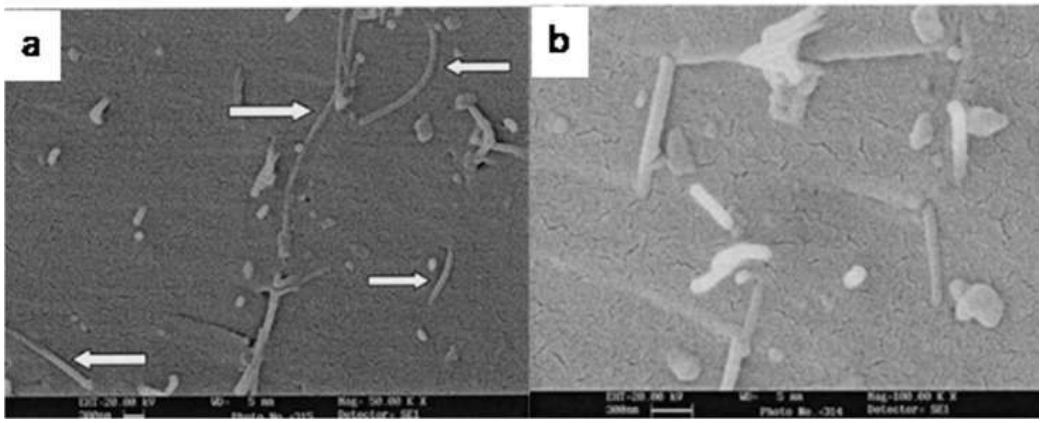

Figure 19: (a) SEM image of longest nanotubes showing the formation of network structures (b) Fractured surface of the EP/MWCNTs nanocomposites on tension (Lau *et al.*, 2003)

Wang *et al.* (2020) used carbon-centred free radical enriched carbon nanotubes (CNT) to reinforce epoxy (EP) resin. The as-prepared nanocomposites were subjected to fire safety and vertical burning tests. In addition to this, its mechanical properties were studied by performing tensile tests, and dynamic mechanical analysis (DMA). It was found that the addition of carbon-centred free radical-enriched CNT to the EP matrix had a substantial effect on the mechanical properties of the nanocomposites. Along with this, it was observed that CNTs with carbon-centred free radicals retard the development of fire in the initial period.

It was reported in the literature that an increment in the concentration of carbon nanotubes increases the limiting oxygen index values. It was also reported that the functionalized MWCNTs bear higher limiting oxygen index (LOI) values than the pristine MWCNTs. From the thermogravimetric analysis (TGA) and LOI test, the EP/MWCNTs composites with 0.5 wt. % of MWCNTs have shown significant improvement in the LOI and thermal stability of the nanocomposites (Kausar *et al.*, 2017).

Pereira (2009) investigated the effects of different nanomaterials namely nanomagnesium hydroxide nano-$Mg(OH)_2$ and carbon nanotubes (CNT) on the flammability of epoxy.

This study suggested that the as-prepared epoxy nanocomposites based on CNT with lower wt. % can bring promising changes in the resin flammability and act as flame retardant materials.

MWCNTs were treated with a 3:1 mixture by volume of concentrated sulphuric acid and nitric acid. After functionalization both pristine and acid-treated MWCNTs were incorporated into the EP matrix. The as-prepared EP/MWCNTs nanocomposites were subjected to tensile tests, morphological tests, and spectroscopic tests. The uniform dispersion was obtained in the case of acid-treated EP/MWCNTs nanocomposites. There was less nanotube pull-out in the sample of acid-treated EP/MWCNTs nanocomposites which was confirmed by scanning electron microscopy (Montazeri *et al.*, 2010).

MWCNTs were purified by using dilute nitric acid to remove amorphous carbon. Thus purified MWCNTs were chemically modified by mixed acids (3:1) mixture of concentrated sulfuric and nitric acids. The modified MWCNTs were reinforced in the

EP matrix by the cast moulding method. The 8 % of acid-treated EP/MWCNTs nanocomposites have a significant improvement in strength (+11.65 %) and fracture strain break (+127.8 %). The tensile strength of value 69.7 MPa was obtained whereas the elastic modulus reduced with the increase of MWCNTs loading (Guo *et al.*, 2007).

EP/MWCNTs nanocomposites of 1 and 2 wt. % were prepared and characterized by dynamic mechanical analysis at different temperatures. There was a considerable improvement in tensile strength and modulus of neat EP on the addition of 1 wt. % MWCNTs whereas reinforcing 2 wt. % MWCNTs had an adverse effect on mechanical behaviour. On examining toughness behaviour 1 wt. % EP/MWCNTs showed higher toughness than that of 2 wt. % EP/MWCNTs nanocomposites. DMA and the tensile test confirmed that 1 wt. % EP/MWCNTs nanocomposites have the optimum storage modulus and tensile behaviour at different temperatures (Revathi *et al.*, 2014).

2.4.2 Properties of epoxy/graphite (EP/GP) nanocomposites

The reinforcement of EP matrix with graphite–graphene structures was studied by Mostovoy and Yakovlev in 2019. The thermally expanded graphite of 0.05 parts by mass is used to prepare the composition of the EP/GP nanocomposites, which provides an increase in the studied complex of physical and chemical properties. The thermally expanded EP/GP nanocomposites are thermal, fire, and heat-resistive in nature. It is also heat conducting along with this it shows flame-resistive properties (Mostovoy & Yakovlev, 2019).

Kaushik *et al.* (2010) prepared the different fractions of EP/GP nanocomposites with graphite wt. % varying from 5-25 wt. % and studied their mechanical, electrical, and morphological properties. The electrical conductivity was found to be increased at increased filler content. Similarly, thus prepared nanocomposites have shown improved tensile modulus and Young's modulus in bending properties with increasing filler content shown in Figure 20.

Suherman *et al.* (2022) aimed to improve the electrical and mechanical performance of EP/GP nanocomposites based on particle size and curing conditions. They further characterized the thermal and microstructural properties. They detected the electrical conductivity value of 32 S/cm after using 10 wt. % smaller graphite particles and further changing the conductivity value of 50 S/cm was achieved. TGA analysis

showed that the nanocomposites were thermally stable.

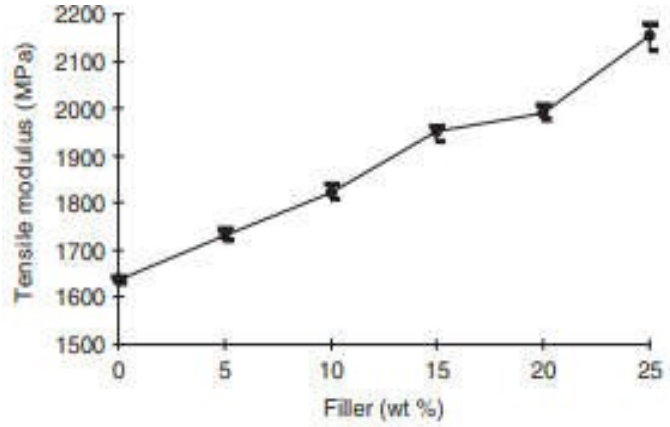

Figure 20: Tensile modulus plot of EP/GP nanocomposites with varying wt. % of GP (Kaushik *et al.*, 2010)

Suherman *et al*. (2010) investigated the electrical conductivity and microhardness of synthetic and natural graphite epoxy composites. The EP/GP nanocomposites were prepared using the compression moulding method and the electrical conductivity was measured by using four probe techniques. The fracture surfaces were analysed by using a scanning electron microscope. They found that the addition of SG and NG to the EP matrix transforms non-conductive EP into conductive. They reported conductivity of natural graphite was higher than that of synthetic graphite at the same wt. % of the filler loading. The conductivity value of 12.6 S/cm and 7 S/cm were found respectively for the two types of graphite as shown in Figure 21. Similarly, the hardness value increased and the highest value was obtained at 60 wt. % for natural graphite and 70 wt. % for synthetic graphite.

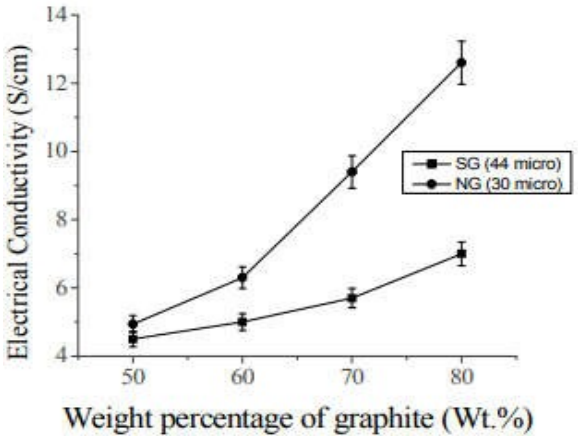

Figure 21: Electrical conductivity of EP/SG and EP/NG nanocomposites (Suherman *et al.*, 2010)

The electrical and mechanical properties of multi-sized graphite filler were studied and the findings of this study suggested that with a 75 wt. % of GP, electrical conductivity reached up to 13 Scm^{-1} as a better network was established in the nanocomposites. The electrical conductivity was found to be 15 Scm^{-1} for two sizes (40/200 μm) than the three sizes (40/100/200 μm) i.e., 13 Scm^{-1}. They reported that EP/GP nanocomposites of 40/200 μm possessed a more stable structure (Pengisi *et al.*, 2021).

Diaz-Chacon *et al.* (2015) prepared and characterized exfoliated graphite nanoplatelets. With increasing filler content, they observed a significant increase in thermal conductivity (sample thickness 4 mm). They end up with the conclusion that the selectivity of resin is an important factor for the high thermal conductivity of the nanocomposites.

Novotna *et al.* (2018) studied the conductivity of EP reinforced with various sizes of carbon fibres (CF). They have used milled carbon fibres as starting materials. In this study, they mainly focused on the sizes of carbon fibres and the conductivity of the EP/CF nanocomposites. They found that the influence of particle size on AC conductivity is increasing with increasing frequency.

The EP and hardener were blended in a 1:3 ratio with various volume fractions of 92 % pure graphite, size 45 m (0, 1, 3, 5, and 7 wt. %) to create the EP/GP nanocomposite. The specific wear rate and coefficient of friction of neat EP and its nanocomposites, based on various GP percentages and date palm fibres with their mechanical properties, were compared in this work by the author. It was found that GP had positive effects on the tribological characteristics of EP/GP nanocomposites as an addition to the EP matrix. The tribological performance of EP/GP nanocomposites reinforced with date palm fibre, either with or without GP, has somewhat improved. There is no relationship between the mechanical properties and the particular wear resistance found by correlation research (Alajmi & Shalwan, 2015).

To investigate the mechanical and physical properties of the EP/GP nanocomposites, Baptista and his teams experimented in 2016. They created nanocomposites with graphite fractions ranging from 5 to 30 wt. % for the study and then used microscopic methods to examine the microstructural characteristics and fracture surfaces of the

composites as they had been created. This investigation found that the mechanical properties of the composites (7.5, 10, 11.5 %) with a homogenous dispersion of filler particles and no pores were found to be improved (Baptista *et al.*, 2016).

The covalent bonding of an epoxy monomer to the surface of expanded GP, through the use of a coupling agent, is a novel method for functionalizing GP nanoparticles in this work. The sp^2 hybridization of the pure graphene sheet is only slightly disturbed by this approach. The effects of incorporating the GP nanoparticles into an EP resin were assessed in terms of the mechanical characteristics and electrical conductivity of the EP/GP nanocomposite. The study revealed that the electrical conductivity was five orders of magnitude higher than the basic resin at a filler concentration of 0.5 wt. % while Young's modulus and the material yield strength increased by 50 % and 30 % respectively (Miller *et al.*, 2010).

The reaction between functionalized graphite and epoxy resin is illustrated in Figure 22.

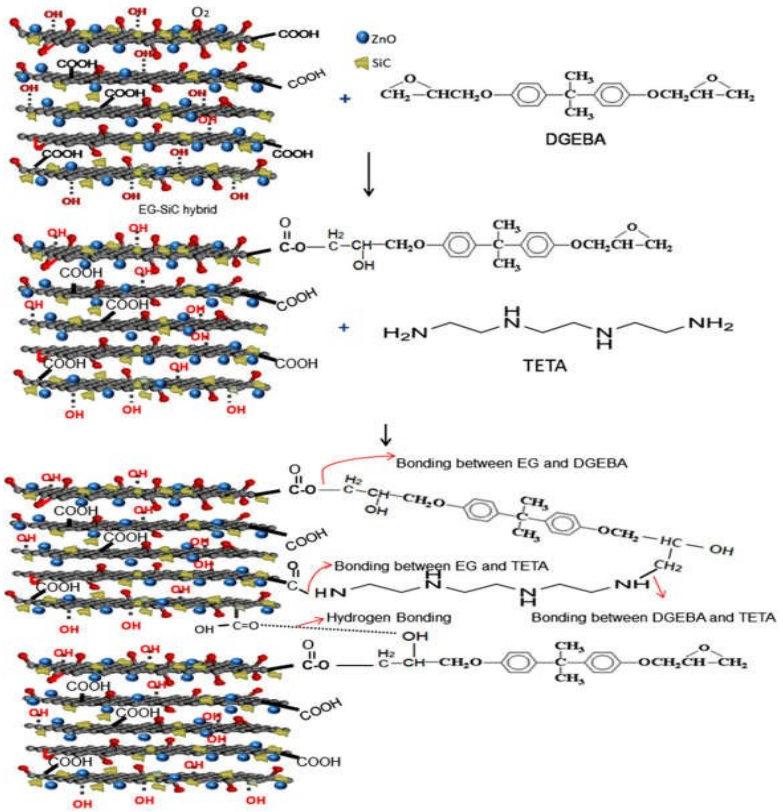

Figure 22: Schematic representation of the reaction between EP and GP (Nayak *et al.*, 2020)

To evaluate the structural, mechanical, viscoelastic, and thermal properties of the EP matrix (DGEBA) containing 2.5–5 wt. % of GP, another team of researchers prepared

different sets of EP/GP nanocomposites. They concluded that the GP still has the same ordered structures. The addition of GP causes the nanocomposite materials' elastic modulus and tensile strength to increase, as well as their thermal stability to exceed that of neat EP (Yasmin & Daniel, 2004).

Suherman *et al.* (2019) investigated the in-plane conductivity and mechanical properties of the EP/GP nanocomposites prepared with the different weight ratios of GP by casting method. The in-plane conductivity of the composites was measured by following the ASTM C61 and the shore hardness by a shore hardness tester. The tensile strength was carried out using ASTMD 3039 and scanning electron microscopy was used to analyse the fracture surface analysis of the EP/GP nanocomposites. This study revealed that the nanocomposites with the higher filler wt. % (85 wt. %) show higher in-plane conductivity and shore hardness while the tensile strength was obtained highest with lower filler wt. % of GP (65 wt. %). The addition of 65 wt. % conductive GP has many gaps or voids shown in Figure 23 which decrease in-plane conductivity and shore hardness of the EP/GP nanocomposites on the other hand if the loadings increased to 80 wt. % of the graphite, the number of voids was reduced (Figure 23. b). This reduction in voids occurs because it occupies the entire area of the EP matrix, thereby increasing the in-plane conductivity and shore hardness.

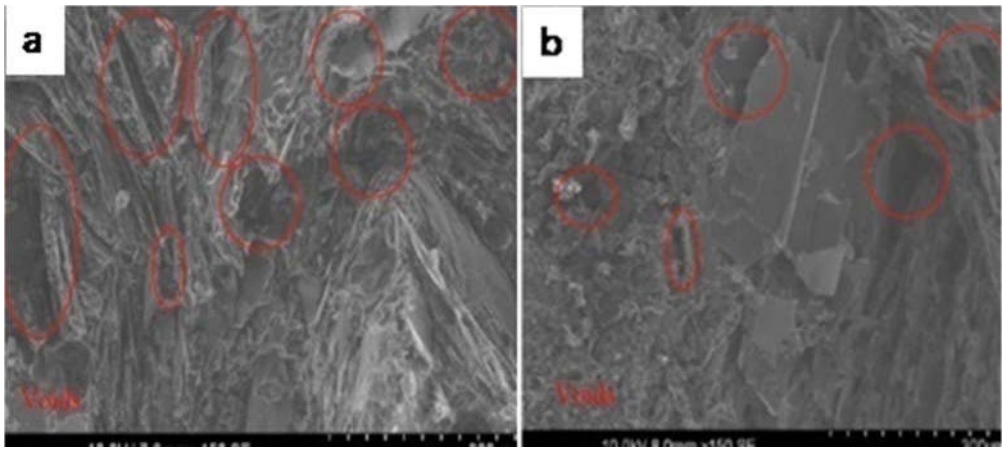

Figure 23: (a) SEM image of 65 wt. % EP/GP and (b) 80 wt. % EP/GP nanocomposites (Suherman *et al.*, 2019)

Aakash & Selvaraj (2020) examined the mechanical properties of the fibreglass/graphite/ epoxy composites. The mechanical properties of the composites were examined by ductile, pressure effect, and water assimilation techniques. The

tensile strength and compressive strength were found to be improved and the water absorption rate was also found to be higher.

Similarly, Mann *et al.* (1999) fabricated the EP/GP nanocomposites with various wt. % of the GP powder to study the variation of filler wt. % on its mechanical properties. The nanocomposites were subjected to the Charpy test, flexural test, impact test, and fracture toughness test. It is evident from this study that the addition of GP from 3 wt. % to 12 wt. % improved the mechanical properties. This improvement in mechanical properties is accounted for by the better dispersion of the GP in the EP matrix and the strong interfacial bonds present between the graphite and epoxy.

Albozahid *et al.* (2021) constructed EP/GP nanocomposites with a different weight ratio of GP (0.5 wt. %, 1 wt. %, 1.5 wt. %, and 2 wt. %) following the dispersion method. The tensile strength, impact strength, and hardness tests were performed to understand the effect of the addition of GP filler on the mechanical properties of the nanocomposites. From this study, they concluded that tensile strength of 67 %, bending strength of 57 %, and impact strength of 85 % were observed for the nanocomposites with 1.5 wt. % of GP. The hardness value was found to be increased up to 1.5 % and then decreased upon further increasing the concentration of the GP.

The mechanical and microstructural properties were studied by Shalwan and his groups. For this study, they prepared the EP/GP nanocomposites of different wt. % (1, 3, 5, and 7 wt. %), and a mechanical test including a tensile test and hardness test was performed. They found out that GP wt. fraction has a substantial impact on the mechanical performance of the nanocomposites. This study also reveals that the nanocomposites with a lower GP wt. % show slight enhancement in hardness and no effect on tensile behaviour whereas the nanocomposites with a higher GP wt. % show a reduction in tensile strength and significant improvement in hardness (Shalwan *et al.*, 2022).

2.4.3 Properties of epoxy/ nanodiamond (EP/ND) nanocomposites

Nanodiamond polymer nanocomposites are utilized in the production of ships, cars, tractors, aeroplanes, and other types of transportation as well as in the chemical and petrochemical industries and protective and friction-reducing coatings (Dolmatov, 2001).

The EP/ND nanocomposites of different weight fractions (0.1, 0.5, and 1 wt. %) were prepared by the sol-gel method, and their physical properties were compared to those of the EP/MWCNTs nanocomposites. It was found that the tensile properties of EP/ND nanocomposites show a slightly higher value than those of EP/MWCNTs nanocomposites. However, it has a lower value for Young's modulus and stress at break. The storage modulus and glass transition temperature for EP/ ND nanocomposites is low, whereas the thermal stability is enhanced (Špitalský *et al.*, 2008).

The EP resin was modified with ND of varied weight fractions (0.4, 0.8, 1.2, 1.6, 2.0, 2.4, and 5 wt. %) to form nanocomposites. Different characterization methods were employed such as microindentation, a contact angle test, and scanning probe microscopy, for the analysis of EP/ND nanocomposites. The findings showed that even a small amount of ND added to EP resin significantly improved the nanocomposite hardness and elastic modulus (Koumoulos *et al.*, 2015).

Ayatollahi *et al.* (2011) investigated the fabrication of EP/ND nanocomposites as well as their mechanical properties. They investigated and discovered that adding ND improved Young's modulus and tensile strength when compared to the neat EP. Additionally, the effect of shear deformation on the fracture properties of nanocomposites was studied, which revealed that the positive effect of ND particles was enhanced as the share of shear deformation in mixed loads increased.

Farooq *et al.* (2021) also looked into how ND affected the thermal and ablative properties of carbon fibre-reinforced nanocomposites. By analysing the pre- and post-burning morphologies of the nanocomposite surfaces and analysing temperature profiles, weight loss, and erosion rates, it was possible to study the ablative reaction of the nanocomposites with 0.2 wt. % and 0.4 wt. % ND. When compared to pristine carbon fibre-epoxy composites, erosion resistance increased by 10.5 % for nanocomposites containing 0.2 wt. % ND and by 12.6 % for those containing 0.4 wt. % ND. The thermal conductivity of nanocomposites showed a similar trend. The incorporation of 0.2 and 0.4 wt. % of ND increased to 37 and 52 wt. %, respectively.

EP resin was mixed with detonation nanodiamond (DND) and carbon nanotubes in small amounts to produce the required nanocomposites. The fractured surfaces of both nanocomposites, in contrast to the neat EP, showed resistance to crack

propagation. DND and CNT reinforcement improved the tensile characteristics of the materials by 6.4 % and 2.9 %, respectively see Figure 24. Additionally, the nanocomposites showed a two orders of magnitude increase in electrical resistivity and a 41 % rise in microhardness for DND and 12 % for CNT. SEM studies of the nanocomposite showed that the nanoparticle dispersion was uniform throughout the epoxy matrix. The rough fracture surface of the nanocomposite signifies increased impact resistance and fracture toughness. Furthermore, the DND showed better mechanical characteristics than the CNT, which had a lower resistance (Roy *et al.*, 2013).

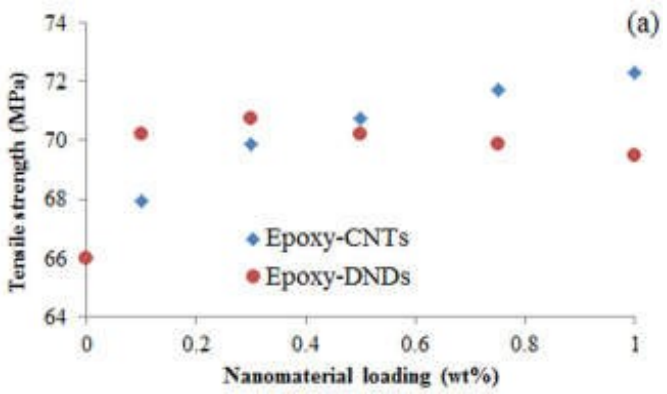

Figure 24: Tensile strength of EP/CNT and EP//DND nanocomposites (Roy *et al.*, 2013)

Due to the tendency of the ND particles to aggregate and deposit in the EP resin, it is challenging to fill high concentrations of ND into EP without surface modification. The ND surface functional groups were adjusted by a simple oxidation process before being blended with EP resin. The FTIR measurements supported the modifications to the ND surface. The thermal and electrical characteristics of EP/OND with various ND levels (5 wt. %, 10 wt. %, and 20 wt. %) were investigated. By maintaining volume resistances identical to those of the neat EP resin, thermal conductivity increased by 36 % while dielectric strengths decreased by 9.7 %, as observed in the case of the 20 % ND nanocomposites (Wang *et al.*, 2016).

The development of vehicles (cars, trains, and aeroplanes) and other lightning-prone things (including wind turbines) requires materials with good electrical characteristics. Epoxy-resin nanocomposites have recently been employed often to lighten structures but due to the insulating nature of the resin, numerous modifications must be made to increase their conductivity. The approaches for increasing conductivity have been divided into three groups: adding layers with higher electrical

conductivity, changing the reinforcement materials, and modifying the matrix with conductive fillers (Krajewski *et al.*, 2022).

Epoxy resin, being a highly cross-linked material, is chosen as the best matrix for the fabrication of ND (Haleem *et al.*, 2015). They are well known because of their fine adhesion, electrical properties, thermal stability, weather stability, wear characteristics, UV stability, and so on (Kausar, 2019). However, the dispersion of ND particles remains a challenge in the fabrication of EP/ND nanocomposites. Because of the high aspect ratio of ND particles, the intrinsic Van der Waals force of attraction produces agglomeration and clustering among ND particles (Zhai *et al.*, 2011).

2.5 Synthesis and Curing of Epoxy Resin

Epoxy resins are cured using different types of curing techniques, including room-temperature curing (Ahmad *et al.*, 2010; Tucker *et al.*, 2010)**,** heat curing (Jin & Park, 2012; Jin & Park, 2009)**,** and photocuring (Esposito Corcione *et al.*, 2009; Foix*et al.*, 2011; Golaz *et al.*, 2013; Morselli *et al.*, 2012) techniques, to produce a strong three-dimensional cross-linked network. There are curing agents (hardeners) that can be classified based on the chemical constituents present in them (Jin *et al.*, 2015)**.** They are amine-type curing agents (Ferdosian *et al.*, 2013; Frank *et al.*, 2013)**,** alkali-curing agents (Hsu *et al.*, 2012; Parildar & Ibik, 2013)**,** (Fan *et al.*, 2013; Flores *et al.*, 2012; Foix *et al.*, 2012; Park & Jin, 2004) and catalytic curing agents.

Novolac epoxy resin: The epichlorohydrin and phenolic novolac resin are reacted to form novolac epoxy resins. The high cross-linking densities in novolac resin are caused by the epoxide groups, which produce good thermal, chemical, and solvent resistance characteristics (Atta *et al.*, 2008). Figure 25 depicts the chemical structure of novolac epoxy resin. The synthesis of different types of epoxy resins and their curing process is discussed below.

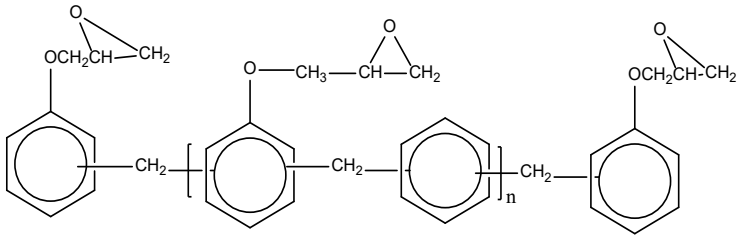

Figure 25: Chemical structure of novolac epoxy resin

Cycloaliphatic epoxy resin: Cycloaliphatic epoxy resin is a saturated molecular structure containing an aliphatic backbone having high UV stability properties, good thermalstability, and good electrical properties. The cycloaliphatic epoxy resin, 3', 4'-epoxycyclohexylmethyl 3,4-epoxycyclohexanecarboxylate is synthesized by the reaction of 3' cyclohexenylmethyl 3-cyclohexenecarboxylate with peracetic acid. They are mostly used in optoelectronic device packaging. The chemical structure is shown in Figure 26.

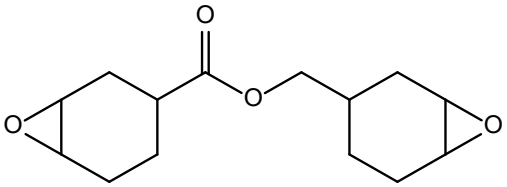

Figure 26: Chemical structure of cycloaliphatic epoxy resin

The curing processes of epoxy are done with various curing agents, like amine type, alkali type, anhydrides, and catalytic curing agents and their chemical structures are shown in Figure 27.

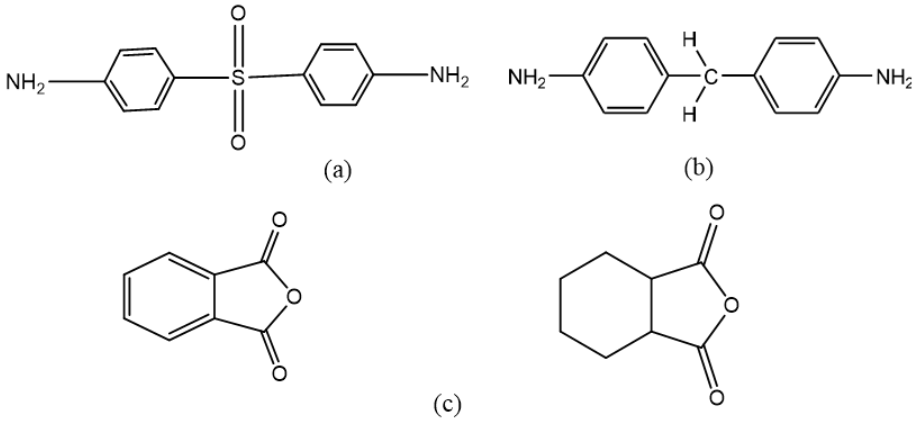

Figure 27: Chemical structure of (a) diaminodiphenylsulfone (b) diaminodiphenyl methane (c) anhydride curing agents

2.6 Summary of Literature Review

The synthesis and functionalization of three distinct nanocarbons (multiwalled carbon nanotubes, graphite, and nanodiamond) of various dimensions have been studied in previous research. According to their findings, the main method for synthesizing nanocarbons includes chemical vapour deposition, laser ablation, and arc discharge. They also discussed different methods to modify nanocarbons like covalent, non-

covalent, direct side walls, and endohedral functionalization. Additional discussion of the functionalization process was covered under various sub-topics for each nanocarbon. The functionalization process has been studied in previous literature related to the functionalization of MWCNTs. Nitric acid, sulfuric acid, nitric and sulphuric acid in combination, non-oxidative techniques, and other treatments were used to functionalize MWCNTs.

Similar information was found in the studied literature, which stated that surface functionalization, oxidation experiments, wet chemical methods, surface amination methods, and remote photocatalytic oxidation methods were used to functionalize graphite. The functionalization of nanodiamonds was accomplished by many researchers using a variety of procedures, including atom transfer radical polymerization, microwave-assisted techniques, grafting of organic compounds, treatment with inorganic acids, and basic oxidative methods. To improve the compatibility of nanocarbons and epoxy polymers to enhance their physical, thermal, mechanical, and electrical properties, the functionalization of nanocarbon was accomplished. The various techniques used to create epoxy/nanocarbon nanocomposites and their electrical, thermal, and mechanical properties were explored. Methods like ultrasonication, high shear mixing, solution casting, sonication, and mixing and moulding were reported in the literature. According to the research on the epoxy/nanocarbon nanocomposites, depending on the preparation process, adding MWCNTs to the EP matrix improved its thermal, electrical, and mechanical properties to a certain filler wt. %. However, if we go beyond that point, their properties start to deteriorate due to the nanocarbon's small size, which causes agglomeration.

Nevertheless, it remains uncertain whether the modification of nanocarbons is influenced by their dimensional properties and whether there exists a correlation between their dimensions and the physical properties of epoxy/nanocarbon nanocomposites. By comparing the functionalization and various properties of these three different nanocarbons, with varying dimensions we were able to discuss the existing problem in this research study. Additionally, earlier researchers had studied the functionalization of nanocarbons to improve the compatibility between epoxy and nanocarbons. However, we studied the electrical conductivity with lower filler

percentages of three different nanocarbons and their comparative dimensional study which is the novelty of the present work.

CHAPTER 3

3. MATERIALS AND METHODS

3.1 Materials

3.1.1 Thermosetting epoxy resin

Lapox L12 is a thermosetting epoxy resin formed by the reaction of epichlorohydrin and bisphenol A (i.e., diglycidyl ether of bisphenol A; DGEBA) used in this study, and the cross-linking agent or hardener (K6) the aliphatic polyamine, diethylenetriamine were purchased from Atul Ltd., Polymer Division, Bangalore, India. Lapox L12 is a low-temperature curing resin with minimal volume shrinkage (Anwar *et al*., 2016) whereas K6 is aliphatic polyamine curable at room temperature (25 °C) with low viscosity. The chemical structures for both DGEBA and polyamine are given in Figure 28.

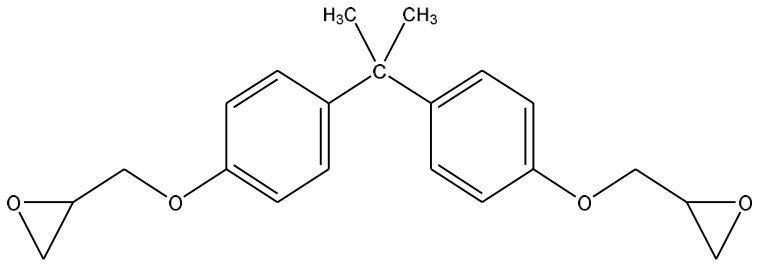

(a) Chemical structures of 5,5-Dimethyl-3,7-dioxa-1,9(2)-bis(oxirana)-4,6(2,4)-dibenzenanonaphane

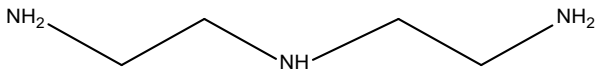

(b) Chemical structures of 2-N'(Aminoethyl)ethane 1,2-diamine

Figure 28: (a) Chemical structures of diglycidyl ether of bisphenol DGEBA and (b) diethylenetriamine

The specification for epoxy and hardener is given in Table 1.

Table 1: Specification chart for epoxy resin and the hardener system (as per supplier's specification)

Materials and specifications	Unit	Value
Lapox L-12		
Epoxide equivalent	gm/eq	182-192
Epoxy value		5.2-5.5
Viscosity at 25 °C		9000-12000

Materials and specifications	Unit	Value
Hardener K6		
Visual appearance		Pale yellow liquid
Refractive index at 25 °C		1.4940-1.5000
Water content		1 % max
Shear strength on A1 alloy lap joint (In combination with Lapox C 51)		1..4 $kgmm^2$ min
Processing parameter		
Lapox L 12		100 pbw
Hardener K6		10-12 pbw
Viscosity at 20 °C	mPa.s	5000-8000
Pot life at 20 °C	Hrs	½-1

3.1.2 Nanocarbons

The three different types of nanocarbons with different dimensionalities (0D nanodiamond, 1D multi-walled carbon nanotubes, and 2D graphite nanoplatelets) were used in this study.

(a) Carbon Nanotube (CNT)

Multiwalled carbon nanotubes, Nanocyl 7000, were purchased from Nanocyl SA, Belgium.

(b) Graphite Nanoplatelets (GnP)

The graphite nanoplatelets, the conductograpgh GFG 50M, were purchased from SGL Carbon GmbH, Meitingen, Germany.

(c) Nanodiamond (ND)

The nanodiamond powder the Nuevo Blend was purchased from Carbodeon, Pakkalankuja, Vantaa, Finland.

3.1.3 Other Chemicals

The different chemicals like concentrated nitric acid (HNO_3), concentrated sulphuric acid (H_2SO_4), sodium carbonate (Na_2CO_3), potassium permanganate ($KMnO_4$), and hydrogen peroxide (H_2O_2) were purchased from Fischer Scientific, India. As a mould-releasing agent, laboratory-grade silicon oil with a viscosity of 370-390 mPa was used. Acetone from Fischer Scientific, India was used as a solvent. The 0.2 μm polycarbonate membrane filter was purchased from the local market.

3.2 Functionalization of Nanocarbons

Different techniques, such as covalent functionalization, can be used to functionalize the nanocarbons. The nanocarbons are subjected to functionalization to introduce the various reactive functional groups. Both dry and wet procedures can be used for functionalization. The functionalization of nanocarbons with various dimensionalities by wet chemical procedure was thoroughly studied in this work.

3.2.1 Functionalization of carbon nanotubes (CNT)

A Pristine multi-walled carbon nanotube powder (0.5 g) was first sonicated in conc. HNO_3 (40 mL) for 15 min. and then refluxed for about 5 hr. The resulting mixture was filtered using a suction apparatus equipped with a membrane filter. The residue was washed with distilled water until a pH value of 7 and oven-dried at 100 °C for an hr. The flow diagram for the functionalization process is shown in Figure 29.

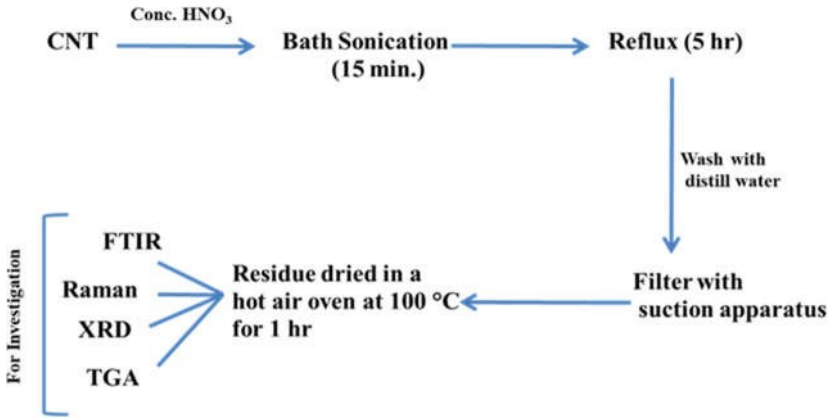

Figure 29: Schematic diagram showing the steps of functionalization of carbon nanotubes

3.2.2 Functionalization of graphite nanoplatelets (GnP)

Initially, pristine graphite nanoplatelets powder (0.5 g) was placed in a graduated borosilicate glass container containing 11.5 mL of concentrated sulphuric acid and the mixture was sonicated for 15 min and functionalized by following the conventional Hummers (Ciszewski & Mianowski, 2013) method and treating the mass with conc. H_2SO_4 along with $NaNO_3$ and $KMnO_4$. It was magnetically stirred for half an hr at 35 °C. The resulting slurry was then diluted with 10 mL of deionized water before being treated with H_2O_2, which turned the blackish green colour to yellow. The resulting mixture was first washed to a pH value of 7 and then filtered through the membrane filter. Finally, the residue was dried in a hot air oven maintained at 50 °C

for 1 hr. The flow diagram for the functionalization process is shown in Figure 30.

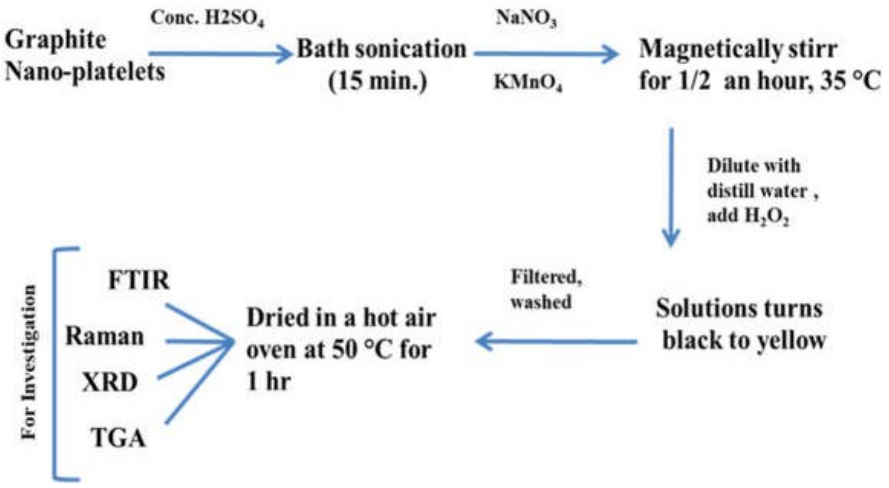

Figure 30: Schematic diagram showing the steps of functionalization of graphite nanoplatelets

3.2.3 Functionalization of nanodiamonds (ND)

Nanodiamond powder (0.5 g) was taken in a round bottom flask containing 25 mL of conc. HNO_3 solution. This mixture was sonicated for 15 minutes before being kept at 60 °C in a magnetic stirrer for 24 hrs. The resulting mixture was then washed with distilled water until it reached pH 7. Finally, it was filtered through polycarbonate membranes using a suction filter and the solid residue was dried in a hot air oven at 100 °C for 1 hr. The flow diagram for the functionalization process is shown in Figure 31.

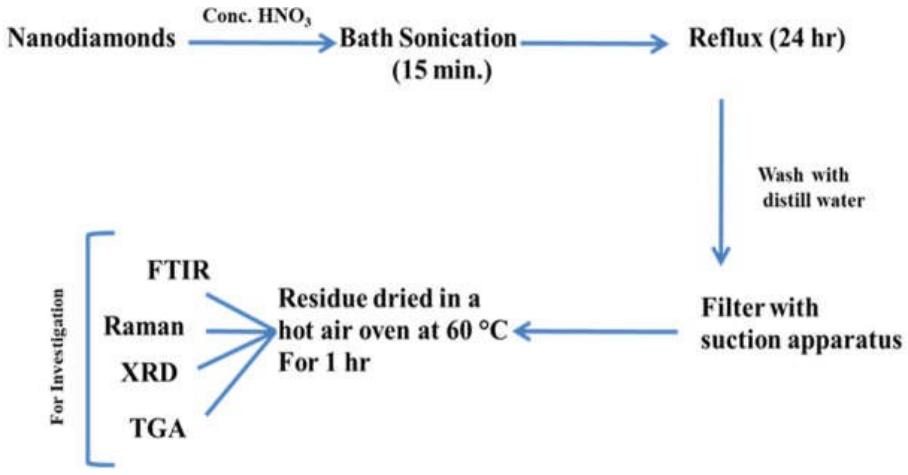

Figure 31: Schematic diagram showing the steps of functionalization of nanodiamonds

The typical experimental setup for the functionalization of different types of nanocarbonsis shown in Figure 32.

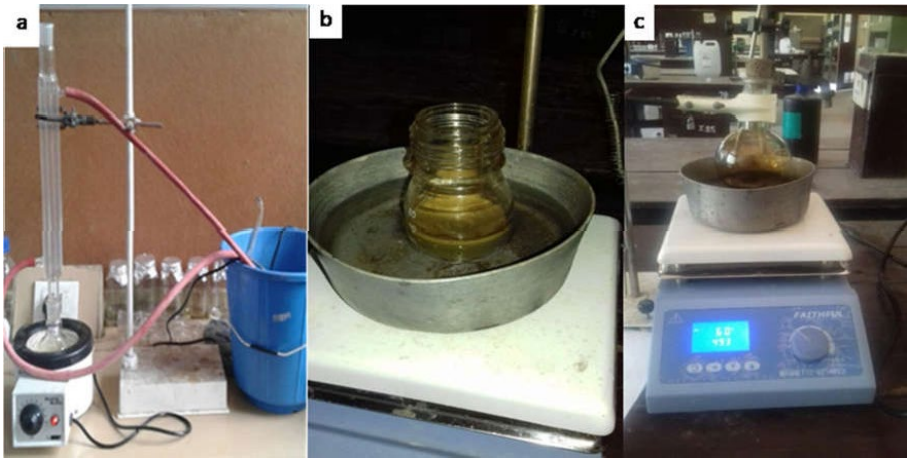

Figure 32: Typical experimental setup showing functionalization procedure (a) carbon nanotubes (b) graphite nanoplatelets and (c) nanodiamonds

3.3 Preparation of Epoxy/Nanocarbons Nanocomposites

The pristine and acid-functionalized three different kinds with varying amounts of nanocarbon (CNT, GnP, and ND) were incorporated into the epoxy matrix *via* physical mixing assisted by ultrasonication. For this purpose, 2.5 g of epoxy was dissolved in 2.5 mL of acetone in a 50 mL beaker followed by 15-minute ultrasonication. The mixture was stirred for 1 hr at 70 ºC with a magnetic stirrer to evaporate the used solvent. Then the resulting mixture was allowed to cool down to room temperature (25 ºC) and a hardener was added (10:1). Finally, the mixture was poured into a plastic mould and pre-cured at 25 ºC for 24 hr before being post-cured at 70 ºC for 5 hr. The flow diagram for the epoxy/nanocarbon nanocomposite preparation is shown in Figure 33.

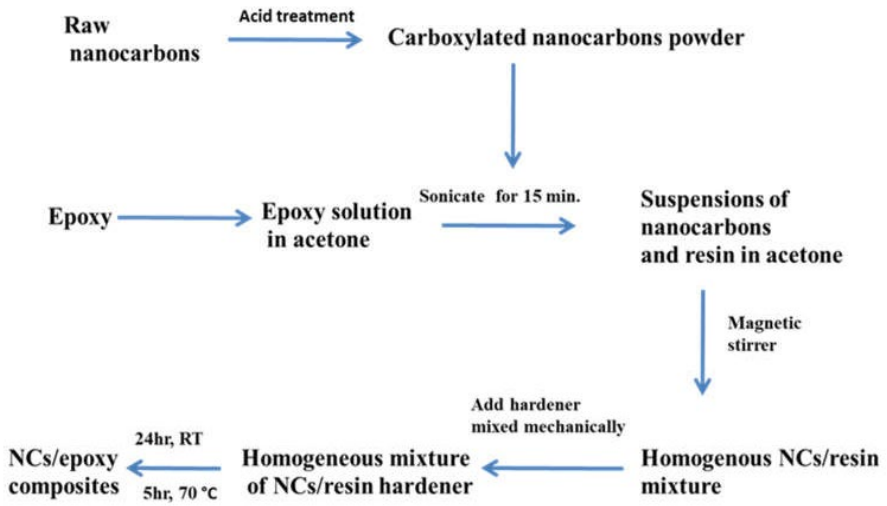

Figure 33: Schematic diagram showing different steps involved in the preparation of EP/nanocarbon

The synthetic procedure for the epoxy resin that is used as the matrix in this work is also schematically illustrated in Figure 34.

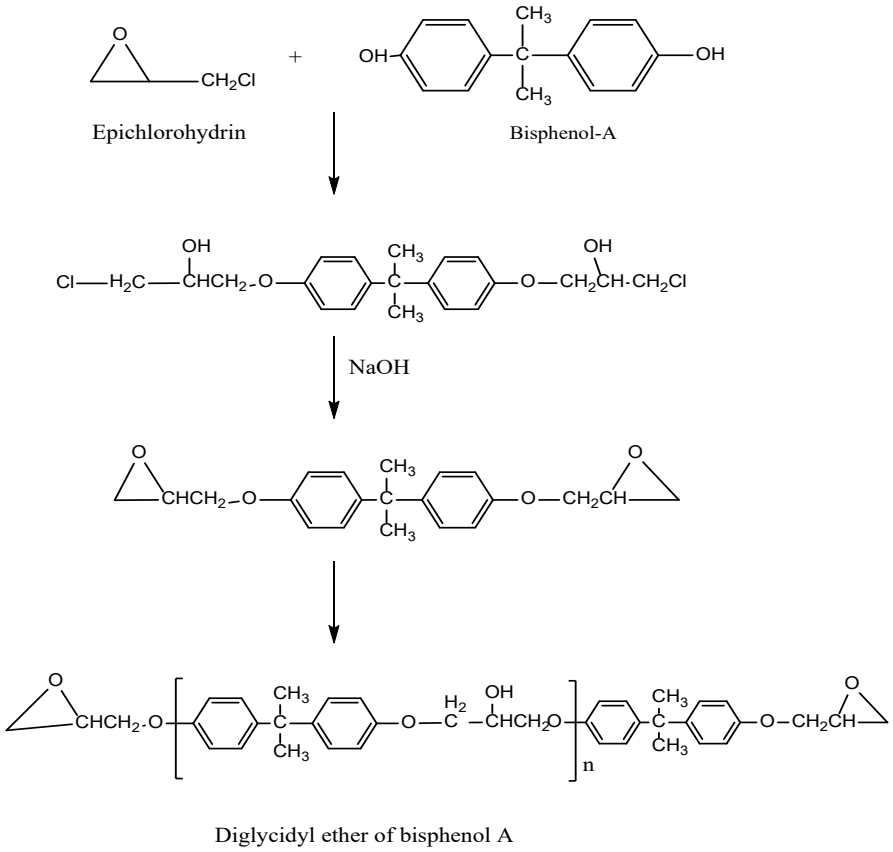

Figure 34: Reaction scheme for the synthesis of DGEBA epoxy resin (Haas, 2014)

The nanocomposites curing method mould for 24 hrs at room temperature (25 °C) and composites post-cured at 70 °C a hot air oven for 5 hrs (McCoy *et al.*, 2016) is shown in Figure 35.

Figure 35: Epoxy/nanocarbon nanocomposites procured at plastic mould for 24 hrs at room temperature (25 °C)

The samples prepared from the method explained above are indexed in Table 2.

Table 2: Different series of material with their respective code explanation

S.N.	Sample code	Remarks
1	EP	Pure resin comprising DGEBA and amine hardener
2	pCNT	Pristine multi-walled carbon nanotubes
3	mCNT	Modified multi-walled carbon nanotubes
4	pGnP	Pristine graphite nano-platelets
5	mGnP	Modified graphite nano-platelets
6	pND	Pristine Nanodiamond
7	mND	Modified Nanodiamond
8	EP/pCNT$_{0.05}$	EP containing 0.05 wt. % of pristine MWCNTs
9	EP/mCNTs$_{0.05}$	EP containing 0.05 wt. % of modified MWCNTs
10	EP/pCNT$_{0.1}$	EP containing 0.1 wt. % of pristine MWCNTs
11	EP/mCNTs$_{0.1}$	EP containing 0.1 wt. % of modified MWCNTs
12	EP/pCNT$_{0.2}$	EP containing 0.2 wt. % of pristine MWCNTs
13	EP/mCNT$_{0.2}$	EP containing 0.2 wt. % of modified MWCNTs
14	EP/pCNT$_{0.5}$	EP containing 0.5 wt. % of pristine MWCNTs
15	EP/mCNT$_{0.5}$	EP containing 0.5 wt. % of modified MWCNTs
16	EP/pGnP$_{0.05}$	EP containing 0.05 wt. % of pristine GnP
17	EP/mGnP$_{0.05}$	EP containing 0.05 wt. % of modified GnP
18	EP/pGnP$_{0.1}$	EP containing 0.1 wt. % of pristine GnP
19	EP/mGnP$_{0.1}$	EP containing 0.1 wt. % of modified GnP
20	EP/pGnP$_{0.2}$	EP containing 0.2 wt. % of pristine GnP
21	EP/mGnP$_{0.2}$	EP containing 0.2 wt. % of modified GnP
22	EP/pGnP$_{0.5}$	EP containing 0.5 wt. % of pristine GnP
23	EP/mGnP$_{0.5}$	EP containing 0.5 wt. % of modified GnP
24	EP/pND$_{0.05}$	EP containing 0.05 wt. % of pristine ND
25	EP/mND$_{0.05}$	EP containing 0.05 wt. % of modified ND
26	EP/pND$_{0.1}$	EP containing 0.1 wt. % of pristine ND
27	EP/mND$_{0.1}$	EP containing 0.1wt. % of modified ND
28	EP/pND$_{0.2}$	EP containing 0.2 wt. % of pristine ND
29	EP/mND$_{0.2}$	EP containing 0.2 wt. % of modified ND
30	EP/pND$_{0.5}$	EP containing 0.5 wt. % of pristine ND
31	EP/mND$_{0.5}$	EP containing 0.5 wt. % of modified ND

3.4 Characterization Techniques

3.4.1 Fourier Transform Infrared (FTIR) Spectroscopy

Molecular absorption of electromagnetic radiation in the infrared region facilitates the transitions between the rotational and vibrational energy levels of the ground (lowest) electronic energy state. In contrast, changes in the electronic, vibrational, and rotational energy levels result from the absorption of energetically stronger visible and ultraviolet radiation. The fundamental goal of infrared spectroscopy is to study molecular vibrations since transitions between various rotating states can only be observed in the infrared spectra of small molecules in the gas phase (Ismail *et al.*, 1997).

FTIR spectroscopy is a very helpful tool for learning about the functional groups contained in specific materials. In FTIR spectroscopy, the raw data of the interferogram is transformed into the actual spectrum using the mathematical method the Fourier transformation. The FTIR method is used to analyse the sample's infrared transmission or absorption spectra and to determine whether it contains organic or inorganic substances. The spectra data in the automated spectroscopy software will identify the specific chemical groups present in the sample based on the infrared absorption frequency range 400–4000 cm^{-1} (Shameer & Nishath, 2019).

The spectra of nanocarbon were recorded using a Perkin Elmer ATR instrument with a resolution of 20 cm^{-1} and 20 scans per sample at Polymer Service GmbH, Merseburg, Germany, and those of nanocomposites were recorded using an IR Prestige 21 with a ZnSe ATR crystal instrument with a resolution of 4 cm^{-1} and 20 scans per sample at Mahatma Gandhi University, Kottayam, India.

To collect the FTIR spectra for nanocarbons, the sample was crushed into a fine powder and put in a sample holder. The nanocomposite samples were first chopped into tiny pieces, a few of which were then taken, and placed in a sample holder to record the spectra.

The vibrational frequency range of some common functional groups is shown in Table 3.

Table 3: Characteristics of the vibrational frequency range of some common functional groups (Ones, 1978)

S.No.	Wavenumber (cm^{-1})	Functional group	Typical chemical species
1	3700-3250	-OH	Alcohols, Phenols
2	3520-3320	0	Primary aromatic amines, amides
3	3360-3340	0	Primary amides
4	3320-3250	-OH	Oximes
5	3300-3250	-CH	Acetylenes
6	3300-3280	-NH	Secondary amides
7	3200-3180	0	Primary amides
8	3100-2400	-OH	Carboxylic acids
9	3100-3000	=CH	Aromatics unsaturated
10	2990-2850	$-CH_3$, $-CH_2$	Aliphatics
11	2750-2650	-CHO	Aldehydes
12	2285-2250	-N=C=O	Isocyanates
13	2260-2200	-C=N	Nitriles
14	1870-1790	-C=O	Anhydrides
15	1780-1760	-C=O	Lactones
16	1750-1740	-C=O	Esters
17	1740-1720	-C=O	Aldehydes
18	1720-1700	-C=O	Ketones
19	1710-1690	-C=O	Carboxylic acids
20	1670-1650	-C=O	Primary amides
21	1550-1490	0	Aromatic nitro
22	1400-1310	$-COO^-$	Carboxylic acid salts
23	1000-950	$-CH=CH_2$	Vinyl
24	980-960	-CH=CH-	Trans alkenes

3.4.2 Raman Spectroscopy

Raman spectroscopy involves illuminating a sample with a monochromatic laser beam, which interacts with the sample's molecules to create scattered light. The Raman spectrum is generated by the inelastic collisions between the sample molecules and the incident monochromatic light. Monochromatic light of a single wavelength strikes a sample and scatters in all directions. When the frequency of the dispersed radiation matches the frequency of the incident radiation, Rayleigh scattering occurs. Raman scattering giving rise to Stoke's line in the spectrum happens when a little portion of the scattered radiation has a frequency that is different from the frequency of the incident radiation. However, when the frequency of incident radiation is lower than that of scattered radiation, anti-Stokes lines can be observed in the Raman spectrum (Bumbrah & Sharma, 2016).

Raman spectroscopy has established itself as a sensitive instrument for identifying defects and the electronic structure of carbon nanotubes. In the first-order Raman spectra of CNTs, a disorder in a double resonance process causes the D mode at about 1300 cm^{-1}. The relative intensity of this mode directly displays the covalent modification and defects. When estimating the defect concentration, the D mode intensity is typically normalized concerning the intensity of the G mode at about 1600 cm^{-1}, which results from a single resonant Raman process (Murphy *et al.*, 2006).

Raman spectroscopy is a powerful tool to characterize carbon-based nanomaterials, especially in the study of the structural order of the substance. Hence, it was used to extract more information on structural variations caused by acid treatments and was recorded by BRUKER Senterra I Raman- Microscope within the wavenumber ranges of 2000 cm^{-1}- 400 cm^{-1} with the excitation wavelength of 532 nm.

The carbon tape was placed in the sample holder after being cleaned up with ethanol and above that carbon tape respective sample was put down precisely which was pressed with the cleaned cover glass. The measurements of the samples were carried out after the removal of a glass slide.

3.4.3 X-ray Diffraction (XRD)

The fundamental principle behind X-ray diffraction is the constructive interference of monochromatic X-rays with crystalline material. A cathode ray tube produces the X-rays, which are then filtered to produce monochromatic radiation, concentrated by collimation, and pointed at the sample. When the conditions satisfy Bragg's law, the interaction of the incident ray and the sample results in constructive interference (Bunaciu *et al.*, 2015).

XRD follows Bragg's law. Under Bragg's law see Figure 36, the reflected X-rays from different crystal layers with long-range order encounter constructive interference in XRD. Thus, the spectra are characterized by sharp peaks and these peaks are not seen in amorphous systems or other materials with long-range disorder. XRD is a commonly used technique to evaluate the crystallinity and structure of solid samples (Selva *et al*., 2020). The structural properties of the nanocarbons were studied by X-ray wide-angle diffraction technique.

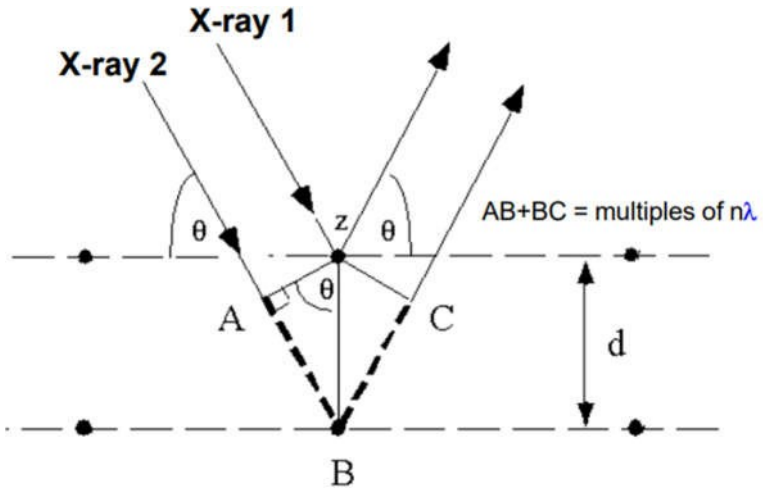

Figure 36: Schematic diagram to explain Bragg's law: where A, B, and C stand for perpendicular drawn, atoms and perpendicular drawn on diffracted second ray respectively (Selva *et al.*, 2020)

In the X-ray diffractogram, the average particle size D was calculated using the Scherrer equation 3.1.

$$D = \frac{0.9\lambda}{\beta \cos\theta} \qquad (3.1)$$

where λ is the wavelength of the X-ray used (0.154nm) and β is the full-width half maxima (FWHM) of the peak in radians.

Figure 37 shows the schematic diagram of the XRD peak and the way of calculating the full-width half maxima (FWHM) of the peak in radians.

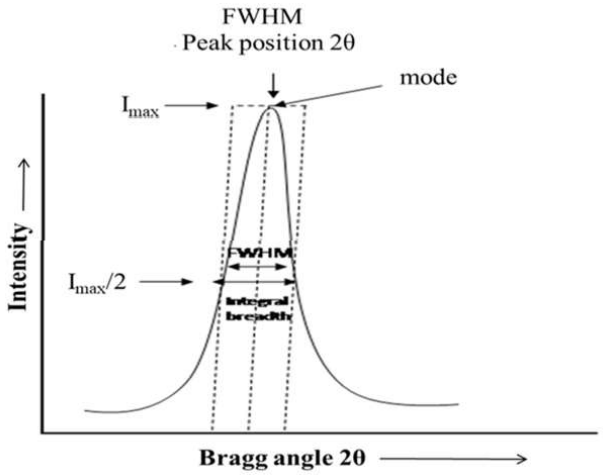

Figure 37: Schematic diagram showing XRD peak and calculation of FWHM (Selva *et al.*, 2020)

FWHM can be theoretically calculated by using the quadratic equation of the total probability function. Here, I_{max} in the figure represents the maximum peak height and

$I_{max}/2$ is the centre of the parabolic curve between I_{max} and the baseline. The interlayer spacing d between the planes is calculated by equation 3.2

$$d=\frac{n\lambda}{2\sin\theta} \qquad (3.2)$$

X-ray diffraction of the samples was carried out on the powder form of the nanocarbon at the Nepal Academy of Science and Technology, Lalitpur. The radiation source used was Cu Kα with a wavelength of 0.15406 nm. The specimens were scanned over a diffraction angle of 2θ ranging between 5° and 80° whereas the nanocomposites were scanned with a Rigaku D/MAX-2500/pc diffractometer.

The nanocarbon powder 200 mg was loaded into the sample holder and XRD measurements were taken, whereas the nanocomposites were cut into 1.6 cm x 1.6 cm before being measured.

3.4.4 Microscopic Studies (SEM)

The investigation of the morphological characteristics of the fillers and the fractured surfaces of the materials was conducted using scanning electron microscopy. An appropriate source, usually a tungsten filament or field emission cannon, produces an electron beam. To create a thin beam of electrons, the electron beam is subjected to high voltage acceleration (for example, 20 kV) and travels through a set of electromagnetic lenses and apertures. The laser then scans the sample's surfaces. The scanning beam causes electrons to be emitted from the specimen; detectors then gather these secondary or backscattered electrons and use them to create a signal that is relayed to a viewing screen, creating an image (Henning & Adhikari, 2017; Akhtar *et al*., 2018).

The microscopy of the nanocarbons and fractured surface was recorded using conductive carbon tape. All these experiments were carried out using scanning electron microscopy (SEM; S400 111 μA with a magnification range of 200-700 at 15 kV, and a field emission scanning electron microscope; FE-SEM, Hitachi SU8010, Japan, with an acceleration voltage of 3 kV) was used for morphological studies of the nanocarbon/epoxy composites. The specimens were fixed on SEM stubs with double-sided carbon tape after applying a 10 nm gold layer on the surface.

3.4.5 Thermogravimetric Analysis (TGA)

The sample is gradually heated in a specific atmosphere (air, N_2, He, or Ar) during thermogravimetric analysis. As a function of time and temperature, the substance's weight changes are noted. To determine the weight changes as a function of temperature at various time intervals, the temperature is raised steadily for a substance with known initial weight. The underlying principle of thermogravimetric analysis is represented by the graph of weight change versus temperature, also known as a thermogravimetric curve or thermogram.

The TGA method was used to study the thermal stability of the materials. The mass loss is recorded as a function of temperature under a controlled atmosphere. TGA is also useful to determine the decomposition temperature of the materials. Thermal stability, oxidative stability, impacts of various atmospheres, moisture, volatile content, and occasionally the composition of multi-component systems are just a few of the many parameters that may be determined using TGA. TGA also determines whether and how various parts of a material are differently bonded. The first derivative of the weight concerning temperature or time yields a differential thermogravimetry curve or DTG. Both quantitative and qualitative data about the sample can be obtained using the DTG curves. The finger printing of a substance and the distinction between two or more overlapping reactions are examples of qualitative modalities of analysis. Peak height and temperature at maximum weight loss measurements are examples of quantitative modes (Pan *et al.*, 2005).The typical TGA and DTG curves are schematically given in Figure 38.

Thermogravimetric measurements of the nanocarbons were carried out at Polymer Service GmBH, Merseburg, Germany, using TGA Mettler Toledo TGA/SDTA 851 equipment in an oxygen environment over a temperature range of 23 °C to 1000 °C at a rate of 10 °C/min, and those of the nanocomposites were carried out at Mahatma Gandhi University, Kottayam, India, using SDT Q600, TA instruments over a temperature range of 30 °C to 700 °C at a rate of 10 °C/min in a nitrogen atmosphere.

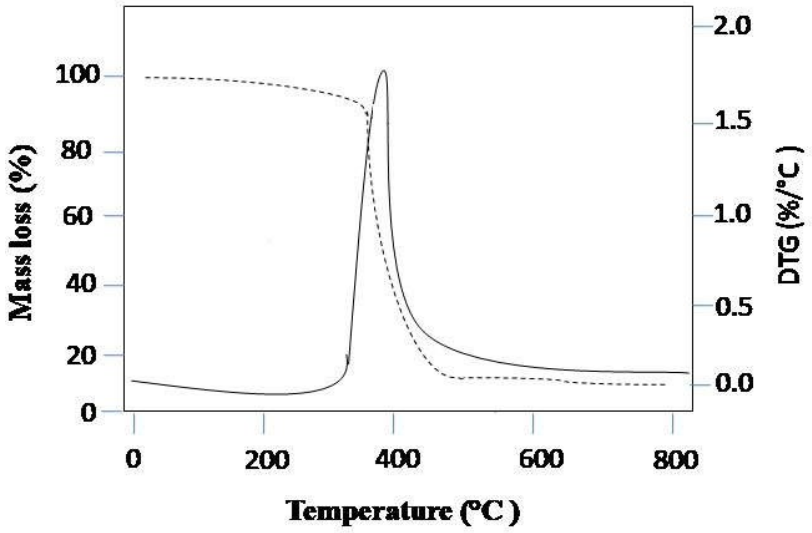

Figure 38: Schematic representation of thermogravimetric analysis (TGA) curves of mass loss and differential thermogram (DTG) (Pandit, 2015)

A small piece of the sample was cut with a Hacksaw blade and 10-15 mg of the sample was kept in the aluminium trioxide (Al_2O_3) crucible for the measurement. After the sample was cut, it was placed in a sample stub, and the necessary measurements were recorded.

3.4.6 Conductivity Measurements

The two-probe method, which involves placing two probes or contacts on a sample and measuring the voltage while a current is supplied between the probes, is the most popular methodology for determining the electrical conductivity of a sample (*Rojo et al*., 2015).

The conductivity test was measured using a DC conductivity meter (Model ADEC Embedded Tech) by the two-probe method with a fixed voltage of 3 V and varying its current in milli, nano, and microamperes at temperatures of 30 °C. The sample was cut into dimensions of 1 cm x 1 cm x 1 mm with the help of a Hacksaw blade and subjected to a conductivity test.

3.4.7 Contact Angles Measurements

The contact angle can be measured as a practical means of identifying a surface's hydrophobicity or hydrophilicity. The angle formed by a liquid at the point where a liquid, gas, and solid meet at a three-phase boundary is known as the contact angle measured see Figure 39. It is based on studies of the intermolecular interactions that

occur when a drop of water comes into contact with a surface. It is mostly utilized to assess a surface's wettability.

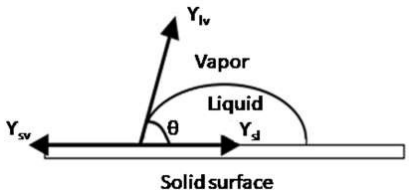

Figure 39: Schematic diagram of the contact angle and interfacial tensions of the three surfaces at the three-phase boundary (Subedi, 2011)

Contact angles less than 90° indicate that wetting of the surface is beneficial and the fluid will spread over a vast area on the surface, whereas contact angles greater than 90° often indicate that wetting of the surface is unfavourable and the fluid will minimize its contact with the surface and form a compact liquid droplet. When the contact angle is 0°, for instance, complete wetting happens and the droplet transforms into a flat puddle. The "lotus effect" (Bracco & Holst, 2013) contact angle and wetting properties can be explained by superhydrophobic surfaces, where water contact angles are typically more than 150°, indicating essentially no contact between the liquid drop and the surface. The formation of contact angles on a smooth surface is displayed in Figure 40.

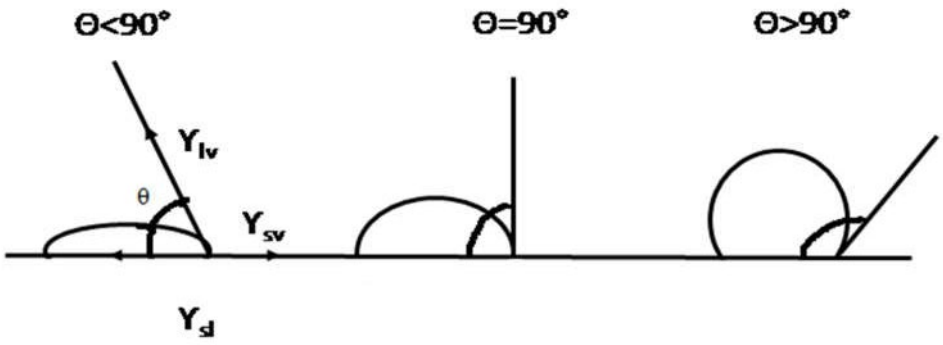

Figure 40: Illustration of contact angles formed by sessile liquid drops on a smooth homogeneous solid surface (Bracco & Holst, 2013)

Young's equation helps to relate the contact angle θ, liquid/vapour surface tension γ_{lv}, solid /vapour surface free energy γ_{sv}, and solid-liquid surface tension γ_{sl} as expressed in eq. (3.3)

$$\gamma_{sv} = \gamma_{ls} + \gamma_{lv}\cos\theta \qquad (3.3)$$

The contact angles of the nanocomposites were measured in the FTA 100 series (First Ten Angstrom, Portsmouth, Virginia, 23704, USA) using distilled water. The sample dimensions of 1 cm x 1 cm x 1 mm were subjected to test at room temperature in closed chambers, maintaining the sessile volume drop of 5 µl.

The summary of different characterization methods and the information to be obtained are summarized in Table 4.

Table 4: Summary of different characterization methods and the information to be obtained

S. No	Methods	Information obtained	Limitation
1	FTIR	Functional groups	Can't detect elements, simple ionic compounds
2	Raman	Chemical structures and composition	Can't detect metal or Alloy samples
3	XRD	Atomic or molecular structure of material/phase, for identification of materials	Only 2 % detection limit in thecase of the mixed samples
4	SEM	Surface fracture morphology, homogeneous/non-homogeneous	Working with liquid samples ischallenging
5	TGA	Thermal stability of the materials	Glass transition temperature and crystallization can't be known
6	Conductivity	Resistivity/conductivity of the materials	High contact and spreading resistance resulting in low accuracy
7	Contact angle	Determines whether the surface is hydrophilic or hydrophobic; wettability	The purity of liquid is very important, vague information on surface chemistry

CHAPTER 4

4. RESULTS AND DISCUSSION

4.1 Functionalization of Nanocarbons

It is challenging to adhere other particles to the surfaces of nanocarbons in their pristine state because of their high degree of chemical inertness. Therefore, the introduction of different oxygen groups on their surface through an oxidation process is always necessary. Many oxidants have been used to oxidize surfaces, such as aquaregia, concentrated nitric acid, concentrated hydrochloric acid, etc. As already discussed in the experimental section, the nanocarbons (CNT, GnP, and ND) were functionalized by treatment with acid. The introduction of the functional groups on the surface of nanocarbons was characterized by different methods including spectroscopic, thermal, and microscopic studies.

The functionalization was done by the acid oxidation method and found to be more effective than other methods because acid-oxidation method is one of the simple and viable methods that do not need any sophisticated method which minimizes the cost additionally this method plays a vital role in the removal of metal impurities that are used as a catalyst during the nanocarbon synthesis.

4.1.1 Structural analysis of nanocarbons

Fourier transform infrared (FTIR) spectroscopic studies

FTIR is mainly used in the chemical identification and evaluation of functional groups present in substances. Here, this technique is used to detect the oxygen-containing functional groups on the surface of oxidized nanocarbons after acid treatment whereas the acidic oxidative treatment may cause a major change in the structural properties. In FTIR spectra of pristine and oxidized CNTs (pCNT and mCNT), the spectrum of pristine CNTs did not show any sharp infrared peaks, indicating that it did not contain any functional groups on comparing the infrared spectrum of the acid-oxidized CNTs to that of pristine ones, see Figure 41.

Due to the acid treatment of pristine CNTs, several oxygen-containing functional groups were introduced. The appearance of the peak at 1700 cm^{-1} is due to the C=O stretching of the carboxyl group, while the transmittance band at 1306 cm^{-1} and 1150

cm^{-1} are associated with the O–H bending and C–O stretching, respectively. The integrity of the hexagonal structure on CNTs was confirmed by the appearance of a peak at 1600 cm^{-1} which showed the existence of carbon-carbon double bonding (Yudianti *et al.*, 2011).

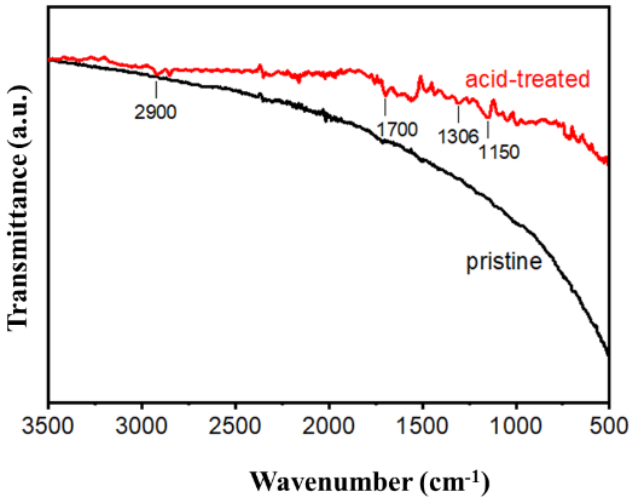

Figure 41: FTIR spectra of pristine (pCNT) and acid-treated (mCNT) carbon nanotubes

The peak around 2900 cm^{-1} indicated the C–H asymmetric and symmetric stretching vibrations of the long-chain nature of the alkyl group (Yadav *et al.*, 2011; Yudianti *et al.*, 2011). Furthermore, the O–H stretching vibration of the hydroxyl group was seen at 3200 cm^{-1} (Liu *et al.*, 2018).

Similarly, FTIR spectra were obtained for pristine and acid-treated graphite nanoplatelets (pGnP and mGnP) samples. The results are shown in Figure 42.

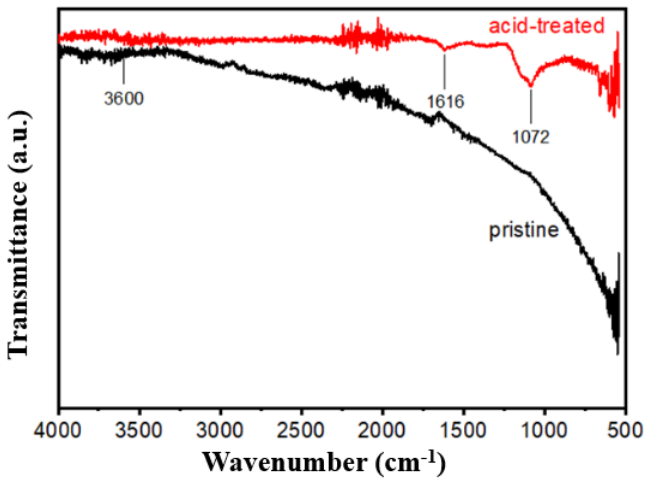

Figure 42: FTIR spectra of pristine (pGnP) and acid-treated (mGnP) graphite nanoplatelets

On acid oxidation of graphite nanoplatelets, the slightly broad signal appears at around 3600 cm^{-1} which is due to the hydroxyl group suggesting that there are –OH functional groups on graphite nanoplatelets surfaces (Chua *et al.*, 2012). Along with this observation, the peak signal at around 1616 cm^{-1} suggests that there is –C=C stretching from the pristine graphitic domain (Guo *et al.*, 2009; Lin, 2014).

Figure 43 shows the FTIR spectrum of pristine and acid-treated nanodiamonds (pND and mND). The detonation nanodiamonds have previously been purified using the acid treatment (Huang *et al.*, 2008; Viboral, 2011).

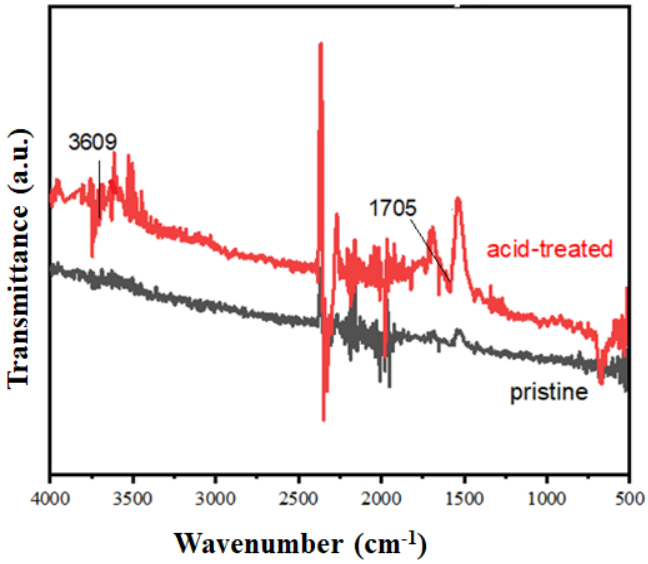

Figure 43: FTIR spectra of pristine (pND) and acid-treated (mND) nanodiamond

The stretching vibration of C=O (1705 cm^{-1}) appears to be sharpened to varying degrees after acid oxidation treatment (nitric acid). This represents the successful incorporation of oxygen containing functional groups on the surface of ND. However, pristine ND is already rich in carboxyls (Wang, 2011). The spectra show that pristine ND has broad and small peaks but on the contrary, acid-treated ND has sharp peaks. This is a clear indicator that during the functionalization process, carboxyl and hydroxyl functional groups were attached to the ND surface (Haleem *et al.*, 2016).

Raman spectroscopic investigation

The result of Raman spectroscopy for three different nanocarbons is summarized in Figure 44. In the case of CNTs, the two intense peaks corresponding to the D and G bands were prominently seen in Raman spectra. The D band is due to the presence of

structural defects (defects due to the generation of amorphous carbon generated during oxidation and conversion of sp^2 carbon to sp^3 carbon) in the nanocarbon whereas the G band occurs due to the tangential stretching of the carbon-carbon bonds. The D band occurs due to the presence of amorphous or disordered carbon in the CNTs because of its nanosized structure. The D and G bands in pristine and treated CNTs were seen at 1334 cm^{-1} and 1572.5 cm^{-1} as well as 1341.5 cm^{-1}, and 1581.5 cm^{-1}, respectively. It has been suggested that the intensity ratio of the D band (I_D) and the G band (I_G), I_D/I_G, determines the degree of disorder, sp^2 domain sizes (Dewangan *et al.*, 2021), and presence of the defects in the nanocarbons. Indeed, the value of I_D/I_G, for (pCNT) was found to be 1.13 whereas for (mCNT) was 1.22. In this way, the magnitude of the ratio I_D/I_G can be used to evaluate the defect density of the carbon nanotube (Jawhari *et al.*, 1995; Murphy *et al.*, 2006).

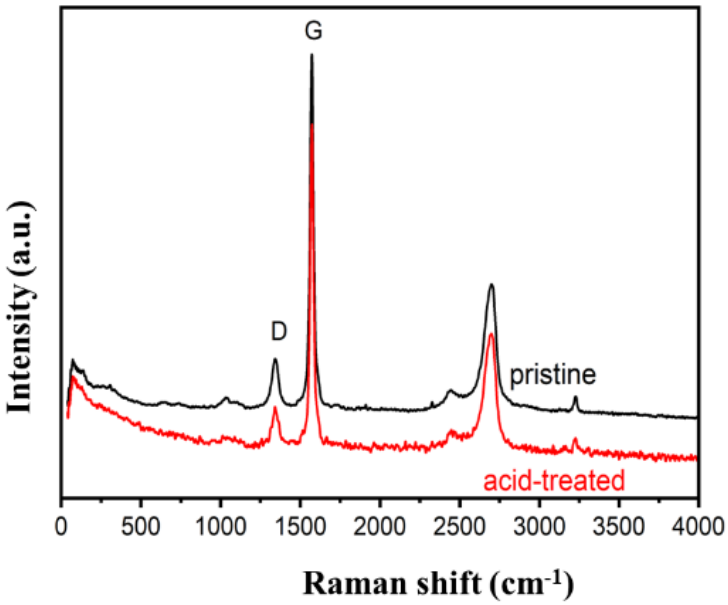

Figure 44: Raman spectra of pristine (pCNT) and acid-treated (mCNT) carbon nanotubes

Similarly, the intense peaks at 1342 cm^{-1} and 1572 cm^{-1} as well as 1341.5 cm^{-1} and 1573 cm^{-1}, respectively, in Figure 45 correspond to D and G bands which are typical for nano graphitic materials before and after oxidation. The value of I_D/I_G was found to be 0.22 and 0.24 for the pristine and the acid-functionalized graphite nano-platelets (pGnP and mGnP), respectively (Maultzsch *et al.*, 2002; Pimenta *et al.*, 2007). It indicates the increase in defect sites on the surface of graphite nanoplatelets. These defect sites may be amorphous carbon generated during oxidation and conversion of

sp^2 carbon to sp^3 carbon.

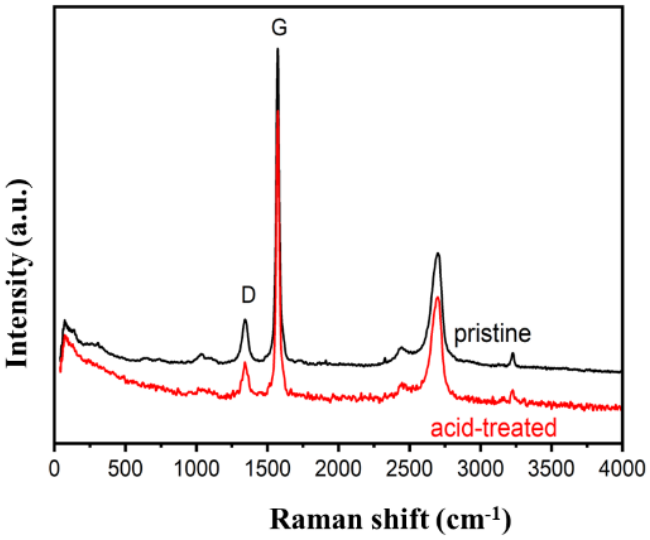

Figure 45: Raman spectra of pristine (pGnP) and acid-treated (mGnP) graphite nanoplatelets

In both nanocarbons, the position of the D and G bands are shifted towards the higher wavelength which may be due to the doping effect upon acid treatment. The presence of these two characteristic peaks after oxidation suggested that there is no damage to the graphitic integrity of nanocarbons (Scheibe *et al.*, 2010).

The Raman spectra of pristine nanodiamond (pND) and acid-functionalized nanodiamond (mND) powder are shown in Figure 46.

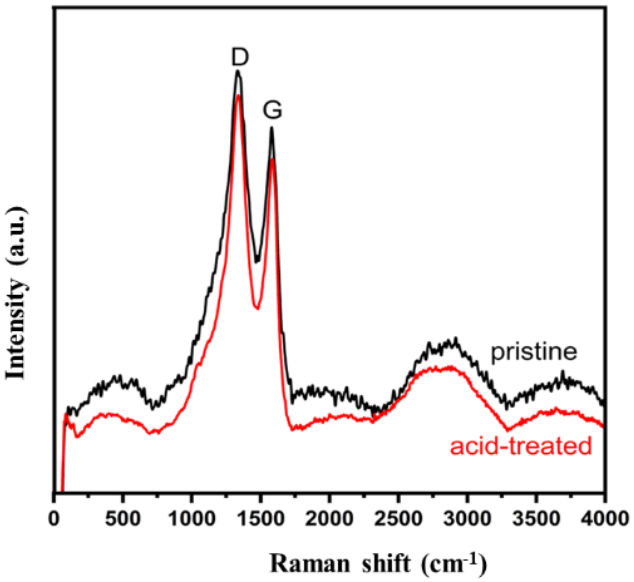

Figure 46: Raman spectra of pristine (pND) and acid-treated (mND) nanodiamond

Pristine nanodiamond exhibits the characteristic Raman features of graphitic carbon: the D band at 1334 cm^{-1} and the disorder-induced G band at 1579 cm^{-1}. Similarly, acid-treated nanodiamonds exhibit D and G bands at 1339 cm^{-1} and 1584 cm^{-1} respectively (Nigmatullin *et al.*, 2013).

The G band denotes sp^2-hybridized carbon atoms and the D band denotes disordered carbon atoms (sp^3 types) and the intensity ratio (I_D/I_G) values were 1.025 and 1.042 for pristine nanodiamond (pND) and acid functionalized nanodiamond (mND) respectively. The slightly increased I_D/I_G ratio in the case of mND indicates that the acid-functionalized nanodiamond sample contains a low number of defects introduced during the acid treatment. The value of Raman peaks and intensity ratios are indexed in Table 5.

Table 5: The pristine and acid-treated nanocarbons with their respective Raman peaks and intensity ratios.

S. No	Sample	D-band (cm^{-1})	G-band (cm^{-1})	I_D/I_G
1	Pristine CNT	1334	1572	1.13
2	Functionalized – CNT	1341	1581	1.22
3	Pristine GnP	1342	1572	0.22
4	Functionalized – GnP	1341	1573	0.24
5	Pristine ND	1334	1579	1.025
6	Functionalized – ND	1339	1584	1.042

Similar results were also reported in previous work (Omalanga, 2015). The increase in the magnitude of I_D/I_G value suggests that the structural defect occurs by the transformation of the sp^2 structure (that is representative of a graphite-like structure) to the sp^3 (diamond-like structure). In contrast to pristine and acid-treated nanocarbons, pGnP was discovered to have the lowest I_D/I_G ratio value which could be a result of the high purity of graphite nanoplatelets with minimal structural flaws (i.e., less amorphous carbon).

4.1.2 Morphological analysis

i. X-ray diffraction (XRD)

The XRD pattern of pristine multiwall carbon nanotubes (pCNT) and multiwall carbon nanotubes that have been subjected to acid oxidation is shown in Figure 47. For pCNT and mCNT, the Bragg peak (002) appeared at 25.92° and 25.68°, respectively. As a result of the acid oxidation, the pCNT undergoes a minor shift in

the (002) peak, which causes an increase in the d-spacing value, indicating the removal of carbon impurities from the starting materials (Das *et al.*, 2014).

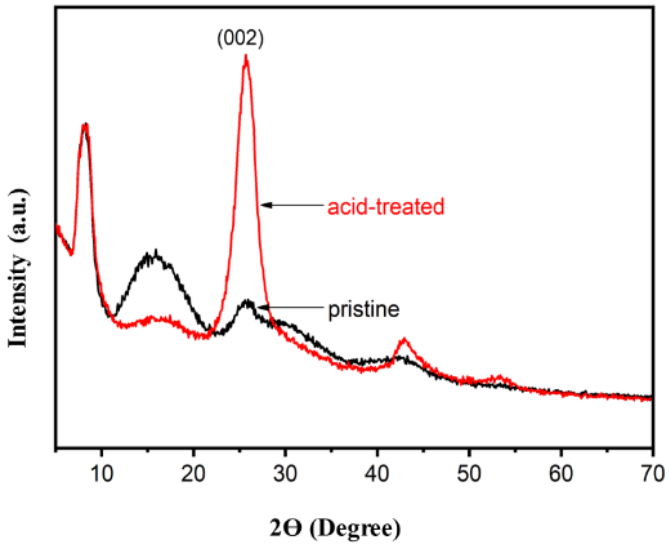

Figure 47: XRD spectra of pristine (pCNT) and acid-treated (mCNT) carbon nanotubes

In the case of graphite nanoplatelets see Figure 48, the Bragg peak corresponding to the (002) plane was observed at 26.33° for pristine graphite nanoplatelets (pGnP) corresponding to a d-spacing of 0.301 nm in the XRD pattern of the graphite nanoplatelets sample. On oxidation of pGnP, the (002) peak shifted to a lower angle at 10.14° (d-spacing: 0.783 nm). This increase in d-spacing is due to the interaction of water molecules and the generation of oxygen functionality in the interlayer spacing of graphite nanoplatelets which is in agreement with the above-presented results (Shalaby *et al.*, 2015).

There was not much change in the particle size of CNTs before and after acid functionalization but in the case of graphite nanoplatelets, the particle size decreased from 17 nm to 3 nm. This was because the oxidizing agents partially broke the graphite nanoplatelets into smaller particles indicating that it has been subjected to the highest degree of molecular distortion in graphite (Gong *et al.*, 2015). The (002) broad peak was observed for acid-treated graphite nanoplatelets than the pristine sample which implies that the degree of crystallinity deteriorated after the acid treatment process further confirmed by calculation.

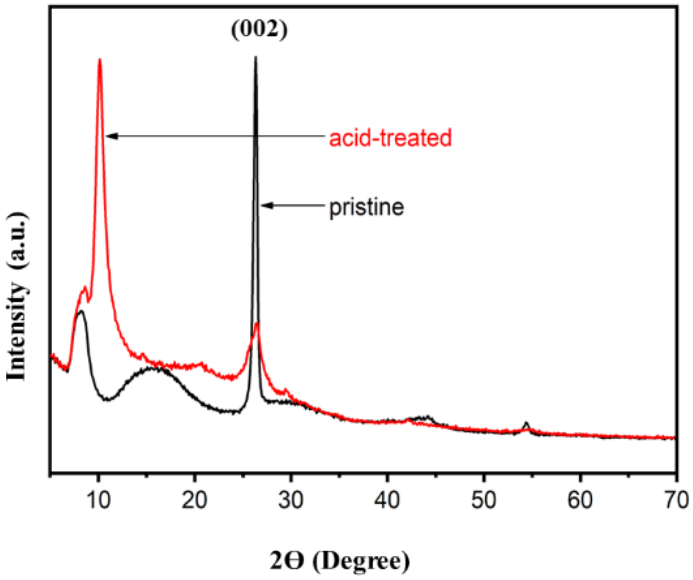

Figure 48: XRD pattern of pristine (pGnP) and acid-treated graphite nanoplatelets (mGnP)

The size of the particles along with interlayer distance highly varies in the case of graphite nanoplatelets compared with CNTs. The degree of crystallinity is also found to deteriorate after the acid treatment in the case of graphite (16.39 %-15.48 %) whereas the opposite trend was found in the case of MWCNTs (20.32 %-29.16 %).

ii. Scanning electron microscopy (SEM) analysis

Figure 49 shows the SEM images of pristine and acid-treated nanocarbons (CNT, GnP, and ND) used in this work. The morphology of the pristine multiwall carbon nanotubes (pCNT) and acid-treated multiwall carbon nanotubes (mCNT) is shown in Figure 49.a and d using SEM images with a resolution of 30 µm. The pCNT appeared to be in an aligned bundle-type nature (Purified *et al.*, 2019) with size variation. The average diameter and length of pCNT were found to be 1.7 µm and 10.27 µm respectively (Ye *et al.*, 2020). However, in the case of mCNT bundles are not visible which might be due to treatment with acids. The pure graphite nanoplatelets (pGnP) in Figure 49.b show flakes-like structures with many graphene layers. The investigation (Oliveira *et al.*, 2018) further supports the exfoliation of these layers after acid treatment, as observed in 49.e which is in agreement with the above presented XRD results. The appearance of multiple graphite flakes in various locations that are a bit separated from one another in pGnP indicates the presence of strong interlayer interactions. This interlayer interaction was disrupted by acid

treatment. The agglomeration of various kinds of largest to smaller particles can be seen. (Kovářík *et al.*, 2020). It was observed that the thick clusters transformed into fine powders after acid-treatment.

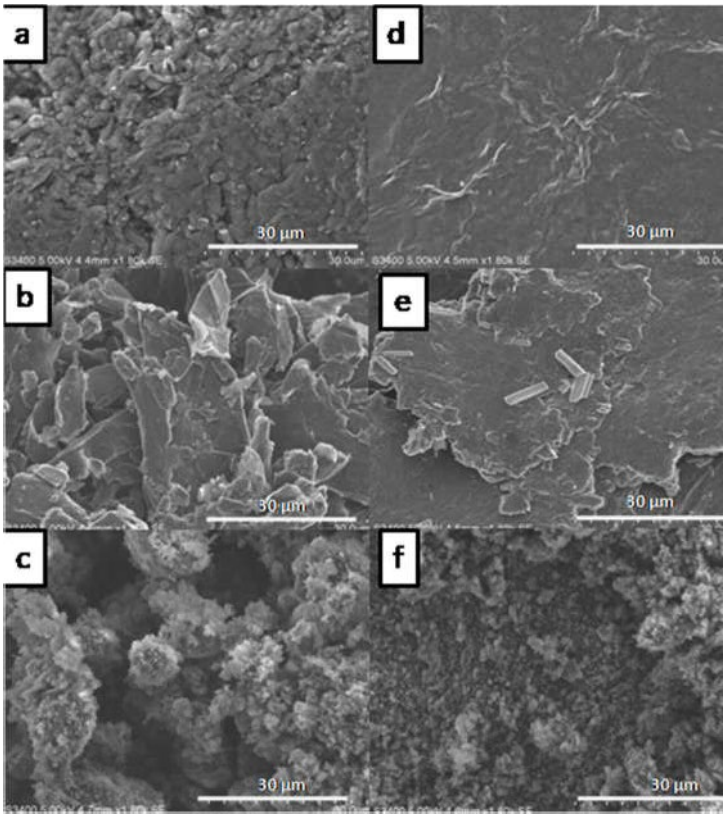

Figure 49: Left (pristine) and right (acid–treated) SEM images of carbon nanotubes, graphite nanoplatelets, and nanodiamond

The geometries of the exfoliated graphite are nearly rectangular with an average dimension of 6.3 µm x 2.4 µm. The acid-treated graphite nanoplatelets sample has a visible colour contrast. The exfoliated sheets' pale colour indicates that they are monolayer, while the slightly darker image in the surrounding area demonstrated a multilayer nature (Dimiev *et al.*, 2012). On the contrary pristine nanodiamond pND shows a dense, thick powder with clump-like shapes.

A morphological examination of three different dimensions of nanocarbons showed aligned bundles in one dimension (CNT), however, these were not apparent after acid oxidation. In contrast to zero-dimensional nanocarbons (ND), which changed into powders, two-dimensional nanocarbons (GnP) changed into rectangular layers with persisting flakes.

4.1.3 Thermogravimetric Analysis (TGA)

Figure 50 shows the TGA thermograms of pristine and acid-treated CNTs (pCNT and mCNT). In the case of pCNT, drastic weight loss occurred (approximately 80 %) at temperatures ranging from 550 °C to 650 °C. This revealed that all CNTs were burned out at this temperature range and the weight remained constant up to 1000 °C. The residue left (about 20 %) corresponds to the weight expected for some of the oxidized metals present as impurities (Dillon *et al.*, 1999; Mansfield *et al.*, 2013).

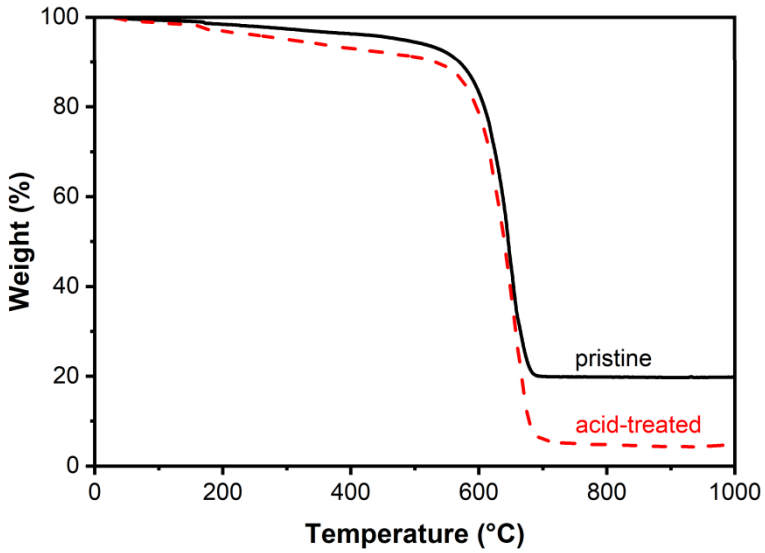

Figure 50: TGA curves of pristine (pCNT) and acid-treated (mCNT) carbon nanotubes

However, in the case of the mCNT see Figure 50, the weight loss from 100 °C–200 °C was due to the loss of water molecules due to the hydrophilic nature of mCNTs. At around 200 °C–350 °C, some weight loss was seen in the TGA curve. The weight loss may be due to the loss of some amorphous carbon, which might have been generated due to the decomposition of different functional groups formed after the acid treatment. This observation thus confirmed the introduction of oxygen-containing functional groups after the acid treatment (Shrestha *et al.*, 2010). The significant weight loss occurred at around 550 °C–650 °C indicating the combustion of all CNTs. The lower weight percentage compared with the pristine (about 3 %) is definite evidence of the removal of the metal impurities after acid treatment.

Figure 51 shows the thermogravimetric curve of pristine and acid-treated graphite nanoplatelets. Pristine graphite nanoplatelets (pGnP) have no weight loss until 650

°C. However, the acid-treated graphite nanoplatelets (mGnP) have a reduction in Van der Waals interactions compared to pGnP, and hence lower thermal stability was observed.

The noticeable stepwise thermal degradation in acid-treated mGnP suggested the removal of water molecules, hydrogen atoms, and hydroxyl groups showing effective functionalization (Jeong *et al.*, 2009).

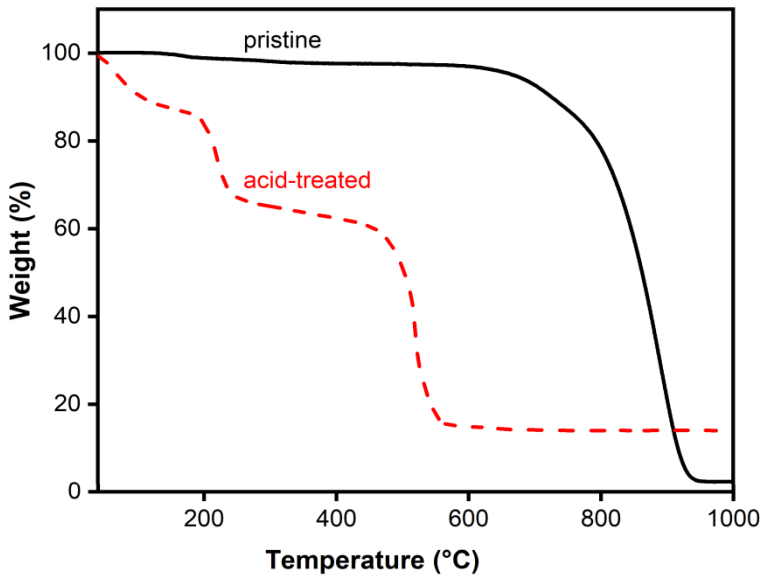

Figure 51: TGA curves of pristine (pGnP) and acid-treated graphite (mGnP) nanoplatelets, showing stepwise degradation of modified graphite nanoplatelets

However, a trace of impurities of about 20 % was seen in the mGnP due to the considerable amounts of residual manganese because of the use of permanganate oxidant (Wong *et al.*, 2014) during acid treatment. The stepwise removal of impurities hence was observed clearly in the thermogram in the case of acid-treated and hydroxyl groups added after the oxidation.

The TGA thermogram of nanodiamonds is shown in Figure 52. In the case of pristine nanodiamond (pND), there is no evidence of loss of weight up to 500 °C, and drastic weight loss occurs (approximately 90 %) at temperatures ranging from 500 °C to 600 °C. However, in the case of acid-treated nanodiamonds (mND), a gradual loss in weight was observed at the initial stages of heating. The initial weight loss (3 wt. %) in the range of (30 °C-220 °C) is attributed to the desorption of adsorbed water (Stehlik *et al.*, 2015). This suggests that the presence of C=O groups on the surface of

ND-COOH makes it somewhat more hydrophilic than pristine nanodiamond (Bouša *et al.*, 2016; Wahab *et al.*, 2015). In addition, sharp weight loss was observed between 500 °C–600 °C.

The decomposition of the diamond phase starts at the temperature of 550 °C. Importantly, the pristine and acid-treated nanodiamond sample had a residual mass of about 7 % and 4 % at 700 °C (Banisaid & Kharat, 2018). In the 200 °C-500 °C range, about 4 % weight loss occurs (Stehlik *et al.*, 2015).

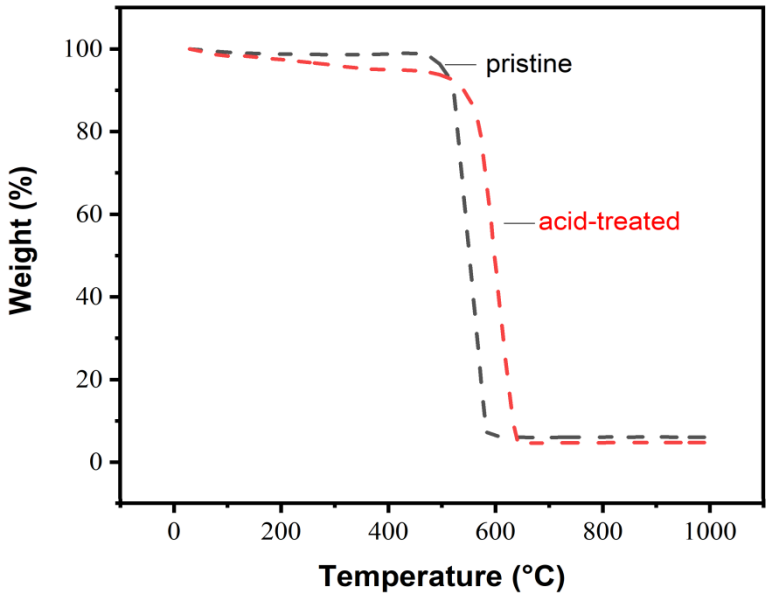

Figure 52: TGA curves of pristine (pND) and acid-treated (mND) nanodiamond

4.1.4 Summary of section 4.1

In summary, the acid oxidation method is found to be effective for the functionalization of nanocarbons (CNT, GnP, and ND) of different dimensionalities. This is confirmed by various spectroscopic, thermal, and microscopic investigations. FTIR shows the attachment of the oxygen-containing functional groups (–COOH and –OH) on the nanocarbon surfaces. The oxidation of the nanocarbon with acid increases their defect population as confirmed by Raman spectroscopy. The comparative high interlayer distance in GnP compared to other nanocarbons after acid treatment suggested that graphite particles are exfoliated into sheets of graphene and smaller particles. The SEM analysis revealed that one-dimensional aligned bundles of CNT were not clearly visible after acid oxidation. In contrast to zero-dimensional nanocarbons ND, which changed into powders, two-dimensional nanocarbons GnP

changed into rectangular layers with persisting flakes. The thermal degradation of acid-treated nanocarbons occurs at a lower temperature compared to that of pristine indicating that functionalization has occurred. The high (20 %) impurities are seen in acid-oxidized graphite nanoplatelets due to the manganese used during the acid treatment.

4.2 Structure-Properties Correlation of EP/CNT Nanocomposites

4.2.1 Structural analysis of nanocomposites

Fourier transform infrared spectroscopic (FTIR) studies

The FTIR spectra reveal information regarding the functional groups as well as the variations in mechanical and thermal properties of various samples with their molecular structures (Charles *et al.*, 2009). The FTIR spectra of neat EP, EP/pCNT$_{0.05}$, and EP/mCNT$_{0.05}$ are shown in Figure 53.

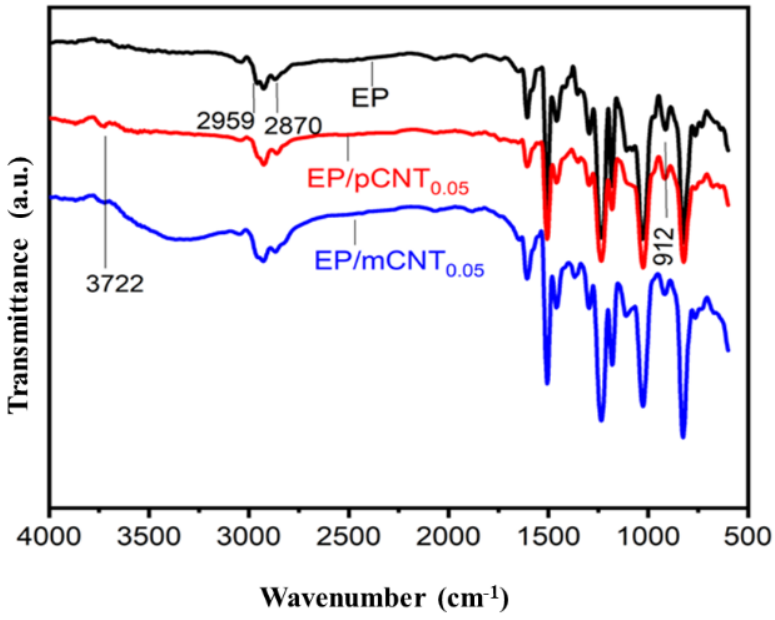

Figure 53: FTIR spectra of neat EP, EP/pCNT$_{0.05}$, and EP/mCNT$_{0.05}$ nanocomposites

The peaks at 2959 cm^{-1} and 2870 cm^{-1} in neat EP are due to the symmetric and asymmetric stretching vibration of methylene and 1506 cm^{-1} represents the stretching vibration of benzene (Qi *et al.*, 2018). The EP group present in all the samples is further denoted by the bands at around 825 cm^{-1}, 912 cm$^{-1,}$ and 1234 cm^{-1}. The appearance of a peak at 3722.61 cm^{-1} of EP/pCNT$_{0.5}$ is ascribed to some unreacted –OH groups of the epoxy resin. It can also be noticed that the peak centred at 2959 cm^{-}

^{1} is eliminated. In addition, the peak centred at 912 cm^{-1} has slightly shifted in peak position in the case of both composites comprising pristine and acid-treated CNT which may be due to the uniform dispersion of CNT on the EP matrix (Mahmood *et al.*, 2021).

The broadband was observed in the range of 3132 cm^{-1}-3783 cm^{-1} in EP/$mCNT_{0.05}$ indicating the presence of hydroxyl groups which might be responsible for creating hydrogen bonds with other nucleophilic groups. The intensity of these bands is found to increase in the nanocomposites comprising acid-treated CNT, which may be due to the interaction of the epoxy groups of the resin with the -COOH groups introduced onto the surface of the nanotubes through acid treatment, thereby enabling the formation of hydrogen bonds between the –COOH group and EP resin and also the formation of hydrogen bond between the unreacted carboxylic groups and –OH groups within the mixture (Rahaman *et al.*, 2012).

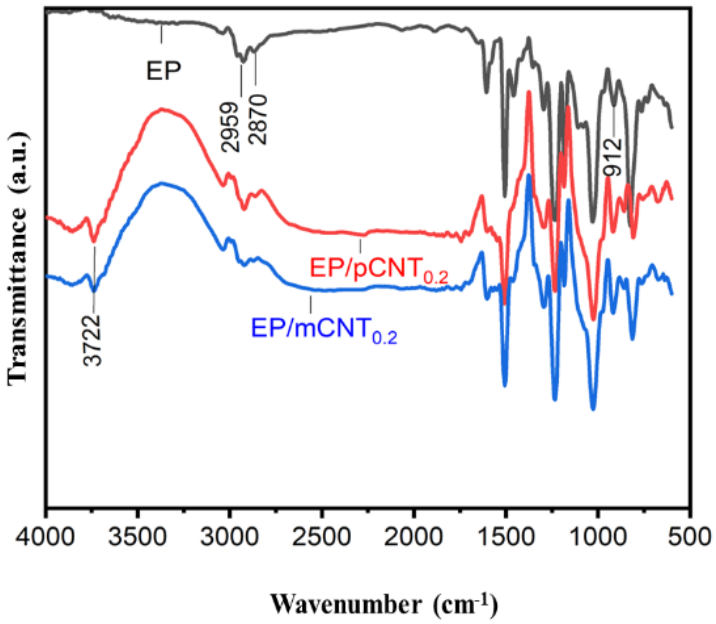

Figure 54: FTIR spectra of neat EP, EP/$pCNT_{0.2}$, and EP/$mCNT_{0.2}$ nanocomposites

Figure 54 shows FTIR spectra of neat EP, EP/$pCNT_{0.2}$, and EP/$mCNT_{0.2}$ nanocomposites. The EP/$pCNT_{0.2}$ and EP/$mCNT_{0.2}$ nanocomposites show broad peaks from 3400 cm^{-1} to 3900 cm^{-1} indicating the formation of -OH bond in the nanocomposites (Păun *et al.*, 2019). The shifting of a peak at 912 cm^{-1} was also observed in both the case of EP/$pCNT_{0.2}$ and EP/$mCNT_{0.2}$ nanocomposites indicating

good dispersion of CNT in the EP matrix caused by the interaction of nanoparticle and the polymer matrix (Mahmood *et al.*, 2021).

When the structural characteristics of the nanocomposites with lower and higher CNT concentrations were analysed, it was discovered that EP, pristine CNT, and modified CNT are well dispersed in both conditions. However, the broad peak of EP/mCNT at about 3100-3700 cm^{-1} sharpens for the increased filler content (0.2 wt.%), indicating stronger interaction between the EP and mCNT resulting in the more cross-linked character of the composites.

4.2.2 Morphological analysis of nanocomposites

(i) X-ray diffraction (XRD) analysis

The XRD patterns of neat EP, EP/$pCNT_{0.5}$, and EP/$mCNT_{0.5}$ nanocomposites are displayed in Figure 55.

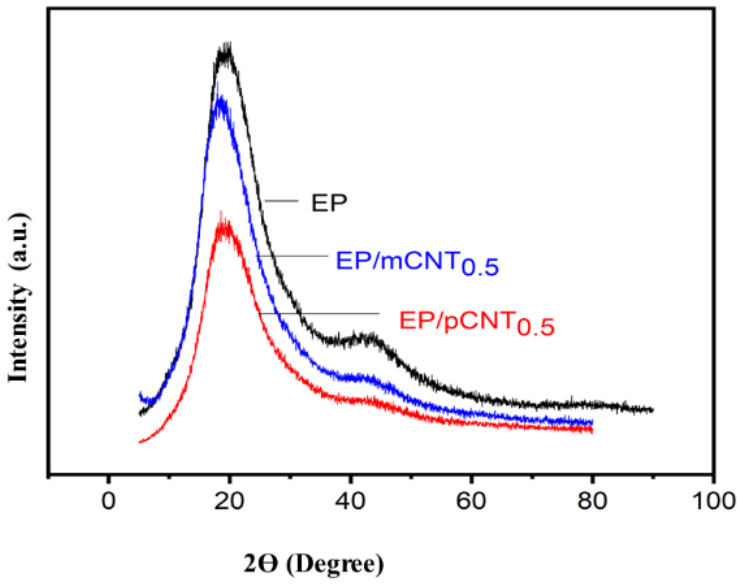

Figure 55: XRD pattern of neat EP, EP/$pCNT_{0.5}$, and Ep/$mCNT_{0.5}$ nanocomposites

XRD patterns of neat EP represent broadly amorphous peaks observed at 2θ values ranging from 7-36° with a peak centred at 19° and 43° because of the scattered crosslinked structures, which typically ascribed to the amorphous nature of EP (Kumar *et al.*, 2018). Both pristine and acid-treated (EP/$pCNT_{0.5}$ and EP/$mCNT_{0.5}$) nanocomposites also show a broad band with a peak centred at 19°, and 43° due to dispersion in the EP matrix indicating the amorphous nature of both the

nanocomposites (Păun *et al.*, 2019).

The decreased peak intensity is observed in the case of both the nanocomposites, which is due to the intercalation of CNT with the EP matrix (Jamal & Abdullah, 2023). In both nanocomposites, the characteristic peak of CNT was not observed, due to the use of filler in lower wt. %. The XRD patterns of EP, EP/$pCNT_{0.5,}$ and EP/$mCNT_{0.5}$ show that the incorporation of CNT in epoxy did not influence the amorphous nature of epoxy (Alhumade *et al.*, 2019).

XRD was performed to extract information regarding the crystallinity, intercalation, and exfoliation of materials within the EP matrix.

(ii) Microscopic studies

Figure 56 displays the neat epoxy resin fracture surface morphology as imaged by FESEM at lower and higher magnifications. The micrograph reveals that cracks and island-like features are present together with smooth, flat fracture surfaces. The island-like structures may have developed as a result of impurities or coating materials that were used during the morphological investigation. Additionally, crack propagation was observed to occur in a specific direction. This analysis leads to the conclusion that neat epoxy materials have a weak resistance to cracking and rupturing. The cured epoxy resin hardens and becomes brittle like glass as a result of cross-linking between the epoxy and the hardener, according to earlier research that was published in the literature. In summary, the neat epoxy resin is brittle like glass and bears different fracture planes.

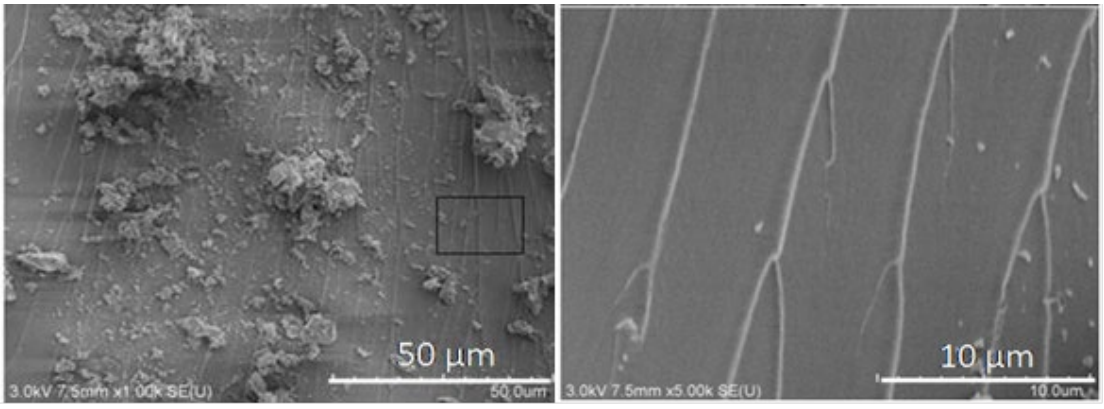

Figure 56: Lower (left) and higher (right) magnification of FESEM micrographs showing the fracture surface morphology of the neat EP; the rectangular part of the upper figure is magnified at the bottom

The FESEM images presented in Figure 57 show the morphologies of the nanocomposites formed by the Epoxy resin with 0.2 wt. % of pristine and acid-treated multi-walled carbon nanotubes (pCNT and mCNT), EP/$pCNT_{0.2}$ and EP/$mCNT_{0.2}$ nanocomposites.

Figure 57.a displays a character somehow similar to that of neat epoxy composites i.e., flat smooth terraces-like structures with crack propagation in a definite direction while EP/$mCNT_{0.2}$ 57.d shows cloud patch structures representing surface roughness leading to greater energy dissipation (Kumar *et al.*, 2017).

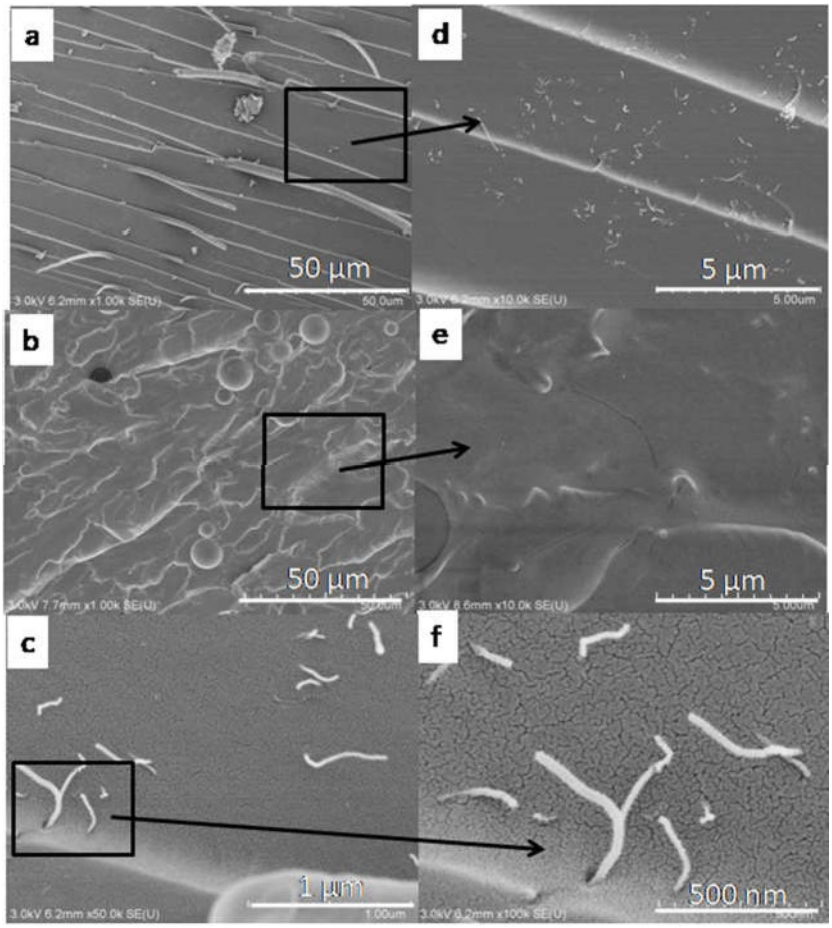

Figure 57: Lower (left) and higher (right) magnification of surface morphology of the pristine and acid-treated carbon nanotubes epoxy nanocomposites; the rectangular part of the left figure is magnified at the right

In 57.b, EP/pCNT nanocomposites, pCNT are clearly visible with a white short strand. These pCNT are almost well distributed however, there is agglomeration visible in some parts of the nanocomposites. The mCNT are not clearly visible compared with pCNT, this is because they are embedded in the EP matrix see Figure

57.e (Anas *et al.*, 2015). The fracture surfaces of EP/mCNT$_{0.2}$ also show cracks created due to the entrapment of air during nanocomposite preparation (Anas *et al.*, 2015). The pull-out, network formation, and crack initiation processes are well displayed in 57.c and f (Anas *et al.*, 2015; Z. Qi *et al.*, 2018). The strongly oxidizing nitric acid shortens the length of the nanotubes during functionalization processes (Smoleń *et al.*, 2021).

EP/pCNT$_{0.2}$ nanocomposites have flat, smooth structures with clear crack propagation and homogeneous distribution patterns with low agglomeration, whereas EP/mCNT$_{0.2}$ has cloud patches indicating surface roughness and energy dissipation.

4.2.3 Thermal, electrical, and surface properties

(i) Thermal (TGA) analysis

Thermal analysis is a very valuable tool for determining the thermal stability of the material. The neat EP, EP/pCNT$_{0.2}$, and EP/mCNT$_{0.2}$ nanocomposite samples were subjected to thermogravimetric analysis (TGA) and derivative thermogravimetric analysis (DTG) to study the impact of adding CNT (pristine and functionalized) on the thermal behaviour of nanocomposite. Figure 58 shows the TGA/DTG thermogram of EP, EP/pCNT$_{0.2}$, and EP/mCNT$_{0.2}$.

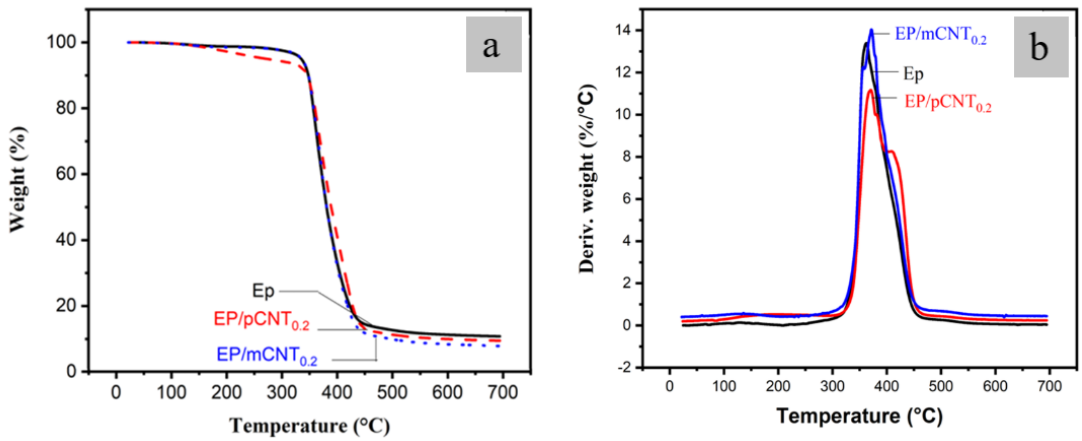

Figure 58: (a) TGA curves of neat EP resin, EP/pCNT$_{0.2}$, and EP/mCNT0.2 nanocomposites (b) DTG curve of neat EP resin, EP/pCNT$_{0.2}$, and EP/mCNT$_{0.2}$ nanocomposites

In neat EP there is no weight loss below 315 ºC, and drastic weight loss (89 %) occurs at a temperature ranging from 315 ºC to 450 ºC with a single DTG curve at 362 ºC

showing a single-step degradation process. However, in EP/pCNT$_{0.2}$, the 5 % weight loss occurs below at around 315 ºC and major weight loss (91 %) occurs at a temperature ranging from 315 ºC to 450 ºC with their respective DTG curve at 371 ºC and 409 ºC. The 5 % wt. loss may be due to the voids formed from the pull-out of nanotubes from the EP matrix shown in Figure 58. EP/mCNT$_{0.2}$ curve displays major weight (92 %) loss at around 315 ºC to 450 ºC with the DTG curve representing 371 ºC.

The residual masses of the EP, EP/pCNT$_{0.2}$, and EP/mCNT$_{0.2}$ nanocomposites are around 11, 9, and 8 wt. %, respectively (Cheng *et al*., 2008). The thermal stability was slightly observed better for EP/mCNT$_{0.2}$ than EP/pCNT$_{0.2}$. The incorporation of pCNT and mCNT into the EP matrix leads to a slight change in the decomposition temperature of the EP matrix and both nanocomposites (EP/pCNT$_{0.2}$ and EP/mCNT$_{0.2}$) from 362 ºC to 371ºC.

On careful examination, it is found that, as compared to neat EP, EP/pCNT$_{0.2}$ and EP/mCNT$_{0.2}$ nanocomposites showed slightly greater thermal stability. The well-dispersed nanotubes and interfacial adhesion are also supported by Figure 59 between the carbon nanotubes and the EP matrix contributing to the nanocomposites' enhanced thermal stability (Cao *et al.*, 2010).

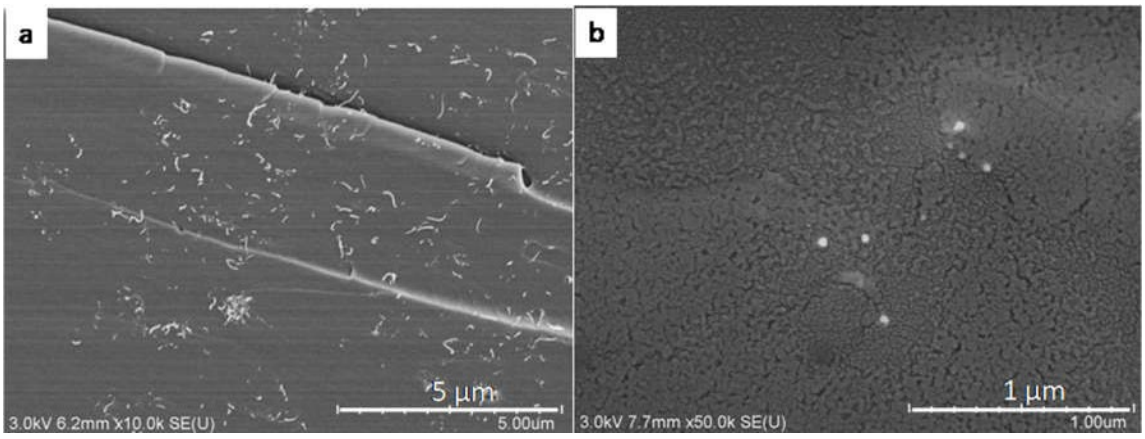

Figure 59: Lower (left) and higher (right) magnification of well-dispersed pristine and acid-treated nanotubes

(ii) Electrical properties

The resistivity of the nanocomposites is measured by taking into account the resistance and the thickness of the sample. The measurement of the resistivity of the

samples was calculated and represented in Figure 60 depending on the mass fraction of CNTs in the nanocomposites. The study indicates that the addition of pCNT reduces the resistivity of the nanocomposites for 0.05, 0.1, and 0.2 wt. % of EP/pCNT nanocomposites and then increased in the case of 0.5 wt. % which might be the formation of agglomeration due to the use of the high amount of CNT contents. In addition to this EP/mCNT shows increasing resistivity values on increasing mCNT content with an exceptional case of 0.1 wt. %. Both EP/pCNT and EP/mCNT nanocomposites exhibit conductivity however EP/mCNT shows more conductivity comparatively within the given study range of filler concentration. All compositions with modified MWCNTs nanocomposites are found to be less conductive which might be due to the decrease in length of carbon nanotubes through severe degradation caused by the acid treatment which hindered the formation of the conductive network (Smoleń *et al.*, 2021).

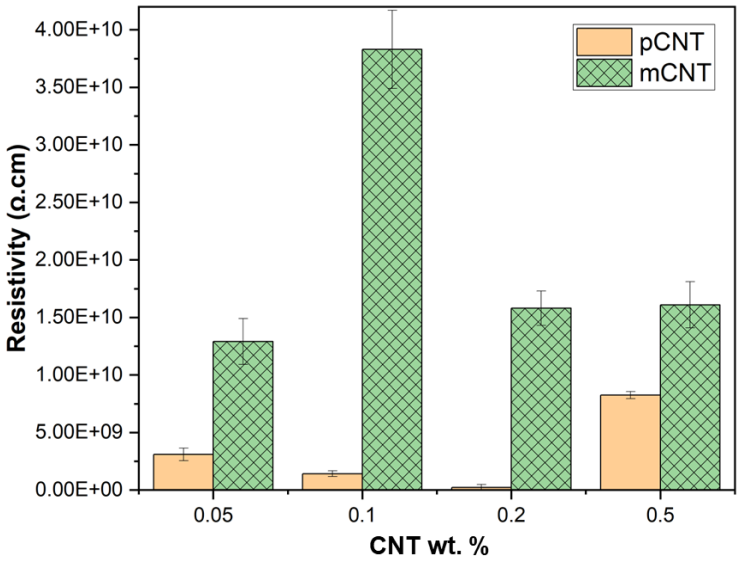

Figure 60: Resistivity measurement of EP/pCNT and EP/mCNT nanocomposites with a variation of CNT wt. %

According to the electrical conductivity measurement, EP/pCNT and EP/mCNT nanocomposites (0.05, 0.1, 0.2, and 0.5) are found to be conductive. However, among the various filler concentrations, EP/pCNT nanocomposites with 0.2 wt.% demonstrate good conductivity. CNT strands are embedded within the EP matrix, creating an interconnected network that extends in all directions. It is believed that this intertwined CNT web is responsible for the composite's electrical conductivity (Earp *et al.*, 2021).

(iii) Surface properties

The water contact angle indicates the wettability of the solid. The contact angle is important wherever the intensity of the phase contact between liquid and solid substances needs to be assisted, such as in coating, painting, cleaning, printing, bonding, dispersing, etc.

The wettability of the neat EP and its nanocomposites comprising 0.05 wt. % and 0.2 wt. % were studied by measuring the contact angle with the help of the sessile drop technique. The contact angles (θ) of various samples are shown in Table 6 and their plot is shown in Figure 61. The contact angle of nanocomposites incorporated with both pristine and acid-treated nanotubes was found to be higher than that of the neat EP, indicating that nanocomposites are slightly less hydrophilic than the neat EP matrix.

The arrangement of the CNT nanostructure in the EP matrix may have an impact on the surface behaviour, and heterogeneity effects may be responsible for the increase in contact angle (Kim, 2008).

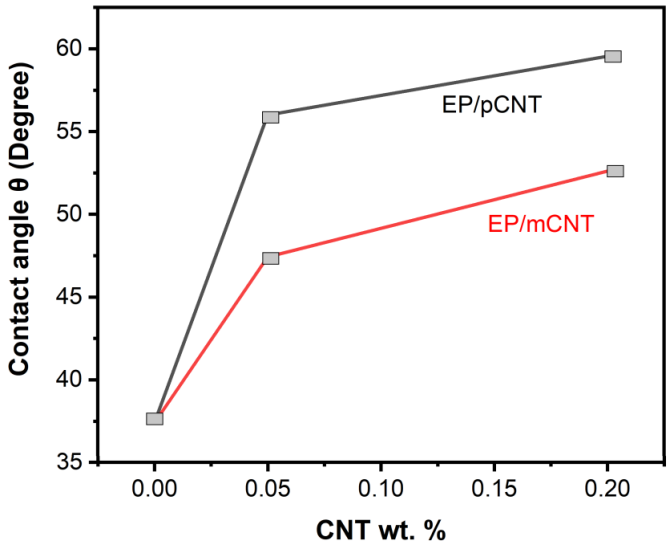

Figure 61: Plot of contact angle measurement EP/pCNT and EP/mCNT with a variation of CNT wt. %

The contact angle value for neat EP is found to be 37º representing its hydrophilic nature. The contact angle values for EP/pCNT$_{0.05}$, EP/pCNT$_{0.2}$, EP/mCNT$_{0.05}$, and EP/mCNT$_{0.2}$ are found to be 56º, 60º, 47º and 52º respectively. The contact angle value increased after the incorporation of the CNT and again rose, with the increasing wt. % of CNT for both pristine and acid-treated cases on comparing to neat EP, which

is attributed to the change in microscale roughness of the epoxy matrix and nanoscale roughness of the CNT. However, altering the filler incorporation i.e., pCNT to acid-treated mCNT, the value of the contact angle is found to be decreased due to the chemical heterogeneity effects of oxygen-containing functional groups introduced during functionalization (Ardjmand *et al.*, 2015). Both EP/pCNT and EP/mCNT are hydrophobic as compared to neat EP, according to the contact angle measurement. In contrast, EP/mCNT exhibits a hydrophilic character when compared to EP/pCNT, enhancing the wettability of the prepared nanocomposites.

Table 6: Contact angle measurement of EP, EP/$pCNT_{0.05}$, EP/$pCNT_{0.2}$, EP/$mCNT_{0.2}$, and EP/$mCNT_{0.2}$ nanocomposites

S.N.	Sample Name	Contact angle value (θ)
1	EP	37 º
2	EP/$pCNT_{0.05}$	56º
3	EP/$mCNT_{0.05}$	47 º
4	EP/$pCNT_{0.2}$	60 º
5	EP/$mCNT_{0.2}$	52 º

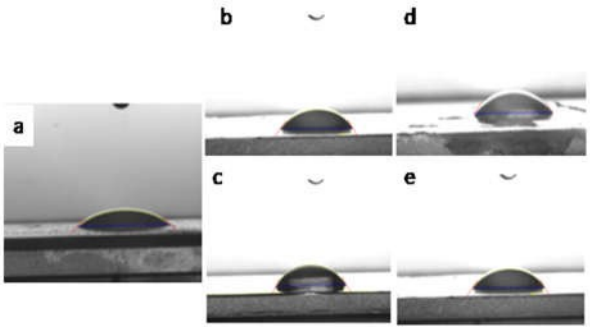

Figure 62: Evolution of droplet geometric shapes of (a) neat EP, (b) EP/$pCNT_{0.05}$, (c) EP/$pCNT_{0.2}$, (d) EP/$mCNT_{0.05}$, and (e) EP/$mCNT_{0.2}$

4.2.4 Summary of section 4.2

The structural analysis of the nanocomposites reveals that with the addition of CNT to the EP matrix, both constituents are well cross-linked in both the pristine and acid-treated cases, enhancing their physical properties. The intensified peak corresponding to higher filler content (0.2 wt. %) implies stronger interaction between the EP and mCNT, leading to highly interlinked nanocomposites enhancing the physical properties for structural applications. From XRD, it is concluded that the incorporation of CNT in epoxy does not show any impact on the degree of crystallinity of epoxy. Furthermore, the nanocomposites show similar diffraction to that of epoxy but with a less intense peak. The microscopic study confirms that pristine and acid-treated CNT are homogeneously dispersed on the EP matrix and are

acid-treated and responsible for the roughness of the surface, displaying a different pattern of fractured surface to that of the neat EP and EP/pCNT nanocomposites. It also shows the degradation of nanotubes caused by refluxed acid. The results of the thermal investigation indicate that the addition of CNT to an EP matrix slightly improves (9-13 °C) the thermal stability of the EP/pCNT and EP/mCNT nanocomposites. The electrical resistivity measurement sums up the conclusion that resistivity of EP/pCNT nanocomposites was found to be decreased as high as about 40 times compared to acid-treated nanocomposites. The higher resistivity of Ep/mCNT was due to the prolonged, long-hour treatment with strongly oxidizing nitric acid, which shortens the length of the chain of the acid-treated CNT. The EP/pCNT is slightly hydrophobic according to the contact angle measurement, whereas the EP/mCNT displays hydrophilic behaviour with improved wettability.

4.3 Structure Properties Correlation of EP/GnP Nanocomposites

4.3.1 Structural analysis of nanocomposites

Fourier transform infrared (FTIR) spectroscopic studies

To analyse the chemical structure of nanocomposites, FTIR spectroscopy was a useful tool. The FTIR spectra of neat EP, EP/pGnP$_{0.05}$, and EP/pGnP$_{0.2}$ nanocomposites are presented in Figure 63. The peaks at 2959 cm^{-1} and 2870 cm^{-1} in neat EP are due to the symmetric and asymmetric stretching vibration of methylene and 1506 cm^{-1} represents the stretching vibration of benzene (Qi *et al.*, 2018).

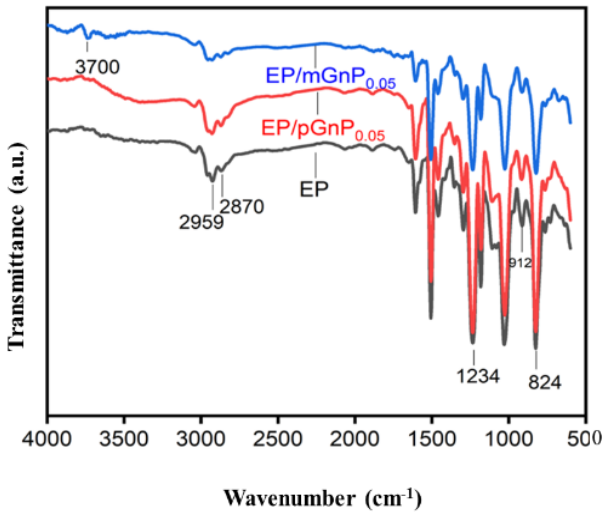

Figure 63: FTIR spectra of neat EP, EP/pGnP$_{0.05}$, and EP/mGnP$_{0.05}$ nanocomposites

The EP group present in all the samples is further denoted by the bands at 824 cm^{-1}, 912 $cm^{-1,}$ and 1232 cm^{-1}. The addition of pGnP to the neat EP matrix has somewhat changed the structures of EP/$pGnP_{0.05}$ nanocomposites compared with the EP matrix. It shows a broad band at 3100 cm^{-1} to 3600 cm^{-1} indicating the presence of hydrogen bonding.

On the other hand, incorporation of mGnP into the EP, matrix leads to the formation of broad peaks from 3400 to 3900 cm^{-1} with a sharp peak at 3700 cm^{-1} which is observed due to the presence of hydroxyl groups attached due to acid treatment on the surface of the samples which is responsible for creating hydrogen bonds with other nucleophilic groups. Additionally, the peak at 2959 cm^{-1} becomes diminished in both of the nanocomposites. In addition, the peak centred at 912 cm^{-1} has a slight position shift in the case of the EP/GnP nanocomposites which may be due to the uniform dispersion of MWCNT on the EP matrix (Mahmood *et al.*, 2021).

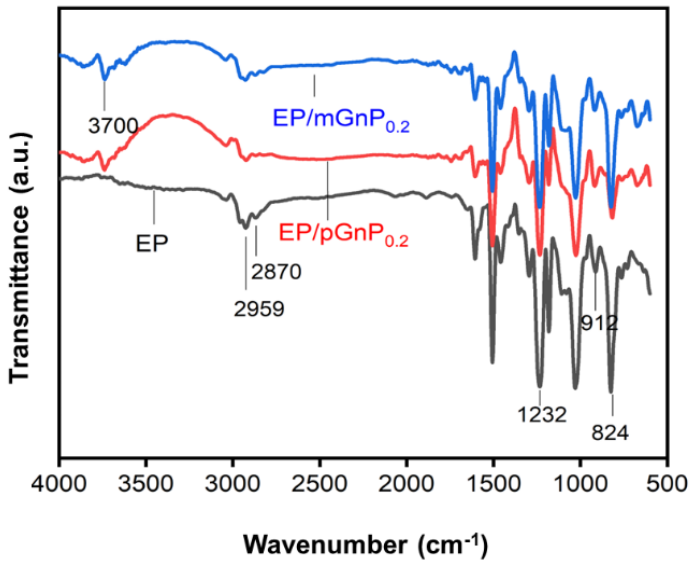

Figure 64: FTIR spectra of neat EP, EP/$pGnP_{0.2}$, and EP/$mGnP_{0.2}$ nanocomposites

Figure 64 shows FTIR spectra of neat EP, EP/$pGnP_{0.2}$, and $mGnP_{0.2}$ nanocomposites. The EP/$pGnP_{0.2}$ and EP/$mGnP_{0.2}$ nanocomposites show broad peaks from 3400 cm^{-1} to 3900 cm^{-1} with a sharp peak at 3700 cm^{-1} indicating well dispersion of GnP into the EP matrix by forming -OH bond (Păun *et al.*, 2019).

Similar to EP/GnP nanocomposites, neat EP, pristine GnP, and modified GnP are discovered to be well dispersed in the case of both filler concentrations (0.05 and 0.2

wt.%). However, they demonstrate a better result at higher filler concentrations.

4.3.2 Morphological analysis of nanocomposites

i. X-ray diffraction (XRD) Analysis

The X-ray diffractogram of neat EP, EP/pGnP$_{0.5}$, and EP/mGnP$_{0.5}$ nanocomposites are shown in Figure 65 XRD patterns of neat EP represent broadly amorphous peaks observed at 2θ values ranging from 7-36° with a peak centred at 19° and 43°, which are typically ascribed to the amorphous nature of EP (Kumar *et al.*, 2018). The EP/pGnP$_{0.5}$ and EP/mGnP$_{0.5}$ nanocomposites exhibit broad peaks rather than sharp diffraction peaks. This is because the crystallite phase disappeared as a result of the graphite having been previously dissolved in the epoxy matrix or separated by networks of cross-linked epoxy resin (Qi *et al.*, 2014).

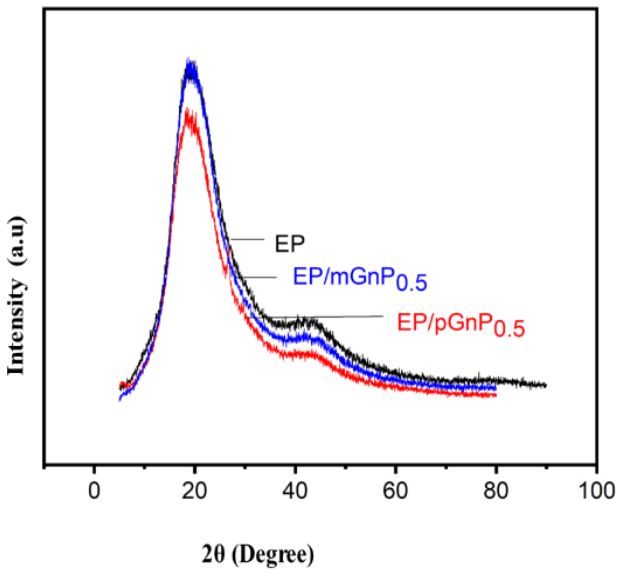

Figure 65: XRD pattern of neat EP, EP/pGnP$_{0.5}$, and EP/mGnP$_{0.5}$ nanocomposites

(ii) Microscopic studies

The fracture surface morphology of the neat EP, EP/pGnP$_{0.2}$, and EP/mGnP$_{0.2}$ nanocomposites are characterized by field emission electron microscope under high and low resolution and are shown in Figure 66. The neat EP depicts typical brittle fracture surfaces with a uniform section and smooth-appearing terrace like-pattern. The fracture surfaces of EP/pGnP$_{0.2}$, and EP/mGnP$_{0.2}$ are rougher than the neat EP indicating more energy dissipated by the GnP nanoparticles (Tang *et al.*, 2014).

These microscopic investigations show that the addition of both pristine and acid-treated GnP nanoparticles to the EP matrix changes the fractured pattern from smooth to an increased wavy rougher surface indicating the GnP particles acted as an obstacle to crack propagation (Abdullah & Ansari, 2015). The graphite nanoparticles distorted the path of the crack tip (Singh & Mohanty, 2020). The whitened parts were observed in 66.e are damaged parts that occurred during the physical fracturing of the nanocomposites. The absence of graphite nanoplatelets in EP/pGnP$_{0.2}$ and EP/mGnP$_{0.2}$ nanocomposites suggests that epoxy resin surrounds the nanoplatelets and that there is a strong interfacial bonding between them.

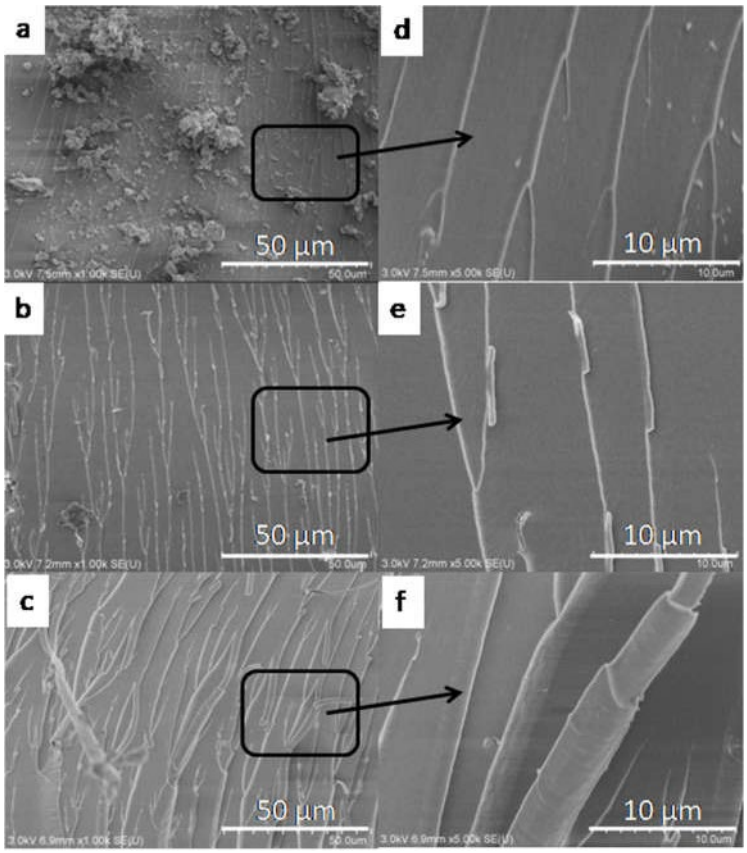

Figure 66: Lower (left) and higher (right) magnification of surface morphology of the neat epoxy, pristine, and acid-treated graphite nanocomposites; the rectangular part of the left figure is magnified at the right

According to the results of microscopic studies, adding GnP to the epoxy matrix can lessen its brittleness by increasing the density of wavy structures, which increases surface roughness and energy dissipation.

4.3.3 Thermal, electrical, and surface properties

(i) Thermogravimetric (TGA) analysis

The neat EP, EP/pGnP$_{0.2}$, and EP/mGnP$_{0.2}$ nanocomposite samples were subjected to thermogravimetric analysis (TGA) and derivative thermogravimetric analysis (DTG) to study the impact of adding GnP (pristine and functionalized) on the thermal behaviour of nanocomposite. Figure 67.a shows the TGA thermogram of EP, EP/pGnP$_{0.2}$, and EP/mGnP$_{0.2}$. In EP and EP/mGnP$_{0.2}$ there is no weight loss, <320 ºC, and drastic weight loss (about 83 %) occurs at a temperature range from 320 ºC to 447 ºC with a single DTG curve at 361 ºC (EP), 372 ºC (EP/pGnP$_{0.2}$) and 366 ºC (EP/mGnP$_{0.2}$), which showed one-step degradation mechanism see Figure 67.b. The weight loss is seen for EP/pGnP$_{0.2}$ <320 ºC. The nature of the TGA and DTG curves indicates that the presence of GnP filler does not affect the breakdown of the EP matrix but a slight improvement of thermal stability was observed for EP/pCNT$_{0.2}$. The residual masses of the EP, EP/pGnP$_{0.2}$, and EP/mGnP$_{0.2}$ nanocomposites are around 10, 10, and 11 wt. %, respectively (Cheng *et al.*, 2008).

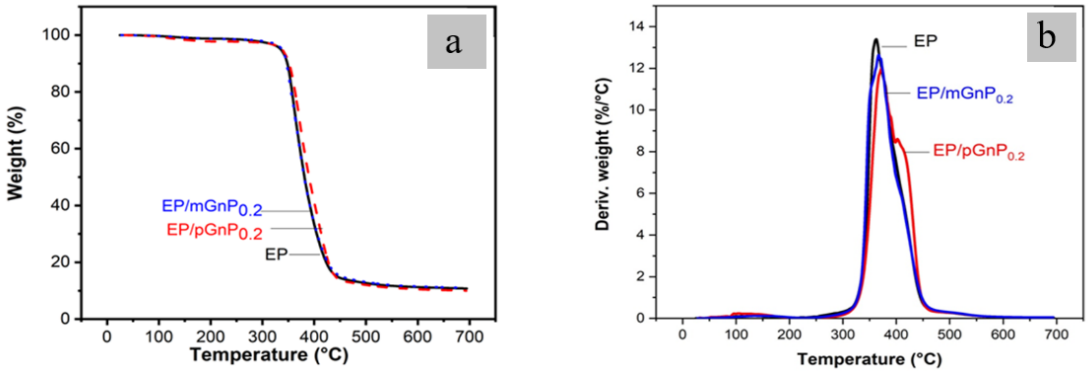

Figure 67: (a) TGA spectra of neat EP, EP/pGnP$_{0.2}$, and EP/mGnP$_{0.2}$ nanocomposites (b) DTG curve of neat EP, EP/pGnP$_{0.2}$, and EP/mGnP$_{0.2}$ nanocomposites

The first weight loss of EP/pGnP$_{0.2}$ is attributed to the removal of moisture. The second weight loss percentages of EP/pGnP$_{0.2}$ and EP/mGnP$_{0.2}$ nanocomposites are found to be 83 % at the highest breakdown temperatures for both samples. This is due to epoxy's deterioration (Suherman *et al.*, 2022). The third weight loss is due to the oxidation of the remaining degradation products of the epoxy (Bera *et al.*, 2018). The decrease in deteriorated weight is attributed to the incorporation of graphite nanoplatelets into the epoxy matrix (Mochane *et al.*, 2017).

Based on a thermogravimetric study, the pristine graphite (EP/pGnP$_{0.2}$) nanocomposites were discovered to be thermally stable in comparison to the acid-treated (EP/mGnP$_{0.2}$) and neat epoxy (EP).

(ii) Electrical properties

The measurement of the electrical resistivity of EP/pGnP and EP/GnP with the mass fraction of pristine and acid-treated GnP in the nanocomposites is Figure 68 respectively. The planar structure of graphite enables electrons to travel freely between its planes due to which graphite nanoplatelets conduct electricity. Graphite nanoplatelets were useful in creating a conductive network as the concentration increased, there was an improvement in the conductivity value. The resistivity value of EP/pGnP nanocomposites seems to be decreased on increasing the concentration of the pristine graphite nanoplatelets exceptional case of nanocomposites with 0.1 graphite wt. %. This exception case might be due to the formation of clusters or agglomeration during the nanocomposite preparation. However, in the case of EP/mGnP nanocomposites, the resistivity value was found to be increased up to the concentration of 0.2 wt. % and drastically decreased in the case of 0.5 wt. % indicating more conductive (Kaushik *et al.*, 2010). In this study, nanocomposites with EP/mGnP are found to be more conductive.

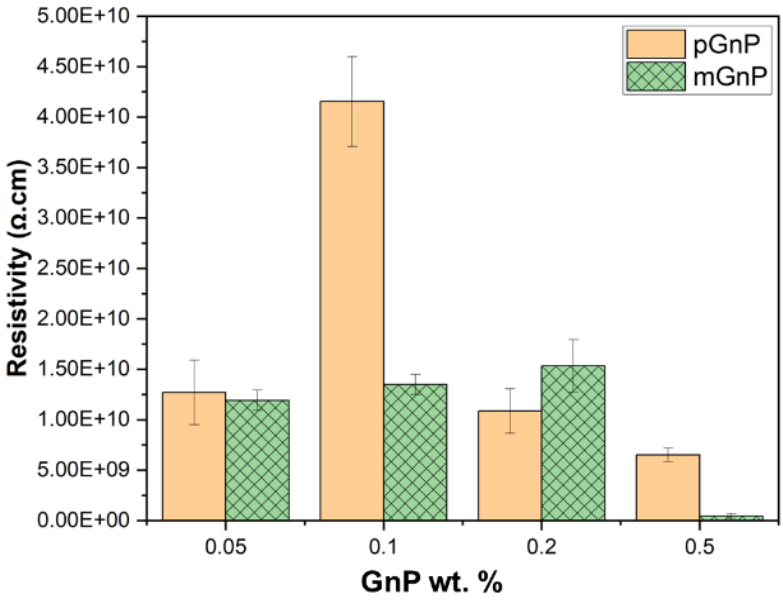

Figure 68: Resistivity measurement EP/pGnP and EP/mGnP with a variation of GnP wt. %

It is concluded that the acid-treated GnP nanocomposites show higher conductivity than that of the pristine GnP because of the homogeneous dispersion of GnP nanoparticles on the EP matrix on acid treatment.

(iii) Surface properties

Graphite, a stacked graphene layer bears a high contact angle value indicating the hydrophobic surface. It was reported in the literature that highly oriented pyrolytic graphite (HOPG) has a contact angle in the range of 60 (Aria *et al.*, 2016; Ondarçuhu *et al.*, 2016; Raj *et al.*, 2013; Shin *et al.*, 2010). The surface properties of EP, EP/pGnP$_{0.05}$, EP/pGnP$_{0.2}$, EP/mGnP$_{0.05,\ and}$ EP/mGnP$_{0.2}$ were studied by contact angle measurement methods and shown in Figure 69. The contact angle values for the EP/pGnP are found to be 58º and 66º respectively for lower and higher filler wt. % which is higher than that of the neat EP i.e., 38º. On incorporating the acid-treated GnP (EP/mGnP$_{0.2}$), the contact angle value simultaneously decreased to 51º and 65º.

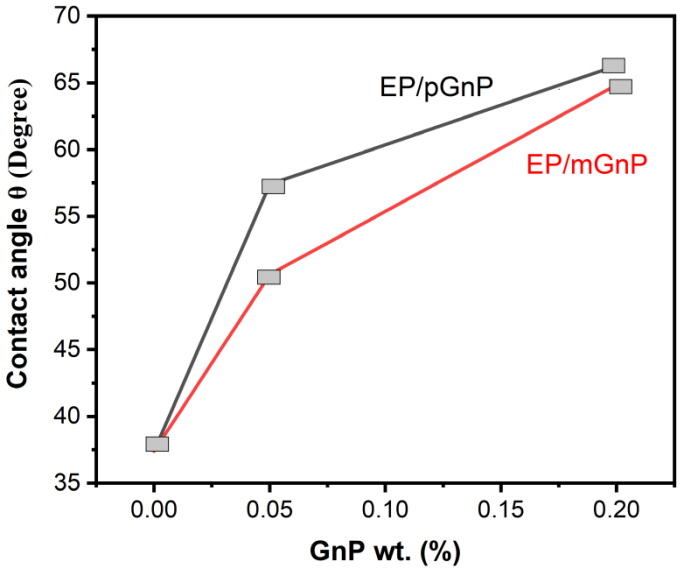

Figure 69: Plot of contact angle measurement EP/pGnP and EP/mGnP with the variation of GnP wt. %

The increased contact angle value of the EP/pGnP nanocomposites is attributed to the surface roughness created after the incorporation of the filler particles. However, the decrease in the value of the contact angle was observed in the case of the EP/mGnP sample which is attributed to the presence of oxygen-containing functional groups on the surface of the graphite nanofiller attached after the acid treatment (Pitchiya *et al.*, 2021).

The contact angle measurement values are indexed in Table 7 as follows.

Table 7: Contact angle measurement of EP, EP/pGnP$_{0.05}$, EP/pGnP$_{0.2}$, EP/mGnP$_{0.05}$, and EP/mGnP$_{0.2}$ nanocomposite

S.N.	Sample Name	Contact angle value(θ)
1	EP	38º
2	EP/pGnP$_{0.05}$	58º
3	EP/mGP$_{0.05}$	51º
4	EP/pGnP$_{0.2}$	66 º
5	EP/mGnP$_{0.2}$	65º

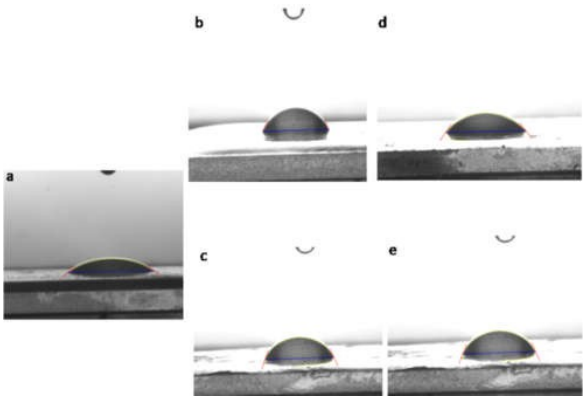

Figure 70: Evolution of droplet geometric shapes (a) neat EP, (b) EP/pGnP$_{0.05}$, (c) EP/pGnP$_{0.2}$, (d) EP/mGnP$_{0.05}$ and (e) EP/mGnP$_{0.2}$

The surface modification of graphite enhances the hydrophilicity and wettability of the epoxy nanocomposites (EP/mGnP) incorporated with acid-treated graphite nanoplatelets.

4.3.4 Summary of section 4.3

The presence of -OH in the graphite and EP matrix is determined by the FTIR analysis, indicating the formation of well-dispersed EP/GnP nanocomposites in cases of both filler concentrations (0.05 and 0.2 wt. %) but they are likely to yield good dispersion at higher concentrations. In comparison to neat EP, the diffraction pattern of EP/mGnP nanocomposite exhibits a single broad peak, indicating the elimination of the graphite crystallite phase. The conclusion drawn from microscopic studies is that adding GnP to the epoxy matrix can reduce its brittleness by altering the crack's path and forming an intense number of wavy structures, thereby creating surface roughness and energy dissipation. According to a thermal study, EP/GnP nanocomposite is slightly more (5-10 ℃) thermally stable than neat EP and acid-treated EP/mGnP nanocomposites. EP/mGnP nanocomposite showed as high as about 35 times decrease in resistivity than that of the pristine graphite because of the homogeneous dispersion of graphite particles on the EP matrix. The higher value accounts for the higher filler content and well dispersion of acid-treated GnP

nanoparticles on the EP matrix. The hydrophilic character of the EP/mGnP nanocomposites with improved wettability is revealed by the contact angle studies.

4.4 Structure-Properties Correlation of EP/ND Nanocomposites``

4.4.1 Structural analysis of nanocomposites

Fourier transform infrared spectroscopy (FTIR) studies

Figure 71 depicts the FTIR spectroscopy of neat EP, EP/$pND_{0.05}$, and EP/$mND_{0.05}$ nanocomposites. In the FTIR spectra of neat EP, the peaks at 2959 cm^{-1}, 2870 cm^{-1}, and 1502 cm^{-1} represent the benzene ring (Zhan *et al*., 2011). The EP group present in all the samples is further denoted by the bands at 824 cm^{-1}, 912 cm^{-1}, and 1232 cm^{-1}. It can be noticed that the peak centred at 2959 cm^{-1} is eliminated in the case of EP/pND nanocomposites only. In addition, the peak centred at 912 cm^{-1} has a slight position shift in the case of both nanocomposites which may be due to the uniform dispersion of ND on the EP matrix (Mahmood *et al.*, 2021).

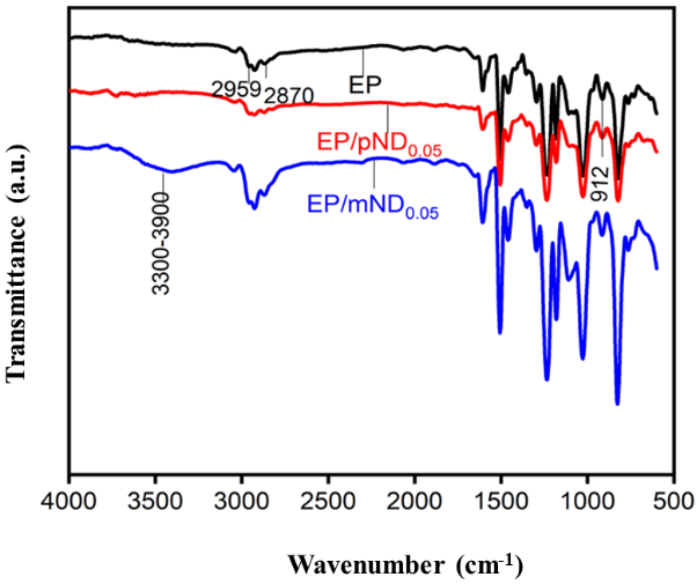

Figure 71: FTIR spectra of neat EP, EP/$pND_{0.05}$, and EP/$mND_{0.05}$ nanocomposites

The broadband was observed in the range of around 3100 cm^{-1}-3700 cm^{-1} indicating the presence of hydroxyl groups attached due to acid treatment on the surface of the samples which is responsible for creating hydrogen bonds with other nucleophilic groups. The intensity of these bands is found to increase in the nanocomposites comprising acid-treated ND, which may be due to the interaction of the EP groups of the resin with the -COOH groups introduced onto the nanodiamond surface through

acid treatment, thereby enabling the formation of hydrogen bonds between the –COOH group and EP resin and also the formation of hydrogen bond between the unreacted carboxylic groups and –OH groups within the mixture (Rahaman *et al.*, 2012).

The FTIR spectra of neat EP, EP/pND$_{0.2,}$ and EP/mND$_{0.2}$ nanocomposites are shown in Figure 72. The chemically modified ND incorporated sample shows the wide band in the region of 4000-3300 cm^{-1} that appeared in the acid-treated sample, indicating the O–H bond formation in the composites confirmed the successful formation of EP/ND nanocomposites (Păun *et al.*, 2019).

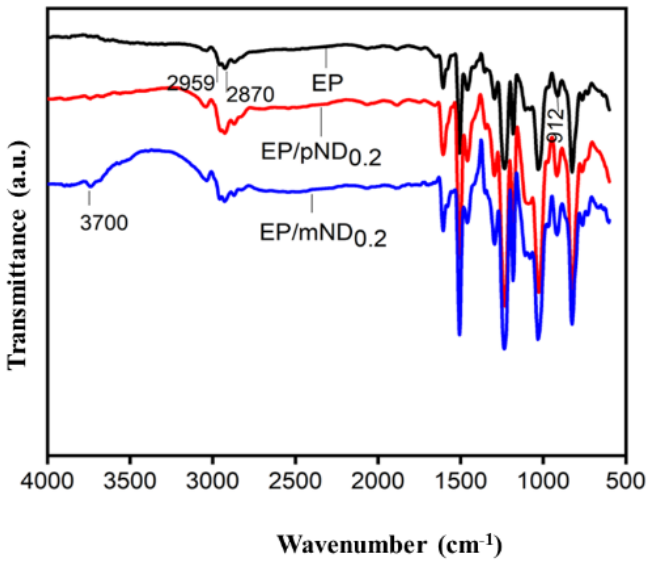

Figure 72: FTIR spectra of neat EP, EP/pND$_{0.2}$, and EP/mND$_{0.2}$ nanocomposites

The structural study of the nanocomposites demonstrates that both constituents are effectively dispersed i.e., ND to the EP matrix in both the pristine and acid-treated cases, improving their physical qualities. Highly interlinked nanocomposites with improved physical characteristics for structural applications are indicated by a sharp peak that corresponds to greater filler content (0.2 wt. %).

4.4.2 Morphological analysis of nanocomposites

(i) X-ray diffraction (XRD) analysis

The XRD patterns of neat EP, EP/pND$_{0.5,}$ and EP/mND$_{0.5}$ nanocomposites are displayed in Figure 73. XRD patterns represent broadly amorphous peaks observed at

2θ values ranging from 7-36° with a peak centred at 19° and 43°, which are typically ascribed to the amorphous nature of epoxy (Kumar *et al.*, 2018). Both pristine and acid-treated nanocomposites also show a broad band with a peak centred at 19° and 43° which is due to the dispersion of nanodiamonds in the epoxy network (Păun *et al.*, 2019). The XRD patterns of EP, EP/pND$_{0.5}$, and EP/mND$_{0.5}$ show that the incorporation of ND in EP did not influence the amorphous phase of epoxy (Alhumade *et al.*, 2019).

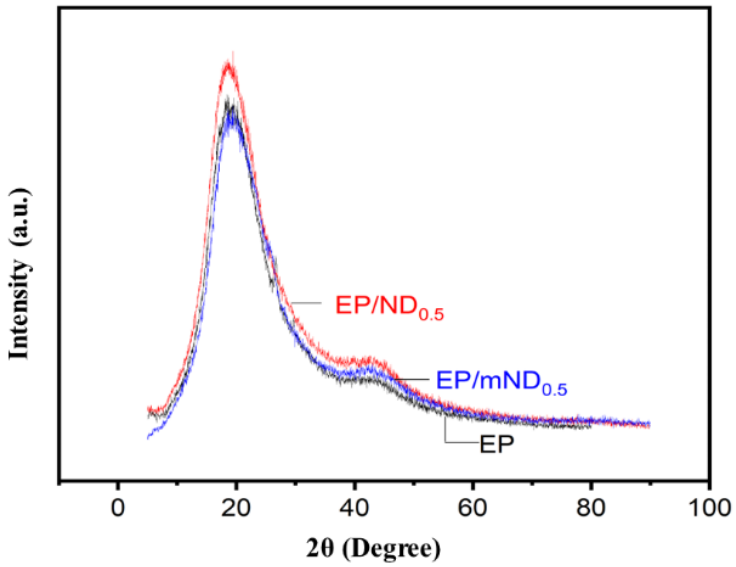

Figure 73: XRD pattern of neat EP, EP/pND$_{0.5}$, and EP/mND$_{0.5}$ nanocomposites

The peak intensity of the EP/mND is almost identical to the neat EP matrix whereas EP/pND possesses a highly intense peak indicating there is no intercalation of ND into the EP matrix (Jamal & Abdullah, 2023). In both nanocomposites, the characteristic peak of ND was not observed, indicating the homogeneous dispersion of ND in the epoxy matrix (Gantayat *et al.*, 2018). There is no shifting of peaks in both EP/pND and EP/mND which suggests that the addition of ND to the EP matrix does not affect the microstructure of the nanocomposite through the interfacial bonding between the ND and EP matrix (Wang & Zhao, 2013).

The XRD patterns of neat epoxy are almost identical with epoxy incorporated pristine and acid-treated ND nanocomposites and also reveal that the addition of ND to the EP matrix does not affect the microstructure of the nanocomposite.

(ii) Microscopic studies

Figure 74 illustrates the comparison of the fracture surfaces of neat EP and EP/$pND_{0.2}$ nanocomposites using FESEM. The fracture surface of neat epoxy contains larger single cracks that show brittleness see Figure 74.c, which results in a weak resistance to cracking and rupturing (Zhang *et al.*, 2018). The incorporation of 0.2 wt. % of pND into the neat EP matrix also shows a few voids that are created during nanocomposite preparation see Figure 74.b (Bisht *et al*., 2019). The fractured surface of EP/$pND_{0.2}$ has several tiny cracks as ND resists crack propagation causing the crack path to become more complex and branched (Zehua & Guojian, 2012). The ND nanoparticle of size ranging from 5.97-9.30 µm is spotted in 74.b. It also shows that EP/$pND_{0.2}$ nanocomposites have a rougher wavy surface than the neat EP indicating the presence of a strong interface (Haleem *et al*., 2016).

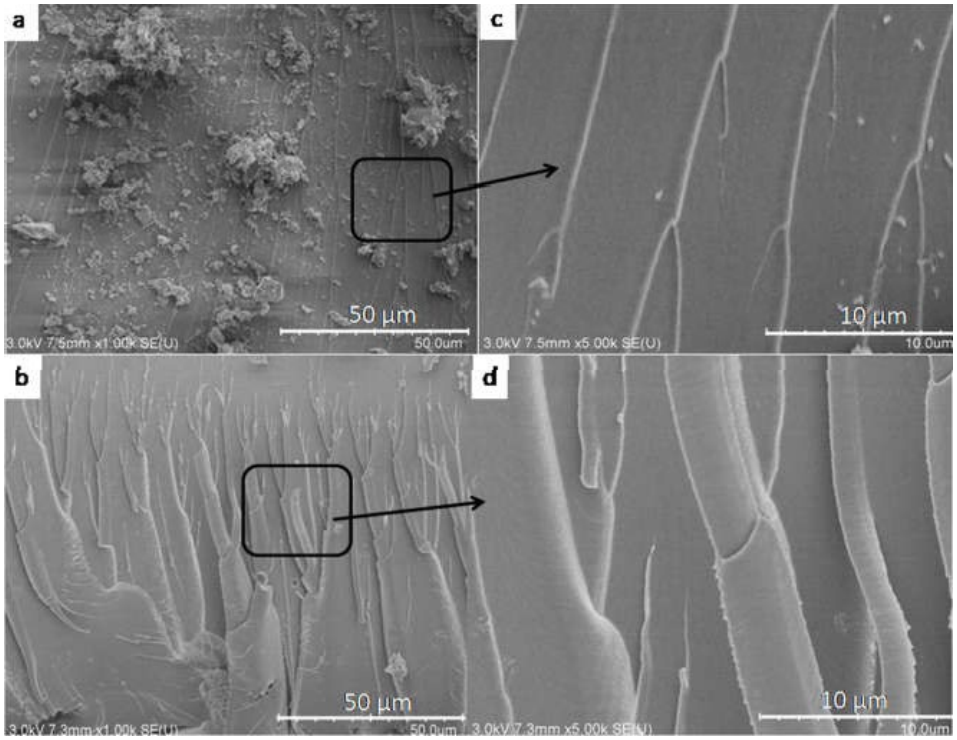

Figure 74: Lower (left) and higher (right) magnification of surface morphology of the neat epoxy and pristine ND nanocomposites; the rectangular part of the left figure is magnified at the right

The microscopic studies of the fractured surface of the EP/ND conclude that adding pristine ND to the EP matrix can lessen the brittleness of EP by resisting crack propagation and energy dissipation mechanism thereby increasing surface roughness.

4.4.3 Thermal, electrical, and surface properties

(i) Thermogravimetric (TGA) analysis

The thermogravimetric analysis was performed to understand the thermal stability of the neat epoxy and composites. The TGA and DTG curves of the neat EP, EP/pND$_{0.2}$, and EP/mND$_{0.2}$ nanocomposites are recorded in Figure 75.a and 75.b. The neat EP started to degrade at around 320 ºC which is attributed to the pyrolysis of an epoxy network (Sahoo *et al*., 2015) and completely degraded at 360 ºC. All three samples exhibit only one decomposition process. The complete decomposition of EP/pND$_{0.2}$ nanocomposites occurs at around 365 ºC and that of acid treated occurs at 370 ºC. The slight increase in the decomposition temperature of EP/mND$_{0.2}$ nanocomposites may be due to the good adhesion of acid-treated ND to the EP matrix (Saw *et al.*, 2013). The char residue was found less in the case of EP/mND$_{0.2}$ nanocomposites. However, on careful examination, the shift of around 10 ºC increase in decomposition temperature was observed on moving from neat EP to EP/mND$_{0.2}$.

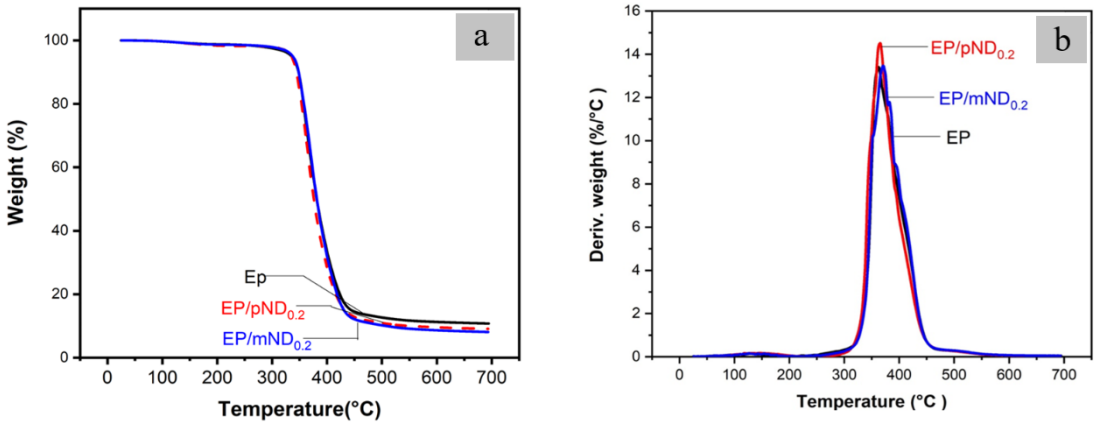

Figure 75: (a) TGA curves of neat EP, EP/pND$_{0.2}$, and EP/mND$_{0.2}$ nanocomposites (b) DTG curves of neat EP, EP/pND$_{0.2}$, and EP/mND$_{0.2}$ nanocomposites

The nanocomposites with acid-treated ND were found to be thermally stable in comparison with the nanocomposites with pristine ND and neat EP on thermal analysis.

(ii) Electrical properties

Figure 76 displays the resistivity measurement of EP/pND and EP/mND with 0.2 wt. % of ND. The electrical resistivity value of nanodiamonds lies at the borderline of

the range of conductive materials showing both pristine and acid-treated nanodiamond conductive at 30 ºC. The resistivity value increased for the epoxy nanocomposites incorporated with acid-treated nanodiamond implying that EP/pND are more conductive comparative with EP/mND. This might be due to the homogeneous dispersion of pND.

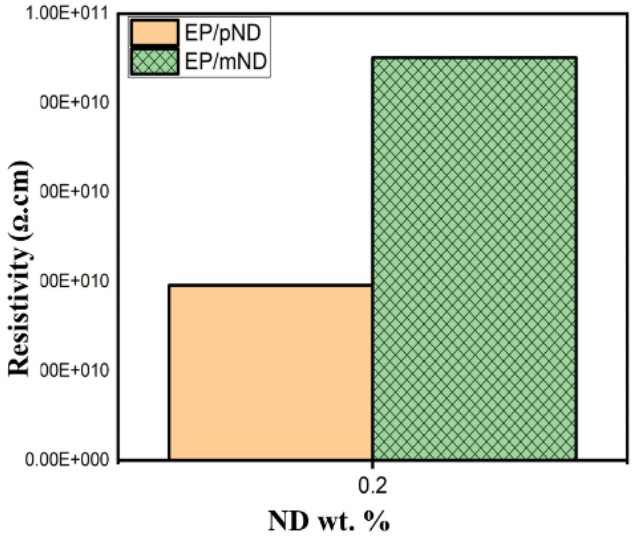

Figure 76: Resistivity measurement of EP/pND$_{0.2}$ and EP/mND$_{0.2}$ nanocomposites

(ii) Surface properties

As shown in Figure 77, we investigated the contact angle test in neat EP, EP/pND$_{0.05}$, EP/pND$_{0.2}$, EP/mND$_{0.05}$, and EP/mND$_{0.2}$ nanocomposites. The contact angle in both the concentrations of pristine ND samples increased sharply and then decreased in terms of the acid-treated ND sample. The increase in the contact angle value from neat EP to EP/pND of both concentrations accounts for the surface roughness created after the incorporation of ND filler particles into the next EP. However, the contact angle value was found to be decreased when we shifted from EP/pND to EP/mND nanocomposites because of the polar groups introduced during the acid treatment procedure, which makes the nanocomposites a little bit hydrophilic (Ardjmand *et al.*, 2015; Grundke *et al.*, 1996; Hameed *et al.*, 2007).

The decrease in contact angle is more remarkable, indicating the improved wettability of EP/mND nanocomposites, which might be due to the increase of chemical groups and surface roughness of the nanocomposites (Zhao *et al.*, 2018).

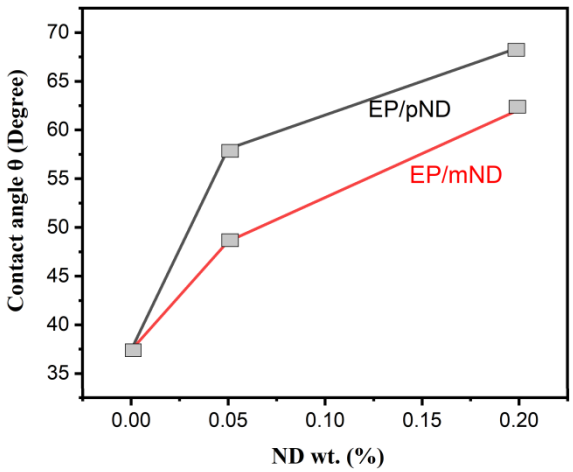

Figure 77: Plot of contact angle measurement EP/pND and EP/mND with a variation of ND wt. %

The measured contact angle values are recorded in Table 8 as follows.

Table 8: Contact angle measurement of EP, EP/pND$_{0.05}$, EP/pND$_{0.2}$, EP/mND$_{0.05}$, and EP/mND$_{0.2}$

S. No	Sample Name	Contact angle value (θ)
1	EP	37º
2	EP/pND$_{0.05}$	58º
3	EP/mND$_{0.05}$	48º
4	EP/pND$_{0.2}$	68 º
5	EP/mND$_{0.2}$	62 º

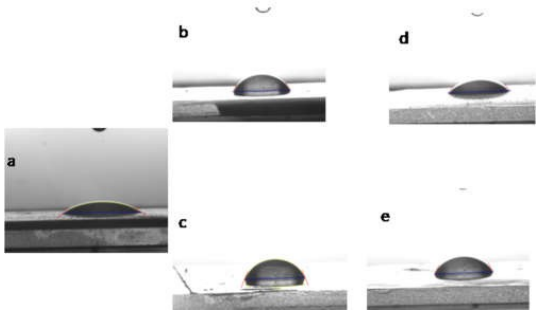

Figure 78: Evolution of droplet geometric shapes of (a) neat EP, (b) EP/pND$_{0.05}$, (c) EP/pND$_{0.2}$, (d) EP/mND$_{0.05}$, and (e) EP/mND$_{0.2}$

Summary of section 4.4

In summary, the FTIR reveals that there is well dispersion of ND into the EP matrix in both the pristine and acid-treated cases, improving their physical qualities. Highly interlinked nanocomposites with improved physical characteristics for structural applications are indicated by a sharp peak that corresponds to greater filler content (0.2 wt. %). The XRD patterns of neat epoxy are almost identical to those of epoxy-incorporated pristine and acid-treated ND nanocomposites and also reveal that the addition of ND to the EP matrix does not affect the microstructure of the nanocomposite. The microscopic study of the fractured surface of EP/pND

nanocomposites reveals that in addition to pristine ND added to the EP matrix, the smooth fracture surfaces converted into wavy rougher ones. On thermal analysis, the EP/mND nanocomposites were found to be thermally stable in comparison with the EP/pND nanocomposites and neat EP. The conductivity of EP/pND is found to be higher than that of EP/mND. It is also obtained that surface modification of ND enhances the hydrophilicity and wettability of EP/mND nanocomposites, which makes them applicable in biomedical applications.

CHAPTER 5

5. CONCLUSION AND RECOMMENDATIONS

5.1 Conclusions

a) The acid treatment method effectively functionalizes nanocarbons of various dimensionalities, as confirmed by spectral, thermal, and microscopic investigations. FTIR reveals oxygen-containing functional groups on the surface, while acid oxidation increases defect population, confirmed by Raman spectroscopy, indicating more defective sites. XRD analysis supports acid treatment surface modification of nanocarbons, with graphite nanoplatelets exfoliating into smaller sheets of graphene with high interlayer distance in GnP. The SEM analysis reveals that nanocarbons treated with acid exfoliated CNT bundles and graphene layers, and changed ND clusters into powder. The thermal degradation of acid-treated nanocarbons occurs at lower temperatures, indicating functionalization, while high impurities (20 %) are observed in acid-oxidized graphite nanoplatelets due to the use of manganese.

b) The addition of CNTs to the EP matrix enhances its physical characteristics, with a significant connection between the EP and mCNT, resulting in highly dispersed nanocomposites for structural applications. XRD analysis shows that adding CNT to epoxy doesn't affect the amorphous phase of the epoxy, and nanocomposites have similar diffraction patterns but a less intense peak. Microscopic examination reveals surface roughness in the EP matrix due to homogeneously dispersed CNT. The thermal examination shows that adding CNT to an EP matrix doesn't significantly improve the thermal stability of EP/pCNT and EP/mCNT nanocomposite. The electrical resistivity measurements reveal that the resistivity of EP/pCNT nanocomposites decreased by up to 40 times compared to acid-treated nanocomposites due to the network formation of CNT. However, the modified CNT nanocomposites exhibit increased resistivity because the breakage of CNTs shortens them, impairing efficient charge transport. The EP/pCNT exhibits hydrophobic behaviour, while the EP/mCNT shows hydrophilic behaviour with enhanced wettability, as determined by contact angle measurement.

c) FTIR analysis reveals -OH bond presence in graphite and EP matrix, well-blended EP/GnP nanocomposites at 0.05 and 0.2 wt. % filler concentrations. EP/mGnP

nanocomposite diffraction pattern shows the absence of graphite crystallite phase. Microscopic investigations show GnP incorporation in epoxy matrix enhances toughness and surface roughness, while thermal analysis shows EP/GnP nanocomposites are more thermally stable (5-11 ℃) than neat EP and acid-treated EP/mGnP nanocomposites. The EP/mGnP nanocomposite exhibited a significant decrease in resistivity, up to approximately 35 times compared to pristine graphite, due to the uniform dispersion of graphite particles within the EP matrix. The hydrophilic nature of the EP/mGnP nanocomposites with enhanced wettability was recorded.

d) The FTIR analysis reveals that ND is well dispersed in the epoxy matrix, enhancing its physical properties. Thus, prepared nanocomposites with superior physical properties are suitable for structural applications. XRD patterns show ND doesn't affect the microstructure of the nanocomposite. The microscopic analysis of the fractured surface of EP/pND nanocomposites shows that the smooth fracture surfaces changed into rougher ones with the integration of pristine ND into the EP matrix. EP/ND nanocomposites are thermally stable and have improved hydrophilicity and wettability, making them suitable for biomedical applications.

5.2 Recommendations for Future Work

The structural, morphological, thermal, electrical, and surface properties of different dimensionalities of nanocarbons (multiwall carbon nanotubes (1D), graphite nanoplatelets (2D), and nanodiamond (0D) of various sets of epoxy/nanocarbons nanocomposites have been successfully addressed in this study. However, some interesting topics could be explored which is not studied in this research. The following aspects may be addressed in future work.

1. It has been observed that the nanocomposites, particularly that of MWCNTs may be useful for conductive coating application. The detailed characteristics of this aspect may be further carried out in future work.

2. A detailed study regarding the mechanical properties and deformation behaviour ofthe nanocomposites comprising GnP nanoparticles applicable in various electronics may be performed in future work comprehensively.

3. The ND nanocomposites applicable in the biomedical fields correlating it with, detailed toxicological effects may be one of the most exciting topics for future work.

CHAPTER 6

6. SUMMARY

Aiming at the purposeful functionalization of different forms of nanocarbons and studying their nanocomposites with epoxy resins, extensive research works have been carried out. This chapter gives a glimpse of the entire thesis.

Chapter 1 introduces the general introduction of nanocarbons (NCs) and epoxy (EP) matrices. Nanostructured materials like carbon nanotubes (CNT), graphite nanoplatelets (GnP), and nanodiamonds (ND) are popular due to their high aspect ratio and superior electrical, thermal, optical, and mechanical properties. They are particularly blended with epoxy for application in the aerospace, transportation, automotive, and electronic industries because of the matrix's superior mechanical and bonding properties, exceptional chemical stability, and ease of processing. The non-homogeneous dispersion due to intermolecular Van der Waals interactions is responsible for the difficulties in the fabrication of composites. Commercially available nanocarbons have amorphous carbon, metal catalysts, and impurities, which can degrade their physical properties. The objectives of study are to functionalize nanocarbons of different dimensions and investigate the physical properties of their nanocomposites with thermosetting polymers.

Chapter 2 explores synthesis, functionalization procedures of NCs, composite preparation methods, and their structural, thermal, electrical, morphological, and mechanical properties. It has been found that to improve the compatibility of nanocarbon and epoxy polymers to enhance their physical, thermal, mechanical, and electrical properties, the functionalization of nanocarbon was accomplished *via* oxidation experiments, wet chemical methods, surface amidation methods, and remote photocatalytic oxidation methods, including atom transfer radical polymerization, microwave-assisted techniques, grafting of organic compounds, treatment with an inorganic acid, and basic oxidative methods. The various techniques like ultrasonication, high shear mixing, solution casting, sonication, and mixing and moulding to prepare epoxy/nanocarbon (EP/NCs) nanocomposites and their electrical, thermal, and mechanical properties were explored. It has been reported that the incorporation of NCs into the EP matrix improved its thermal, electrical, and

mechanical properties to a certain filler wt. %. However, if we go beyond a certain point, their properties start to deteriorate due to agglomeration. However, it is still unclear whether the functionalization of nanocarbons varies with their dimensionality and whether there is a relationship between their dimensions and the physical characteristics of epoxy/nanocarbon nanocomposites. By comparing the functionalization and various properties of these three different nanocarbons, with varying dimensions, we were able to discuss the existing problem in this research study.

Chapter 3 discusses the detailed information of materials and methodology adopted to functionalize nanocarbons and to prepare EP/NCs nanocomposites. The three different nanocarbons namely multi-walled carbon nanotubes; Nanocyl 7000, Nanocyl SA, Belgium, graphite nanoplatelets; conductograpgh GFG 50M, SGL Carbon GmbH, Meitingen, Germany, nanodiamond powder; Nuevo Blend Carbodeon, Pakkalankuja, Vantaa, Finland were used in this research work. These three different nanocarbons (NCs) were functionalized by treatment with different inorganic acids. The nanocarbons functionalization process was confirmed through FTIR, Raman, XRD, TGA, and FESEM. Further, the EP/NCs nanocomposites were prepared by incorporating pristine and acid-treated nanocarbons into the EP matrix *via* physical mixing assisted by ultrasonication. These EP/NCs nanocomposites were subjected to structural, morphological, thermal, electrical, and wetting properties. The structural properties of the nanocomposites were determined by FTIR; IR Prestige 21, ZnSe ATR, 4000 cm^{-1}, and 600 cm^{-1}. The morphology of the nanocomposites was studied using XRD; Rigaku, Miniflex 600, Cu Kα, and FESEM; Hitachi SU8010, Japan, with an acceleration voltage of 3 kV. The thermal properties were carried out using TGA; SDT 0600, 30 °C-700 °C at the heating rate of 10 °C /min. Their electrical and surface properties are well studied through two probe methods; ADEC Embedded Tech, 3kV and contact angle measurement test; FTA 100 series, Portsmouth, Virginia, 23704, USA using distilled water.

Chapter 4 covers the results and discussion part. The results are briefly summarized in the following paragraphs. The study investigated electrical and surface properties of EP/NCs nanocomposites with varying wt. % of fillers correlating with structural, thermal and morphological analysis. It first functionalized nanocarbons (multiwall

carbon nanotubes CNTs; 1D, graphite nanoplatelets GnP; 2D, and nanodiamonds ND; 0D) to increase hydrophilicity and reactivity by wet method. The rise in the defect population of sp^3 hybridized carbon atoms and the addition of functional groups containing oxygen were confirmed by spectroscopy. Exfoliation and the transformation of a cluster into powder were explained by XRD and microscopic examination; however, the thermogravimetric study revealed mass loss at lower temperatures.

EP/NCs nanocomposites were developed by adding pristine and functionalized NCs to the EP matrix through physical mixing and ultrasonication. Spectroscopy, thermal, and microscopic methods were used to characterize the nanomaterials. FTIR spectra showed well dispersion of the components, while XRD analysis showed no impact on crystallinity. NCs were uniformly distributed in the EP matrix, displaying a rough, cloud-like fractured and river-like surface pattern. CNTs resist crack propagation and shorten upon acid treatment, proving apotential material for EP/NCs nanocomposites. EP/NCs showed improvement in thermal stability by 5-13 ℃ in TGA thermograms with pristine and acid-treated nanocarbons. The resistivity of EP/pCNT nanocomposites decreased by up to approximately 40 times compared to acid-treated counterparts. The increased resistivity of EP/mCNT was attributed to the shortening of carbon nanotube length, altering its aspect ratio upon acid treatment. Conversely, acid-treated graphite exhibited a resistivity decrease of up to about 35 times compared to pristine graphite due to the uniform dispersion of graphite particles within the EP matrix. The surface properties of acid-treated nanocomposites showed hydrophilic properties.

Chapters 5 and 6 finally conclude and summarize the whole work respectively.

REFERENCES

Aakash, A., & Selvaraj, S. (2020). Mechanical Properties of GFR & Graphite Epoxy Polymer Composites. *International Journal of Innovative Science and Research Technology*, **5**(6): 560–565. https://doi.org/10.38124/ijisrt20jun277

Abdullah, M. P., & Zulkepli, S. A. (2015). The Functionalization and Characterization of Multi-Walled Carbon Nanotubes (MWCNTs). *AIP Conference Proceedings*, **1678**(1). https://doi.org/10.1063/1.4931312

Abdullah, S. I., & Ansari, M. N. M. (2015). Mechanical Properties of Graphene Oxide (GO)/Epoxy Composites. *HBRC Journal*, **11**(2): 151–156. https://doi.org/10.1016/j.hbrcj.2014.06.001

Abuilaiwi, F. A., Laoui, T., Al-Harthi, M., & Atieh, M. A. (2010). Modification and Functionalization of Multiwalled Carbon Nanotube (MWCNT) *via* Fischer Esterification. *Arabian Journal for Science and Engineering*, **35**(1C): 37–48.

Ahmad, M. F., Mazuki, A. A. M., Yusof, N. M., Yahya, R., Zawawi, S. M. M., Mansor, N. A., & Zakaria, O. (2013). Functionalization by Acidic Treatment in the Purification of Multiwalled Carbon Nanotubes (MWCNTs). *Advanced Materials Research*, **685**: 155–158. https://doi.org/10.4028/www.scientific.net/AMR.685.155

Ahmad Mir, I., & Kumar, D. (2012). Carbon Nanotube-Filled Conductive Adhesives for Electronic Applications. *Nanoscience Methods*, **1**(1): 183–193. https://doi.org/10.1080/17458080.2011.602724

Ahmad, Z., Ansell, M. P., & Smedley, D. (2010). Effect of Nano- and Micro-Particle Additions on Moisture Absorption in Thixotropic Room Temperature Cure Epoxy-Based Adhesives for Bonded-in Timber Connections. *International Journal of Adhesion and Adhesives*, **30**(6): 448–455. https://doi.org/10.1016/j.ijadhadh.2010.04.001

Ahmed, D. S., Haider, A. J., & Mohammad, M. R. (2013). Comparison of Functionalization of Multi-Walled Carbon Nanotubes Treated by Oil Olive and

Nitric Acid and Their Characterization. *Energy Procedia*, **36**: 1111–1118. https://doi.org/10.1016/j.egypro.2013.07.126

Akhtar, K., Khan, S. A., Khan, S. B., & Asiri, A. M. (2018). Scanning Electron Microscopy: Principle and Applications in Nanomaterials Characterization. In *Handbook of Materials Characterization*. https://doi.org/10.1007/978-3-319-92955-2_4

Alajmi, M., & Shalwan, A. (2015). Correlation between Mechanical Properties with Specific Wear Rate and the Coefficient of Friction of Graphite/Epoxy Composites. *Materials*, **8**(7): 4162–4175. https://doi.org/10.3390/ma8074162

Alam, A., Wan, C., & McNally, T. (2017). Surface Amination of Carbon Nanoparticles for Modification of Epoxy Resins: Plasma-Treatment vs. Wet-Chemistry Approach. *European Polymer Journal*, **87**: 422–448. https://doi.org/10.1016/j.eurpolymj.2016.10.004

Albozahid, M., Diwan, A. A., & Habeeb, S. A. (2021). The Effect of Addition Graphite Filler on Mechanical Properties of Epoxy Material. *Egyptian Journal of Chemistry*, **64**(10): 5747–5754. https://doi.org/10.21608/ejchem.2021.73645.3638

Alhumade, H., Rezk, H., Nassef, A. M., & Al-Dhaifallah, M. (2019). Fuzzy Logic Based-Modeling and Parameter Optimization for Improving the Corrosion Protection of Stainless Steel 304 by Epoxy-Graphene Composite. *IEEE Access*, **7**: 100899–100909. https://doi.org/10.1109/ACCESS.2019.2930902

Aliyeva, S., Alosmanov, R., Buniyatzadeh, I., Azizov, A., & Maharramov, A. (2019). Recent Developments in Edge-Selective Functionalization of Surface of Graphite and Derivatives–a Review. *Soft Materials*, **17**(4): 448–466. https://doi.org/10.1080/1539445X.2019.1600549

Allaoui, A., Bai, S., Cheng, H. M., & Bai, J. B. (2002). Mechanical and Electrical Properties of a MWNT/Epoxy Composite. *Composites Science and Technology*, **62**(15): 1993–1998. https://doi.org/10.1016/S0266-3538(02)00129-X

AlMaadeed, M. A. A., Ponnamma, D., & El-Samak, A. A. (2020). Polymers to Improve the World and Lifestyle: Physical, Mechanical, and Chemical Needs. In *Polymer Science and Innovative Applications*. INC. https://doi.org/10.1016/b978-0-12-816808-0.00001-9

An Wong, C. H., Sofer, Z., Kubešová, M., Kučera, J., Matějková, S., & Pumera, M. (2014). Synthetic Routes Contaminate Graphene Materials with a Whole Spectrum of Unanticipated Metallic Elements. *Proceedings of the National Academy of Sciences of the United States of America*, **111**(38): 13774–13779. https://doi.org/10.1073/pnas.1413389111

Anas, S., Khan, Z., Rehman, G. ur, & Khan, M. B. (2015). Influence of MWCNTs as Secondary Reinforcement Material in Glass Fiber / Epoxy Composites Fabricated Using VARTM. *Applied Polymer Composites,* **2**(1): 17-26.

Ando, T., Tanaka, J., Ishii, M., Kamo, M., Sato, Y., Ohashi, N., & Shimosaki, S. (1993). Diffuse Reflectance Fourier-Transform Infrared Study of the Plasma-Fluorination of Diamond Surfaces Using a Microwave Discharge in CF4. *Journal of the Chemical Society, Faraday Transactions*, **89**(16): 3105–3109. https://doi.org/10.1039/FT9938903105

Anwar, Z., Kausar, A., Rafique, I., & Muhammad, B. (2016). Advances in Epoxy/Graphene Nanoplatelet Composite with Enhanced Physical Properties: A Review. *Polymer - Plastics Technology and Engineering*, **55**(6): 643–662. https://doi.org/10.1080/03602559.2015.1098695

Ardjmand, M., Omidi, M., & Choolaei, M. (2015). The Effects of Functionalized Multi-Walled Carbon Nanotube on Mechanical Properties of Multi-Walled Carbon Nanotube/Epoxy Composites. *Oriental Journal of Chemistry*, **31**(4): 2291–2301. https://doi.org/10.13005/ojc/310457

Aria, A. I., Kidambi, P. R., Weatherup, R. S., Xiao, L., Williams, J. A., & Hofmann, S. (2016). Time Evolution of the Wettability of Supported Graphene under Ambient Air Exposure. *Journal of Physical Chemistry C*, **120**(4): 2215–2224. https://doi.org/10.1021/acs.jpcc.5b10492

Atta, A. M., Shaker, N. O., & Nasser, N. E. (2008). Synthesis of Bisphenol a Novolac Epoxy Resins for Coating Applications. *Journal of Applied Polymer Science*, **107**(1): 347–354. https://doi.org/10.1002/app.26981

Ayatollahi, M. R., Alishahi, E., & Shadlou, S. (2011). Mechanical Behavior of Nanodiamond/Epoxy Nanocomposites. *International Journal of Fracture*, **170**(1): 95–100. https://doi.org/10.1007/s10704-011-9600-3

Bai, R. G., Muthoosamy, K., Manickam, S., & Hilal-Alnaqbi, A. (2019). Graphene-Based 3D Scaffolds in Tissue Engineering: Fabrication, Applications, and Future Scope in Liver Tissue Engineering. *International Journal of Nanomedicine*, 5753–5783. https://doi.org/10.2147/IJN.S192779

Banisaid, M., & Kharat, A.N. (2018). Synthesis and Characterizations of Nanodiamond and Its Application as Anti-Polishing Agent on SiO_2 Substrate. *International Journal of Chemical Sciences*, **16**(2): 1–10. https://doi.org/10.21767/0972-768x.1000262

Baptista, R., Mendão, A., Guedes, M., & Marat-Mendes, R. (2016). An Experimental Study on Mechanical Properties of Epoxy-Matrix Composites Containing Graphite Filler. *Procedia Structural Integrity*, **1**: 74–81. https://doi.org/10.1016/j.prostr.2016.02.011

Basso, L., Cazzanelli, M., Orlandi, M., & Miotello, A. (2020). Nanodiamonds: Synthesis and Application in Sensing, Catalysis, and the Possible Connection with Some Processes Occurring in Space. *Applied Sciences (Switzerland)*, **10**(12): 1–28. https://doi.org/10.3390/APP10124094

Bera, T., Acharya, S. K., & Mishra, P. (2018). *Synthesis , mechanical and thermal properties of carbon black / epoxy composites*. **10**(4): 12–20.

Bikiaris, D., Vassiliou, A., Chrissafis, K., Paraskevopoulos, K. M., Jannakoudakis, A., & Docoslis, A. (2008). Effect of Acid Treated Multi-Walled Carbon Nanotubes on the Mechanical, Permeability, Thermal Properties and Thermo-Oxidative Stability of Isotactic Polypropylene. *Polymer Degradation and Stability*, **93**(5): 952–967. https://doi.org/10.1016/j.polymdegradstab.2008.01.033

Bisht, A., Kumar, R. M., Dasgupta, K., & Lahiri, D. (2019). Spatial Distribution of Nanodiamond and Its Effect on Mechanical Behaviour of Epoxy Based Composite Using 2D Modulus Mapping. *Mechanics of Materials*, **135**: 114–128. https://doi.org/10.1016/j.mechmat.2019.05.008

Bogatyreva, G. P., Marinich, M. A., Ishchenko, E. V., Gvyazdovskaya, V. L., Bazalǐ, G. A., & Oleĭnik, N. A. (2004). Application of Modified Nanodiamonds as Catalysts of Heterogeneous and Electrochemical Catalyses. *Physics of the Solid State*, **46**(4): 738–741. https://doi.org/10.1134/1.1711462

Boukhvalov, D. W., Dreyer, D. R., Bielawski, C. W., & Son, Y. W. (2012). A Computational Investigation of the Catalytic Properties of Graphene Oxide: Exploring Mechanisms by Using DFT Methods. *ChemCatChem*, **4**(11): 1844–1849. https://doi.org/10.1002/cctc.201200210

Bouša, D., Luxa, J., Mazánek, V., Jankovský, O., Sedmidubský, D., Klímová, K., Pumera, M., & Sofer, Z. (2016). Toward Graphene Chloride: Chlorination of Graphene and Graphene Oxide. *RSC Advances*, **6**(71): 66884–66892. https://doi.org/10.1039/c6ra14845j

Bracco, G., & Holst, B. (2013). *Surface Science Techniques*, Springer Science & Business Media. https://doi.org/10.1007/978-3-642-34243-1

Breton, Y., Delpeux, S., Benoit, R., Salvetat, J. P., Sinturel, C., Beguin, F., Bonnamy, S., Desarmot, G., & Boufendi, L. (2002). Functionalization of Multiwall Carbon Nanotubes: Properties of Nanotubes-Epoxy Composites. *Molecular Crystals and Liquid Crystals*, **387**(1): 135–140. https://doi.org/10.1080/10587250215234

Breton, Y., Désarmot, G., Salvetat, J. P., Delpeux, S., Sinturel, C., Béguin, F., & Bonnamy, S. (2004). Mechanical Properties of Multiwall Carbon Nanotubes/Epoxy Composites: Influence of Network Morphology. *Carbon*, **42**(5–6): 1027–1030. https://doi.org/10.1016/j.carbon.2003.12.026

Bumbrah, G. S., & Sharma, R. M. (2016). Raman Spectroscopy – Basic Principle, Instrumentation and Selected Applications for the Characterization of Drugs of Abuse. *Egyptian Journal of Forensic Sciences*, **6**(3): 209–215.

https://doi.org/10.1016/j.ejfs.2015.06.001

Bunaciu, A. A., Udriştioiu, E. gabriela, & Aboul-Enein, H. Y. (2015). X-Ray Diffraction: Instrumentation and Applications. *Critical Reviews in Analytical Chemistry*, **45**(4): 289–299. https://doi.org/10.1080/10408347.2014.949616

Byrne, H. J. (2009). Thomas J. Webster (Ed.): Safety of Nanoparticles. From Manufacturing to Medical Applications. *Analytical and Bioanalytical Chemistry*, **395**(5): 1199–1200. https://doi.org/10.1007/s00216-009-3094-0

Cao, X. T., Patil, M. P., Phan, Q. T., Le, C. M. Q., Ahn, B. H., Kim, G. Do, & Lim, K. T. (2020). Green and Direct Functionalization of Poly (Ethylene Glycol) Grafted Polymers onto Single Walled Carbon Nanotubes: Effective Nanocarrier for Doxorubicin Delivery. *Journal of Industrial and Engineering Chemistry*, **83**: 173–180. https://doi.org/10.1016/j.jiec.2019.11.025

Cao, Y., Feng, J., & Wu, P. (2010). Preparation of Organically Dispersible Graphene Nanosheet Powders through a Lyophilization Method and Their Poly(Lactic Acid) Composites. *Carbon*, **48**(13): 3834–3839. https://doi.org/10.1016/j.carbon.2010.06.048

Charles, J., Ramkumaar, G. R., Azhagiri, S., & Gunasekaran, S. (2009). FTIR and Thermal Studies on Nylon-66 and 30% Glass Fibre Reinforced Nylon-66. *E-Journal of Chemistry*, **6**(1): 23–33. https://doi.org/10.1155/2009/909017

Chauhan, S., Jain, N., & Nagaich, U. (2020). Nanodiamonds with Powerful Ability for Drug Delivery and Biomedical Applications: Recent Updates on in Vivo Study and Patents. *Journal of Pharmaceutical Analysis*, **10**(1): 1–12. https://doi.org/10.1016/j.jpha.2019.09.003

Chemi, A., Zidour, M., Heireche, H., Rakrak, K., & Bousahla, A. A. (2018). Critical Buckling Load of Chiral Double-Walled Carbon Nanotubes Embedded in an Elastic Medium. *Mechanics of Composite Materials*, **53**(6): 827–836. https://doi.org/10.1007/s11029-018-9708-x

Chen, H., Chen, Y., Zhan, H., Wu, G., Xu, J. M., & Wang, J. N. (2019). Preparation

of Carbon Nanotube/Epoxy Composite Films with High Tensile Strength and Electrical Conductivity by Impregnation under Pressure. *Frontiers of Materials Science*, **13**(2): 165–173. https://doi.org/10.1007/s11706-019-0460-5

Chen, J., Hamon, M. A., Hu, H., Chen, Y., Rao, A. M., Eklund, P. C., & Haddon, R. C. (1998). Solution Properties of Single-Walled Carbon Nanotubes. *Science*, **282**(5386): 95–98. https://doi.org/10.1126/science.282.5386.95

Chen, J., Han, J., & Xu, D. (2019). Thermal and Electrical Properties of the Epoxy Nanocomposites Reinforced with Purified Carbon Nanotubes. *Materials Letters*, **246:** 20–23. https://doi.org/10.1016/j.matlet.2019.03.037

Chen, X., & Li, J. (2020). Superlubricity of Carbon Nanostructures. *Carbon*, **158**: 1–23. https://doi.org/10.1016/j.carbon.2019.11.077

Chen, X., Wang, J., Lin, M., Zhong, W., Feng, T., Chen, X., Chen, J., & Xue, F. (2008). Mechanical and Thermal Properties of Epoxy Nanocomposites Reinforced with Amino-Functionalized Multi-Walled Carbon Nanotubes. *Materials Science and Engineering A*, **492**(1–2): 236–242. https://doi.org/10.1016/j.msea.2008.04.044

Chen, X., & Li, J. (2020). Superlubricity of Carbon Nanostructures.*Carbon*,**158**: 1–23. https://doi.org/10.1016/j.carbon.2019.11.077

Cheng, Q., Wang, J., Jiang, K., Li, Q., & Fan, S. (2008). Fabrication and Properties of Aligned Multiwalled Carbon Nanotube-Reinforced Epoxy Composites. *Journal of Materials Research*, **23**(11): 2975–2983. https://doi.org/10.1557/JMR.2008.0356

Chou, C. C., & Lee, S. H. (2010). Tribological Behavior of Nanodiamond-Dispersed Lubricants on Carbon Steels and Aluminum Alloy. *Wear*, **269**(11–12): 757–762. https://doi.org/10.1016/j.wear.2010.08.001

Chow, W. S., & Tan, P. L. (2010). Epoxy/Multiwall Carbon Nanotube Nanocomposites Prepared by Sonication and Planetary Mixing Technique. *Journal of Reinforced Plastics and Composites*, **29**(15): 2331–2342.

https://doi.org/10.1177/0731684409348346

Chua, C. K., Sofer, Z., & Pumera, M. (2012). Graphite Oxides: Effects of Permanganate and Chlorate Oxidants on the Oxygen Composition. *Chemistry - A European Journal*, **18**(42): 13453–13459. https://doi.org/10.1002/chem.201202320

Chung, D. D. L. (2002). Review: Graphite. *Journal of Materials Science*, **37**(8): 1475–1489. https://doi.org/10.1023/A:1014915307738

Ciszewski, M., & Mianowski, A. (2013). Survey of Graphite Oxidation Methods Using Oxidizing Mixtures in Inorganic Acids. *Chemik*, **67**(4): 267–274.

Corcione, C. E., Malucelli, G., Frigione, M., & Maffezzoli, A. (2009). UV-Curable Epoxy Systems Containing Hyperbranched Polymers: Kinetics Investigation by Photo-DSC and Real-Time FT-IR Experiments. *Polymer Testing*, **28**(2): 157–164. https://doi.org/10.1016/j.polymertesting.2008.11.002

Cunningham, B. D., Huang, J., & Baird, D. G. (2007). Development of Bipolar Plates for Fuel Cells from Graphite Filled Wet-Lay Material and a Thermoplastic Laminate Skin Layer. *Journal of Power Sources*, **165**(2): 764–773. https://doi.org/10.1016/j.jpowsour.2006.12.035

Darabi, H. R., Jafar Tehrani, M., Aghapoor, K., Mohsenzadeh, F., & Malekfar, R. (2012). A New Protocol for the Carboxylic Acid Sidewall Functionalization of Single-Walled Carbon Nanotubes. *Applied Surface Science*, **258**(22): 8953–8958. https://doi.org/10.1016/j.apsusc.2012.05.126

Das, R., Hamid, S., Ali, M., Ramakrishna, S., & Yongzhi, W. (2014). Carbon Nanotubes Characterization by X-Ray Powder Diffraction – A Review. *Current Nanoscience*, **11**(1): 23–35. https://doi.org/10.2174/15734137106661408182100 43

Datsyuk, V., Kalyva, M., Papagelis, K., Parthenios, J., Tasis, D., Siokou, A., Kallitsis, I., & Galiotis, C. (2008). Chemical Oxidation of Multiwalled Carbon Nanotubes. *Carbon*, **46**(6): 833–840. https://doi.org/10.1016/j.carbon.2008.02.012

De Juan, A., & Pérez, E. M. (2013). Getting Tubed: Mechanical Bond in Endohedral Derivatives of Carbon Nanotubes? *Nanoscale*, **5**(16): 7141–7148. https://doi.org/10.1039/c3nr01683h

Dervishi, E., Li, Z., Xu, Y., Saini, V., Biris, A. R., Lupu, D., & Biris, A. S. (2009). Carbon Nanotubes: Synthesis, Properties, and Applications. *Particulate Science and Technology*, **27**(2): 107–125. https://doi.org/10.1080/02726350902775962

Desai, C., & Mitra, S. (2013). Microwave Induced Carboxylation of Nanodiamonds. *Diamond and Related Materials*, **34**: 65–69. https://doi.org/10.1016/j.diamond.2013.02.005

Dewangan, R., Asthana, A., Singh, A. K., & Carabineiro, S. A. C. (2021). Control of Surface Functionalization of Graphene-Metal Oxide Polymer Nanocomposites Prepared by a Hydrothermal Method. *Polymer Bulletin*, **78**(8): 4665–4683. https://doi.org/10.1007/s00289-020-03342-w

Dhawane, S. H., Kumar, T., & Halder, G. (2018). Recent advancement and prospective of heterogeneous carbonaceous catalysts in chemical and enzymatic transformation of biodiesel. Energy Conversion and Management, 167, 176-202

Diaz-chacon, L., Metz, R., Dieudonné, P., Bantignies, J. L., Tahir, S., Hassanzadeh, M., Sosa, E., Atencio, R., Lc, L. C. C., Montpellier, U. M. R. C. De, & Lyon, U. (2015). Graphite Nanoplatelets Composite Materials : Role of the Epoxy-System in the Thermal Conductivity. *Journal of Materials Science and Chemical Engineering*, **3**: 75–87. https://doi.org/http://dx.doi.org/10.4236/msce.2015.35009

Dillon, A. C., Gennett, T., Jones, K. M., Alleman, J. L., Parilla, P. A., & Heben, M. J. (1999). Simple and Complete Purification of Single-Walled Carbon Nanotube Materials. *Advanced Materials*, **11**(16): 1354–1358. https://doi.org/10.1002/(SICI)1521-4095(199911)11:16<1354::AID-ADMA1354>3.0.CO;2-N

Dimiev, A., Kosynkin, D. V, Alemany, L. B., Chaguine, P., & Tour, J. M. (2012). Pristine Graphite Oxide. *Jounal of the American Chemical Society*, **134**: 2851–2822. https://doi.org/10.1021/ja211531y

Dolmatov, V. Y. (2001). Detonation Synthesis Ultradispersed Diamonds: Properties and Applications. *Uspekhi Khimii*, **70**(7): 706–708. https://doi.org/10.1070/rc2001v070n07abeh000665

Earp, B., Hubbard, J., Tracy, A., Sakoda, D. & Luhrs, C. (2021). Electrical Behavior of CNT Epoxy Composites under In-Situ Simulated Space Environments. *Composites Part B: Engineering*, **219**: 108874. https://doi.org/10.1016/j.compositesb.2021.108874.

El Moumen, A., Tarfaoui, M., & Lafdi, K. (2017). Mechanical Characterization of Carbon Nanotubes Based Polymer Composites Using Indentation Tests. *Composites Part B: Engineering*, **114**: 1–7. https://doi.org/10.1016/j.compositesb.2017.02.005

Fan, M., Liu, J., Li, X., Cheng, J., & Zhang, J. (2013). Curing Behaviors and Properties of an Extrinsic Toughened Epoxy/Anhydride System and an Intrinsic Toughened Epoxy/Anhydride System. *Thermochimica Acta*, **554**: 39–47. https://doi.org/10.1016/j.tca.2012.12.007

Farooq, U., Ali, M. U., Hussain, S. J., Ahmad, M. S., Zafar, A., Ghafoor, U., & Subhani, T. (2021). Improved Ablative Properties of Nanodiamond-Reinforced Carbon Fiber–Epoxy Matrix Composites. *Polymers*, **13**: 2035. https://doi.org/10.3390/polym13132035

Fatin, M. F., Ruslinda, A. R., Arshad, M. K. M., Hashim, U., Norhafizah, S., & Farehanim, M. A. (2014). Surface Functionalization of Multiwalled Carbon Nanotube for Biosensor Device Application. *IEEE International Conference on Semiconductor Electronics, Proceedings, (ICS2014)E*, 377–379. https://doi.org/10.1109/SMELEC.2014.6920876

Ferdosian, F., Ebrahimi, M., & Jannesari, A. (2013). Curing Kinetics of Solid Epoxy/DDM/Nanoclay: Isoconversional Modelsversus Fitting Model. *Thermochimica Acta*, **568**: 67–73. https://doi.org/10.1016/j.tca.2013.06.001

Ferrari, A. C., & Robertson, J. (2004). Raman Spectroscopy of Amorphous, Nanostructured, Diamond-like Carbon, and Nanodiamond. *Philosophical*

Transactions of the Royal Society A: Mathematical, Physical and Engineering Sciences, **362**(1824): 2477–2512. https://doi.org/10.1098/rsta.2004.1452

Flores, M., Fernández-Francos, X., Ferrando, F., Ramis, X., & Serra, À. (2012). Efficient Impact Resistance Improvement of Epoxy/Anhydride Thermosets by Adding Hyperbranched Polyesters Partially Modified with Undecenoyl Chains. *Polymer*, **53**(23): 5232–5241. https://doi.org/10.1016/j.polymer.2012.09.031

Foix, D., Ramis, X., Serra, A., & Sangermano, M. (2011). UV Generation of a Multifunctional Hyperbranched Thermal Crosslinker to Cure Epoxy Resins. *Polymer*, **52**(15): 3269–3276. https://doi.org/10.1016/j.polymer.2011.05.029

Foix, D., Rodríguez, M. T., Ferrando, F., Ramis, X., & Serra, A. (2012). Combined Use of Sepiolite and a Hyperbranched Polyester in the Modification of Epoxy/Anhydride Coatings: A Study of the Curing Process and the Final Properties. *Progress in Organic Coatings*, **75**(4): 364–372. https://doi.org/10.1016/j.porgcoat.2012.07.013

Frank, K., Childers, C., Dutta, D., Gidley, D., Jackson, M., Ward, S., Maskell, R., & Wiggins, J. (2013). Fluid Uptake Behavior of Multifunctional Epoxy Blends. *Polymer*, **54**(1): 403–410. https://doi.org/10.1016/j.polymer.2012.11.065

Friedrich, K. (1986). *Friction and wear of polymer composites,* Elsevier. https://doi.org/10.1016/0266-3538(87)90078-9

Gantayat, S., Sarkar, N., Prusty, G., Rout, D., & Swain, S. K. (2018). Designing of Epoxy Matrix by Chemically Modified Multiwalled Carbon Nanotubes. *Advances in Polymer Technology*, **37**(1): 176–184. https://doi.org/10.1002/adv.21654

Gao, W., Alemany, L. B., Ci, L., & Ajayan, P. M. (2009). New Insights into the Structure and Reduction of Graphite Oxide. *Nature Chemistry*, **1**(5): 403–408. https://doi.org/10.1038/nchem.281

Gao, W., Majumder, M., Alemany, L. B., Narayanan, T. N., Ibarra, M. A., Pradhan, B. K., & Ajayan, P. M. (2011). Engineered Graphite Oxide Materials for

Application in Water Purification. *ACS Applied Materials and Interfaces*, **3**(6): 1821–1826. https://doi.org/10.1021/am200300u

Giammarco, J., Mochalin, V. N., Haeckel, J., & Gogotsi, Y. (2016). The Adsorption of Tetracycline and Vancomycin onto Nanodiamond with Controlled Release. *Journal of Colloid and Interface Science*, **468**: 253–261. https://doi.org/10.1016/j.jcis.2016.01.062

Golaz, B., Michaud, V., & Månson, J. E. (2013). Photo-Polymerized Epoxy Primer for Adhesion Improvement at Thermoplastics / Metallic Wires Interfaces. *Composites Part A*: Applied Science and Manufacturing, **48**: 171–180. https://doi.org/10.1016/j.compositesa.2013.01.017

Gong, W., He, D., Tao, J., Zhao, P., Kong, L., Luo, Y., Peng, Z., & Wang, H. (2015). Formation of Defects in the Graphite Oxidization Process: A Positron Study. *RSC Advances*, **5**(108): 88908–88914. https://doi.org/10.1039/c5ra14660g

Goze-Bac, C. (2008). *NMR studies of carbon nanotubes and derivatives* (Doctoral dissertation). University Montpellier.

Grundke, K., Bogumil, T., Gietzelt, T., Jacobasch, H. J., Kwok, D. Y., & Neumann, A. W. (1996). Wetting Measurements on Smooth, Rough and Porous Solid Surfaces. *Progress in Colloid and Polymer Science*, **101**: 58–68. https://doi.org/10.1007/bfb0114445

Gu, W., Peters, N., & Yushin, G. (2013). Functionalized Carbon Onions, Detonation Nanodiamond and Mesoporous Carbon as Cathodes in Li-Ion Electrochemical Energy Storage Devices. *Carbon*, **53**: 292–301. https://doi.org/10.1016/j.carbon.2012.10.061

Guo, H., Wang, X., Qian, Q., Wang, F., & Xia, X. (2009). A Green Approach to the Synthesis Of. *ACS Nano*, **3**(9): 2653–2659. https://doi.org/10.1021/nn900227d

Guo, P., Chen, X., Gao, X., Song, H., & Shen, H. (2007). Fabrication and Mechanical Properties of Well-Dispersed Multiwalled Carbon Nanotubes/Epoxy Composites. *Composites Science and Technology*, **67**(15–16): 3331–3337.

https://doi.org/10.1016/j.compscitech.2007.03.026

Guo, T., Wu, J., Gao, H., & Chen, Y. (2017). Covalent Functionalization of Multi-Walled Carbon Nanotubes with Spiropyran for High Solubility Both in Water and in Non-Aqueous Solvents. *Inorganic Chemistry Communications*, **83**: 31–35. https://doi.org/10.1016/j.inoche.2017.06.002

Haleem, Y. A., Song, P., Liu, D., Wang, C., Gan, W., Saleem, M. F., & Song, L. (2016). The Effect of High Concentration and Small Size of Nanodiamonds on the Strength of Interface and Fracture Properties in Epoxy Nanocomposite. *Materials*, **9**(7): 507. https://doi.org/10.3390/ma9070507

Hameed, N., Thomas, S. P., Abraham, R., & Thomas, S. (2007). Morphology and Contact Angle Studies of Poly(Styrene-Co-Acrylonitrile) Modified Epoxy Resin Blends and Their Glass Fibre Reinforced Composites. *Express Polymer Letters*, **1**(6): 345–355. https://doi.org/10.3144/expresspolymlett.2007.49

Hirsch, A. (2002). Functionalization of Single-Walled Carbon Nanotubes. *Angewandte Chemie - International Edition*, **41**(11): 1853–1859. https://doi.org/10.1002/1521-3773(20020603)41:11<1853::AID-ANIE1853>3.0.CO;2-N

Hirsch, A., & Vostrowsky, O. (2005). Functionalization of Carbon Nanotubes. *Topics in Current Chemistry*, **245**: 193–237. https://doi.org/10.1007/b98169

Hoseinpour, S., Jafarzadeh, Y., Yegani, R., & Masoumi, S. (2019). Embedding Neat and Carboxylated Nanodiamonds into Polypropylene Membranes to Enhance Antifouling Properties. *Polyolefins Journal*, **6**(1): 63–74. https://doi.org/10.22063/poj.2018.2264.1120

Hsu, Y. G., Lin, K. H., Lin, T. Y., Fang, Y. L., Chen, S. C., & Sung, Y. C. (2012). Properties of Epoxy-Amine Networks Containing Nanostructured Ether-Crosslinked Domains. *Materials Chemistry and Physics*, **132**(2–3): 688–702. https://doi.org/10.1016/j.matchemphys.2011.11.087

Huang, H., Dai, L., Wang, D. H., Tan, L. S., & Osawa, E. (2008). Large-Scale Self-

Assembly of Dispersed Nanodiamonds. *Journal of Materials Chemistry*, **18**(12): 1347–1352. https://doi.org/10.1039/b716676a

Huang, T. S., Tzeng, Y., Liu, Y. K., Chen, Y. C., Walker, K. R., Guntupalli, R., & Liu, C. (2004). Immobilization of Antibodies and Bacterial Binding on Nanodiamond and Carbon Nanotubes for Biosensor Applications. *Diamond and Related Materials*, **13**(4–8): 1098–1102. https://doi.org/10.1016/j.diamond.2003.11.047

Hunge, Y. M., Yadav, A. A., Khan, S., Takagi, K., Suzuki, N., Teshima, K., Terashima, C., & Fujishima, A. (2021). Photocatalytic Degradation of Bisphenol A Using Titanium Dioxide@nanodiamond Composites under UV Light Illumination. *Journal of Colloid and Interface Science*, **582**. 1058–1066. https://doi.org/10.1016/j.jcis.2020.08.102

Hwang, I. U., Yu, H. N., Kim, S. S., Lee, D. G., Suh, J. Do, Lee, S. H., Ahn, B. K., Kim, S. H., & Lim, T. W. (2008). Bipolar Plate Made of Carbon Fiber Epoxy Composite for Polymer Electrolyte Membrane Fuel Cells. *Journal of Power Sources*, **184**(1): 90–94. https://doi.org/10.1016/j.jpowsour.2008.05.088

Iijima, S. (1991). Helical microtubules of graphitic carbon. *Nature*, **354**(6348), 56–58. https://doi.org/10.1038/354056a0

Iijima, S., & Ichihashi, T. (1993). Single-Shell Carbon Nanotubes of 1-Nm Diameter. *Nature*, **363**: 603–605. https://doi.org/https://doi.org/10.1038/363603a0

Im, J. S., Lee, S. K., In, S. J., & Lee, Y. S. (2010). Improved Flame Retardant Properties of Epoxy Resin by Fluorinated MMT/MWCNT Additives. *Journal of Analytical and Applied Pyrolysis*, **89**(2): 225–232. https://doi.org/10.1016/j.jaap.2010.08.003

Ismail, A. A., Voort, F. R. Van De, & Sedman, J. (1997). Fourier Transform Infrared Spectroscopy : Principles and Applications. In *Techniques and Instrumentation in Analytical Chemistry*, **18**: 93-139, Elsevier.

Ivanov, E., Petrova, I., Kotsilkova, R., & Mihailova, V. (2014). Epoxy/Multi-Walled

Carbon Nanotube Composites - Structure, Viscoelastic and Nanomechanical Properties. *Nanoscience and Nanotechnology Letters*, **6**(7): 624–629. https://doi.org/10.1166/nnl.2014.1698

Jamal, G. M., & Abdullah, O. G. (2023). The Use of Multi-Wall Carbon Nanotube for Improving the Mechanical Performance of Epoxy Resin Based Metal Oxide Hybrid Nanocomposites. *ECS Journal of Solid State Science and Technology,* **12**(9). https://doi.org/10.1149/2162-8777/acf36d

Januszewski, R., Dutkiewicz, M., Nowicki, M., Szołyga, M., & Kownacki, I. (2021). Synthesis and Properties of Epoxy Resin Modified with Novel Reactive Liquid Rubber-Based Systems. *Industrial and Engineering Chemistry Research*, **60**(5): 2178–2186. https://doi.org/10.1021/acs.iecr.0c05781

Jawhari, T., Roid, A., & Casado, J. (1995). Raman Spectroscopic Characterization of Some Commercially Available Carbon Black Materials. *Carbon*, **33**(11): 1561–1565. https://doi.org/10.1016/0008-6223(95)00117-V

Jeon, I., Wook, D., Ashok, N., & Baek, J.-B. (2011). Functionalization of Carbon Nanotubes. In S. Yellampalli (Ed.), *Carbon Nanotubes - Polymer Nanocomposites*. InTech. https://doi.org/10.5772/18396

Jeong, H. K., Lee, Y. P., Jin, M. H., Kim, E. S., Bae, J. J., & Lee, Y. H. (2009). Thermal Stability of Graphite Oxide. *Chemical Physics Letters*, **470**(4–6): 255–258. https://doi.org/10.1016/j.cplett.2009.01.050

Jin, F.L., & Park, S.J. (2012). Thermal Properties of Epoxy Resin/Filler Hybrid Composites. *Polymer Degradation and Stability*, **97**(11): 2148–2153. https://doi.org/10.1016/j.polymdegradstab.2012.08.015

Jin, F. L., Li, X., & Park, S. J. (2015). Synthesis and Application of Epoxy Resins: A Review. *Journal of Industrial and Engineering Chemistry*, **29**: 1–11. https://doi.org/10.1016/j.jiec.2015.03.026

Jin, F. L., & Park, S. J. (2009). Thermal Stability of Trifunctional Epoxy Resins Modified with Nanosized Calcium Carbonate. *Bulletin of the Korean Chemical*

Society, **30**(2): 334–338. https://doi.org/10.5012/bkcs.2009.30.2.334

Kamal, A. S., Othman, R., & Jabarullah, N. H. (2020). Preparation and Synthesis of Synthetic Graphite from Biomass Waste: A Review. *Systematic Reviews in Pharmacy*, **11**(2): 881–894.

Kaur, R., & Badea, I. (2013). Nanodiamonds as Novel Nanomaterials for Biomedical Applications: Drug Delivery and Imaging Systems. *International Journal of Nanomedicine*, **8**: 203–220. https://doi.org/10.2147/IJN.S37348

Kausar, A., Rafique, I. & Muhammad, B. (2016). Review of Applications of Polymer/Carbon Nanotubes and Epoxy/CNT Composites. *Polymer - Plastics Technology and Engineering*, **55**(11): 1167–1191. https://doi.org/10.1080/03602559.2016.1163588.

Kauasr, A., Rafique, I., & Muhammad, B. (2017). Significance of Carbon Nanotube in Flame Retardant Polymer/CNT Composite : A Review. *Polymer - Plastics Technology and Engineering*, **56**(5): 470–487. https://doi.org/https://doi.org/10.1080/03602559.2016.1233267

Kausar, A. (2018). Nanodiamond Reinforced Epoxy Composite: Prospective Material for Coatings. *Advanced Coating Materials*, (pp. 255–274). https://doi.org/10.1002/9781119407652.ch9

Kausar, A. (2019). Review on conducting polymer/nanodiamond nanocomposites: Essences and functional performance. *Journal of Plastic Film & Sheeting*, *35*(4), 331–353. https://doi.org/10.1177/8756087919835870

Kaushik, A., Singh, P., & Jyoti. (2010). Mechanical and Electrical Conductivity Study on Epoxy/Graphite Composites. *Journal of Reinforced Plastics and Composites*, **29**(7): 1038–1044. https://doi.org/10.1177/0731684409103055

Ke, P. L., Wu, Y. N., & Sun, C. (2011). Detonation Gun Sprayed Thermal Barrier Coatings. In *Thermal Barrier Coatings* (pp. 175–189). Elsevier. https://doi.org/10.1533/9780857090829.2.175

Khatiwada, S. P. (2020). *Effect of Block Copolymer (Bcp) Architecture on*

Morphology and Deformation Behaviour of Epoxy Resin / Bcp Blends (Unpublished doctoral dissertation). Central Department of Chemistry, Institute of Science and Technology, Tribhuvan University, Kathmandu, Nepal.

Khlobystov, A. N., Britz, D. A., & Briggs, G. A. D. (2005). Molecules in Carbon Nanotubes. *Accounts of Chemical Research*, **38**(12): 901–909. https://doi.org/10.1021/ar040287v

Kim, J., Cote, L. J., & Huang, J. (2012). Two Dimensional Soft Material: New Faces of Graphene Oxide. *Accounts of Chemical Research*, **45**(8): 1356–1364. https://doi.org/10.1021/ar300047s

Kim, S. H. (2008). Fabrication of Superhydrophobic Surfaces. *Journal of Adhesion Science and Technology*, **22**(3–4): 235–250. https://doi.org/10.1163/156856108X305156

Kocaman, S., Gursoy, M., Karaman, M., & Ahmetli, G. (2020). Synthesis and Plasma Surface Functionalization of Carbon Nanotubes for Using in Advanced Epoxy-Based Nanocomposites. *Surface and Coatings Technology*, **399**: 126144. https://doi.org/10.1016/j.surfcoat.2020.126144

Koo, M. Y., & Lee, G. W. (2015). Thermal Property of Multi-Walled-Carbon-Nanotube Reinforced Epoxy Composites. *International Journal of Chemical, Molecular, Nuclear, Materials and Metallurgical Engineering*, **9**(1): 25–29.

Koo, M. Y., Shin, H. C., Kim, W.-S., & Lee, G. W. (2014). Properties of Multi-Walled Carbon Nanotube Reinforced Epoxy Composites Fabricated by Using Sonication and Shear Mixing. *Carbon Letters*, **15**(4): 255–261. https://doi.org/10.5714/cl.2014.15.4.255

Koumoulos, E. P., Jagadale, P., Lorenzi, A., Tagliaferro, A., & Charitidis, C. A. (2015). Evaluation of Surface Properties of Epoxy-Nanodiamonds Composites. *Composites Part B: Engineering*, **80**: 27–36. https://doi.org/10.1016/j.compositesb.2015.05.036

Kovářík, T., Bělský, P., Rieger, D., Ilavsky, J., Jandová, V., Maas, M., Šutta, P., Pola,

M., & Medlín, R. (2020). Particle Size Analysis and Characterization of Nanodiamond Dispersions in Water and Dimethylformamide by Various Scattering and Diffraction Methods. *Journal of Nanoparticle Research*, **22**(2): 1–17. https://doi.org/10.1007/s11051-020-4755-3

Krajewski, D., Oleksy, M., Oliwa, R., Bulanda, K., Czech, K., Mazur, D., & Masłowski, G. (2022). Methods for Enhancing the Electrical Properties of Epoxy Matrix Composites. *Energies*, **15**(13): 1–18. https://doi.org/10.3390/en15134562

Krueger, A., & Boedeker, T. (2008). Deagglomeration and Functionalisation of Detonation Nanodiamond with Long Alkyl Chains. *Diamond and Related Materials*, **17**(7–10): 1367–1370. https://doi.org/10.1016/j.diamond.2008.01.033

Krueger, A., & Lang, D. (2012). Functionality Is Key: Recent Progress in the Surface Modification of Nanodiamond. *Advanced Functional Materials*, **22**(5): 890–906. https://doi.org/10.1002/adfm.201102670

Krueger, A., Stegk, J., Liang, Y., Lu, L., & Jarre, G. (2008). Biotinylated Nanodiamond: Simple and Efficient Functionalization of Detonation Diamond. *Langmuir*, **24**(8): 4200–4204. https://doi.org/10.1021/la703482v

Krüger, A., Liang, Y., Jarre, G., & Stegk, J. (2006). Surface Functionalisation of Detonation Diamond Suitable for Biological Applications. *Journal of Materials Chemistry*, **16**(24): 2322–2328. https://doi.org/10.1039/b601325b

Kumar, A., Ghosh, P. K., Yadav, K. L., & Kumar, K. (2017). Thermo-Mechanical and Anti-Corrosive Properties of MWCNT/Epoxy Nanocomposite Fabricated by Innovative Dispersion Technique. *Composites Part B: Engineering*, **113**: 291–299. https://doi.org/10.1016/j.compositesb.2017.01.046

Kumar, A., Kumar, K., Ghosh, P. K., & Yadav, K. L. (2018). MWCNT/TiO_2 Hybrid Nano Filler toward High-Performance Epoxy Composite. *Ultrasonics Sonochemistry*, **41**: 37–46. https://doi.org/10.1016/j.ultsonch.2017.09.005

Lau, K.T., Shi, S.Q., Zhou, L.M., & Cheng, H.M. (2003). Micro-Hardness and Flexural Properties of Randomly-Oriented Carbon Nanotube Composites.

Journal of Composite Materials, **37**(4): 365–376. https://doi.org/10.1177/0021998303037004043

Le, V. T., Ngo, C. L., Le, Q. T., Ngo, T. T., Nguyen, D. N., & Vu, M. T. (2013). Surface Modification and Functionalization of Carbon Nanotube with Some Organic Compounds. *Advances in Natural Sciences: Nanoscience and Nanotechnology*, **4**(3): 4–9. https://doi.org/10.1088/2043-6262/4/3/035017

Lee, G. J., Park, J. J., Lee, M. K., & Rhee, C. K. (2017). Stable Dispersion of Nanodiamonds in Oil and Their Tribological Properties as Lubricant Additives. *Applied Surface Science*, **415**: 24–27. https://doi.org/10.1016/j.apsusc.2016.12.109

Lee, S. E., Cho, S., & Lee, Y. S. (2014). Mechanical and Thermal Properties of MWCNT-Reinforced Epoxy Nanocomposites by Vacuum Assisted Resin Transfer Molding. *Carbon Letters*, **15**(1): 32–37. https://doi.org/10.5714/CL.2014.15.1.032

Li, L., Davidson, J. L., & Lukehart, C. M. (2006). Surface Functionalization of Nanodiamond Particles *via* Atom Transfer Radical Polymerization. *Carbon*, **44**(11): 2308–2315. https://doi.org/10.1016/j.carbon.2006.02.023

Li, S., Hao, X., Wang, Z., Le, T., Zou, S., & Cao, X. (2021). Lab-on-a-Chip Analytical Devices. *Micro- and Nanotechnology Enabled Applications for Portable Miniaturized Analytical Systems*, *March*, 355–374. https://doi.org/10.1016/B978-0-12-823727-4.00001-8

Liang, Y., Meinhardt, T., Jarre, G., Ozawa, M., Vrdoljak, P., Schöll, A., Reinert, F., & Krueger, A. (2011). Deagglomeration and Surface Modification of Thermally Annealed Nanoscale Diamond. *Journal of Colloid and Interface Science*, **354**(1): 23–30. https://doi.org/10.1016/j.jcis.2010.10.044

Lin, Z. (2014). *Functionalized Graphene for Energy Storage and Conversion* (Doctoral dissertation), Georgia Institute of Technology.

Liu, H., Wang, J., Wang, J., & Cui, S. (2018). Sulfonitric Treatment of Multiwalled

Carbon Nanotubes and Their Dispersibility in Water. *Materials*, **11**(12). https://doi.org/10.3390/ma11122442

Loh, K. P., Bao, Q., Eda, G., & Chhowalla, M. (2010). Graphene Oxide as a Chemically Tunable Platform for Optical Applications. *Nature Chemistry*, **2**(12): 1015–1024. https://doi.org/10.1038/nchem.907

Mahmood, O. A., Jameel, Z. N., & Abdullah, H. W. (2021). Effect of Different Multi-Walled Carbon Nanotubes MWCNTs on Mechanical and Physical Properties of Epoxy Nanocomposites. *IOP Conference Series: Materials Science and Engineering*, **1094**(1): 012166. https://doi.org/10.1088/1757-899x/1094/1/012166

Maitra, U., Prasad, K. E., Ramamurty, U., & Rao, C. N. R. (2009). Mechanical Properties of Nanodiamond-Reinforced Polymer-Matrix Composites. *Solid State Communications*, **149**(39–40): 1693–1697. https://doi.org/10.1016/j.ssc.2009.06.017

Mann, D., Bos, J. C., & Way, A. (1999). Automotive Plastics and Composites. In *International Journal of Advanced Engineering Research and Studies E*. Elsevier. https://doi.org/10.1016/B978-1-85617-349-0.X5000-4

Mansfield, E., Kar, A., Wang, C. M., & Chiaramonti, A. N. (2013). Statistical Sampling of Carbon Nanotube Populations by Thermogravimetric Analysis. *Analytical and Bioanalytical Chemistry*, **405**(25): 8207–8213. https://doi.org/10.1007/s00216-013-7221-6

Markets, W. (2007). *Automotive Plastics and Composites*,UK, Elsevier Advance Technology.

Maultzsch, J., Reich, S., Thomsen, C., Webster, S., Czerw, R., Carroll, D. L., Vieira, S. M. C., Birkett, P. R., & Rego, C. A. (2002). Raman Characterization of Boron-Doped Multiwalled Carbon Nanotubes. *Applied Physics Letters*, **81**(14): 2647–2649. https://doi.org/10.1063/1.1512330

Mbayachi, V. B., Ndayiragije, E., Sammani, T., Taj, S., Mbuta, E. R., & Khan, A. ullah. (2021). Graphene Synthesis, Characterization and Its Applications: A

Review. *Results in Chemistry*, **3**: 100163. https://doi.org/10.1016/j.rechem.2021.100163

McCoy, J. D., Ancipink, W. B., Clarkson, C. M., Kropka, J. M., Celina, M. C., Giron, N. H., Hailesilassie, L., & Fredj, N. (2016). Cure Mechanisms of Diglycidyl Ether of Bisphenol A (DGEBA) Epoxy with Diethanolamine. *Polymer*, **105**: 243–254. https://doi.org/10.1016/j.polymer.2016.10.028

Meng, L., Fu, C., & Lu, Q. (2009). Advanced Technology for Functionalization of Carbon Nanotubes. *Progress in Natural Science*, **19**(7): 801–810. https://doi.org/10.1016/j.pnsc.2008.08.011

Miller, S. G., Bauer, J. L., Maryanski, M. J., Heimann, P. J., Barlow, J. P., Gosau, J. M., & Allred, R. E. (2010). Characterization of Epoxy Functionalized Graphite Nanoparticles and the Physical Properties of Epoxy Matrix Nanocomposites. *Composites Science and Technology*, **70**(7): 1120–1125. https://doi.org/10.1016/j.compscitech.2010.02.023

Mittal, G., Dhand, V., Rhee, K. Y., Park, S. J., & Lee, W. R. (2015). A Review on Carbon Nanotubes and Graphene as Fillers in Reinforced Polymer Nanocomposites. *Journal of Industrial and Engineering Chemistry*, **21**: 11–25. https://doi.org/10.1016/j.jiec.2014.03.022

Mittal, V., Saini, R. & Sinha, S. (2016). Natural Fiber-Mediated Epoxy Composites - A Review. *Composites Part B: Engineering*, **99**: 425–435. https://doi.org/10.1016/j.compositesb.2016.06.051.

Moaseri, E., Bazubandi, B., Baniadam, M., & Maghrebi, M. (2019). Enhancement in Mechanical Properties of Multiwalled Carbon Nanotube-Reinforced Epoxy Composites: Crosslinking of the Reinforcement with the Matrix *via* Diamines. *Polymer Engineering and Science*, **59**(9): 1905–1910. https://doi.org/10.1002/pen.25191

Mochalin, V. N., & Gogotsi, Y. (2015). Nanodiamond-Polymer Composites. *Diamond and Related Materials*, **58**: 161–171. https://doi.org/10.1016/j.diamond.2015.07.003

Mochalin, V. N., Pentecost, A., Li, X. M., Neitzel, I., Nelson, M., Wei, C., He, T., Guo, F., & Gogotsi, Y. (2013). Adsorption of Drugs on Nanodiamond: Toward Development of a Drug Delivery Platform. *Molecular Pharmaceutics*, **10**(10): 3728–3735. https://doi.org/10.1021/mp400213z

Mochane, M. J., Motaung, T. E., & Molloung, S. V. (2017). Morphology, Flammability, and Properties of Graphite Reinforced Polymer Composites. Systematic Review. *Polymer Composites*, **16**(2): 101–113. https://doi.org/0.1002/pc.24379

Mohl, M., Konya, Z., Kukovecz, A., & Kiricsi, I. (2007). Functionalization of Multi-Walled Carbon Nanotubes. *Materials Science Forum*, **537**: 623–630. https://doi.org/10.4028/www.scientific.net/msf.537-538.623

Montazeri, A., Javadpour, J., Khavandi, A., Tcharkhtchi, A., & Mohajeri, A. (2010). Mechanical Properties of Multi-Walled Carbon Nanotube/Epoxy Composites. *Materials and Design*, **31**(9): 4202–4208. https://doi.org/10.1016/j.matdes.2010.04.018

Moosa, B., Fhayli, K., Li, S., Julfakyan, K., Ezzeddine, A., & Khashab, N. M. (2014). Applications of Nanodiamonds in Drug Delivery and Catalysis. *Journal of Nanoscience and Nanotechnology*, **14**(1): 332–343. https://doi.org/10.1166/jnn.2014.9141

Morselli, D., Bondioli, F., Sangermano, M., & Messori, M. (2012). Photo-Cured Epoxy Networks Reinforced with TiO_2 in-situ Generated by Means of Non-Hydrolytic Sol-Gel Process. *Polymer*, **53**(2): 283–290. https://doi.org/10.1016/j.polymer.2011.12.006

Mostovoy, A. S., & Yakovlev, A. V. (2019). Reinforcement of Epoxy Composites with Graphite-Graphene Structures. *Scientific Reports*, **9**(1): 1–9. https://doi.org/10.1038/s41598-019-52751-z

Murphy, H., Papakonstantinou, P., & Okpalugo, T. T. (2006). Raman Study of Multiwalled Carbon Nanotubes Functionalized with Oxygen Groups. *Journal of Vacuum Science and Technology B: Microelectronics and Nanometer Structures*

Processing, Measurement, and Phenomena, **24**(2): 715–720. https://doi.org/10.1116/1.2180257

Nayak, S. K., Mohanty, S., & Nayak, S. K. (2020). Thermal, Electrical and Mechanical Properties of Expanded Graphite and Micro-SiC Filled Hybrid Epoxy Composite for Electronic Packaging Applications. *Journal of Electronic Materials*, **49**(1): 212–225. https://doi.org/10.1007/s11664-019-07681-x

Neitzel, I., Mochalin, V., Knoke, I., Palmese, G. R., & Gogotsi, Y. (2011). Mechanical Properties of Epoxy Composites with High Contents of Nanodiamond. *Composites Science and Technology*, **71**(5): 710–716. https://doi.org/10.1016/j.compscitech.2011.01.016

Neto, J. S. S., Banea, M. D., Cavalcanti, D. K. K., Queiroz, H. F. M., & Aguiar, R. A. A. (2020). Analysis of Mechanical and Thermal Properties of Epoxy Multiwalled Carbon Nanocomposites. *Journal of Composite Materials*, **54**(30): 4831–4840. https://doi.org/10.1177/0021998320939232

Nigmatullin, R. R., Baleanu, D., Povarova, D., Salah, N., Habib, S. S., & Memic, A. (2013). Raman Spectra of Nanodiamonds: New Treatment Procedure Directed for Improved Raman Signal Marker Detection. *Mathematical Problems in Engineering*, **2013**. https://doi.org/10.1155/2013/847076

Novotna, J., Salacova, J., Tomkova, B., & Mullerova, J. (2018). Study of The Conductivity of Various Size Forms Carbon Particles Used as Fillers of Epoxy Polymer Composites. *European Conference on Composite Materials*, **285**: 1–7.

Omalanga, S. L., Lyuke, S., & Nkazi, B. (2015). *Effect of Functionalized Multi-Walled Carbon Nanotubes on A Polysulfone Ultrafiltration Membrane* (Doctoral dissertation). Faculty of Engineering and the Built Environment, School of Chemical and Metallurgical Engineering, University of the Witwatersrand.

Ondarçuhu, T., Thomas, V., Nuñez, M., Dujardin, E., Rahman, A., Black, C. T., & Checco, A. (2016). Wettability of Partially Suspended Graphene. *Scientific Reports*, **6**(1). https://doi.org/10.1038/srep24237

Ones, D. A. E. J. (1978). Fourier Transform Infrared Spectra. *Fourier Transform Infrared Spectra*. https://doi.org/10.1016/c2009-0-22072-1

Ostyn, N. R., Thijs, B., Steele, J. A., Sree, S. P., Wangermez, W., Teyssandier, J., Minjauw, M. M., Li, J., Detavernier, C., Roeffaers, M. B. J., De Feyter, S., & Martens, J. A. (2021). Controlled Graphite Surface Functionalization Using Contact and Remote Photocatalytic Oxidation. *Carbon*, **172**: 637–646. https://doi.org/10.1016/j.carbon.2020.10.069

Pan, W. P., Xu, W., & Li, S. (2005). Fundamentals of TGA and SDT.

Pandit, R. (2014). *Templating Nanostructures in Epoxy Resin Using Styrenic Block Copolymers* (Unpublished doctoral dissertation). Central Department of Chemistry, Institute of Science and Technology, Tribhuvan University, Kathamandu, Nepal.

Parildar, R. A., & Ibik, A. A. B. (2013). Characterization of Tertiary Amine and Epoxy Functional All-Acrylic Coating System. *Progress in Organic Coatings*, **76**(6): 955–958. https://doi.org/10.1016/j.porgcoat.2012.10.019

Park, S. J., & Jin, F. L. (2004). Thermal Stabilities and Dynamic Mechanical Properties of Sulfone-Containing Epoxy Resin Cured with Anhydride. *Polymer Degradation and Stability*, **86**(3): 515–520. https://doi.org/10.1016/j.polymdegradstab.2004.06.003

Păun, C., Obreja, C., Comănescu, F., Tucureanu, V., Tutunaru, O., Romanitan, C., & Ionescu, O. (2019). Epoxy Nanocomposites Based on MWCNT. In *2019 International Semiconductor Conference (CAS)*, 237-240. IEEE. https://doi.org/10.1109/SMICND.2019.8923947

Pengisi, K., Berbilang, G., & Mekanikal, S. (2021). Effect of Multi-Sized Graphite Filler on the Mechanical Properties and Electrical Conductivity. *Sains Malaysiana*, **50**(7): 2025–2034.

Pereira, C. M. C. (2009). Flame Retardancy of Thermoset Polymers Based on Nanoparticles and Carbon Nanotubes. *Solid State Phenomena*, **151**: 79–87.

https://doi.org/10.4028/www.scientific.net/SSP.151.79

Pham, V. P., Jang, H. S., Whang, D., & Choi, J. Y. (2017). Direct Growth of Graphene on Rigid and Flexible Substrates: Progress, Applications, and Challenges. *Chemical Society Reviews*, **46**(20): 6276–6300. https://doi.org/10.1039/c7cs00224f

Pichler, T., Kukovecz, A., Kuzmany, H., & Kataura, H. (2003). Charge Transfer in Doped Single Wall Carbon Nanotubes. *Synthetic Metals*, **135**–**136**: 717–719. https://doi.org/10.1016/S0379-6779(02)00810-X

Pimenta, M. A., Dresselhaus, G., Dresselhaus, M. S., Cançado, L. G., Jorio, A., & Saito, R. (2007). Studying Disorder in Graphite-Based Systems by Raman Spectroscopy. *Physical Chemistry Chemical Physics*, **9**(11): 1276–1291. https://doi.org/10.1039/b613962k

Pitchiya, A. P., Le, N. T., Putnam, Z. A., Harrington, M., & Krishnan, S. (2021). Microporous Graphite Composites of Tailorable Porosity, Surface Wettability, and Water Permeability for Fuel Cell Bipolar Plates. *Industrial and Engineering Chemistry Research*, **60**(28): 10203–10216. https://doi.org/10.1021/acs.iecr.1c01737

Post, G., Dolmatov, V. Y., Marchukov, V. A., Sushchev, V. G., Veretennikova, M. V., & Sal'ko, A. E. (2002). Industrial Synthesis of Ultradisperse Detonation Diamonds and Some Fields of Their Use. *Russian Journal of Applied Chemistry*, **75**(5): 755–760. https://doi.org/10.1023/A:1020354411417

Prabhakar, N., & Rosenholm, J. M. (2019). Nanodiamonds for Advanced Optical Bioimaging and Beyond. *Current Opinion in Colloid and Interface Science*, **39**: 220–231. https://doi.org/10.1016/j.cocis.2019.02.014

Qi, B., Yuan, Z., Lu, S., Liu, K., Li, S., Yang, L., & Yu, J. (2014). Mechanical and Thermal Properties of Epoxy Composites Containing Graphene Oxide and Liquid Crystalline Epoxy. *Fibers and Polymers*, **15**(2): 326–333. https://doi.org/10.1007/s12221-014-0326-5

Qi, Z., Tan, Y., Zhang, Z., Gao, L., Zhang, C., & Tian, J. (2018). Synergistic Effect of Functionalized Graphene Oxide and Carbon Nanotube Hybrids on Mechanical Properties of Epoxy Composites. *RSC Advances*, **8**(67): 38689–38700. https://doi.org/10.1039/c8ra08312f

Qin, J. X., Yang, X. G., Lv, C. F., Li, Y. Z., Chen, X. X., Zhang, Z. F., Zang, J. H., Yang, X., Liu, K. K., Dong, L., & Shan, C. X. (2021). Humidity Sensors Realized *via* Negative Photoconductivity Effect in Nanodiamonds. *Journal of Physical Chemistry Letters*, **12**(16): 4079–4084. https://doi.org/10.1021/acs.jpclett.1c01011

Qin, J. X., Yang, X. G., Lv, C. F., Li, Y. Z., Liu, K. K., Zang, J. H., Yang, X., Dong, L., & Shan, C. X. (2021). Nanodiamonds: Synthesis, Properties, and Applications in Nanomedicine. *Materials and Design*, **210**: 110091. https://doi.org/10.1016/j.matdes.2021.110091

Rahaman, A., Ventura, I. A., & Lubineau, G. (2012). Influence of Carbon Nanotubes on the Curing and Damage Behavior of Epoxy/Carbon Nanotubes Composites. In *15th European Conference on Composites Materials:Composites at Venice, ECCM 2012.* European Conference on Composite Materials, ECCM.

Rahmam, S., Mohamed, N. M., & Sufian, S. (2014). Effect of Acid Treatment on the Multiwalled Carbon Nanotubes. *Materials Research Innovations*, **18**. https://doi.org/10.1179/1432891714Z.0000000001038

Rahman, A., Ali, I., Al Zahrani, S. M., & Eleithy, R. H. (2011). A Review of the Applications of Nanocarbon Polymer Composites. *Nano*, **6**(3): 185–203. https://doi.org/10.1142/S179329201100255X

Raj, R., Maroo, S. C., & Wang, E. N. (2013). Wettability of Graphene (Supporting Info). *Nano Letters*, **13**(4): 1509–1515.

Rajendran Royan, N. R., Sulong, A. B., Sahari, J., & Suherman, H. (2013). Effect of Acid- and Ultraviolet/Ozonolysis-Treated MWCNTs on the Electrical and Mechanical Properties of Epoxy Nanocomposites as Bipolar Plate Applications. *Journal of Nanomaterials*, **2013**. https://doi.org/10.1155/2013/717459

Revathi, A., Rao, S., Rao, K. V., Rajendra Prakash, M., Sendil Murugan, M., Srihari, S., & Dayananda, G. N. R. (2014). Influence of Temperature on Tensile Behavior of Multiwalled Carbon Nanotube Modified Epoxy Nanocomposites. *Journal of Materials Research*, **29**(15): 1635–1641. https://doi.org/10.1557/jmr.2014.197

Rojo, M. M., Manzano, C. V., Granados, D., Osorio, M. R., Borca-Tasciuc, T., & Martín-González, M. (2015). High Electrical Conductivity in out of Plane Direction of Electrodeposited Bi_2Te_3 Films. *AIP Advances*, **5**(8). https://doi.org/10.1063/1.4928863

Roy, S., Mitra, K., Desai, C., Petrova, R., & Mitra, S. (2013). Detonation Nanodiamonds and Carbon Nanotubes as Reinforcements in Epoxy Composites-a Comparative. *Journal of Nanotechnology in Engineering and Medicine*, **4**(1): 1–7. https://doi.org/10.1115/1.4024663

Saba, N., Jawaid, M., Alothman, O. Y., Paridah, M. T. & Hassan, A. (2016). Recent Advances in Epoxy Resin, Natural Fiber-Reinforced Epoxy Composites and Their Applications. *Journal of Reinforced Plastics and Composites*, **35**(6): 447–470. https://doi.org/10.1177/0731684415618459.

Saha, S., & Bal, S. (2017). Influence of Nanotube Content on the Mechanical and Thermo-Mechanical Behaviour of -COOH Functionalized MWNTs/Epoxy Composites. *Bulletin of Materials Science*, **40**(5): 945–956. https://doi.org/10.1007/s12034-017-1433-x

Sahoo, S. K., Mohanty, S., & Nayak, S. K. (2015). Toughened Bio-Based Epoxy Blend Network Modified with Transesterified Epoxidized Soybean Oil: Synthesis and Characterization. *RSC Advances*, **5**(18): 13674–13691. https://doi.org/10.1039/c4ra11965g

Saleh, H. M., & Koller, M. (2019). Introductory Chapter: Carbon Nanotubes. In H. . Saleh & S. M. . El-Sheikh (Eds.), *Perspective of Carbon Nanotubes* (pp. 1–7). IntechOpen. https://doi.org/10.5772/intechopen.85387

Saw, S. K., Purwar, R., Nandy, S., Ghose, J., & Sarkhel, G. (2013). Fabrication, Characterization, and Evaluation of Luffa Cylindrica Fiber Reinforced Epoxy

Composites. *BioResources*, **8**(4): 4805–4826. https://doi.org/10.15376/biores.8.4.4805-4826

Scheibe, B., Borowiak-Palen, E., & Kalenczuk, R. J. (2010). Oxidation and Reduction of Multiwalled Carbon Nanotubes - Preparation and Characterization. *Materials Characterization*, **61**(2): 185–191. https://doi.org/10.1016/j.matchar.2009.11.008

Schrand, A. M., Hens, S. A. C., & Shenderova, O. A. (2009). Nanodiamond Particles: Properties and Perspectives for Bioapplications. *Critical Reviews in Solid State and Materials Sciences*, **34**(1–2): 18–74. https://doi.org/10.1080/10408430902831987

Schrand, A. M., Huang, H., Carlson, C., Schlager, J. J., Osawa, E., Hussain, S. M., & Dai, L. (2007). Are Diamond Nanoparticles Cytotoxic? *Journal of Physical Chemistry B*, **111**(1): 2–7. https://doi.org/10.1021/jp066387v

Selva, T. M., Selva, J., & Prata, R. B. (2023). *Sensing Materials: Diamond-based Materials*. https://doi.org/10.1016/B978-0-12-822548-6.00081-9

Sengupta, R., Bhattacharya, M., Bandyopadhyay, S., & Bhowmick, A. K. (2011). A Review on the Mechanical and Electrical Properties of Graphite and Modified Graphite Reinforced Polymer Composites. *Progress in Polymer Science (Oxford)*, **36**(5): 638–670. https://doi.org/10.1016/j.progpolymsci.2010.11.003

Setaro, A. (2017). Advanced Carbon Nanotubes Functionalization. *Journal of Physics: Condensed Matter*, **29**(42). https://doi.org/10.1088/1361-648X/aa8248

Shalaby, A., Nihtianova, D., Markov, P., Staneva, A. D., Iordanova, R. S., & Dimitriev, Y. B. (2015). Structural Analysis of Reduced Graphene Oxide by Transmission Electron Microscopy. *Bulgarian Chemical Communications*, **47**(1): 291–295.

Shameer, P. M., & Nishanth, P. M. (2019). Exploration and Enhancement on Fuel Stability of Biodiesel: A Step Forward in the Track of Global Commercialization. In *Advanced Biofuels: Applications, Technologies and Environmental Sustainability*. Elsevier Ltd. https://doi.org/10.1016/B978-0-08-102791-2.00008-

Shalwan, A., Alajmi, F. M., & Alajmi, N. (2022). The Impact of Filler Content on Mechanical and Micro-Structural Characterization of Graphite-Epoxy Composites. *Journal of Materials Science and Chemical Engineering*, **10**(06): 19–29. https://doi.org/10.4236/msce.2022.106003

Shin, Y. J., Wang, Y., Huang, H., Kalon, G., Wee, A. T. S., Shen, Z., Bhatia, C. S., & Yang, H. (2010). Surface-Energy Engineering of Graphene. *Langmuir*, **26**(6): 3798–3802. https://doi.org/10.1021/la100231u

Shirani, A., Hu, Q., Su, Y., Joy, T., Zhu, D., & Berman, D. (2019). Combined Tribological and Bactericidal Effect of Nanodiamonds as a Potential Lubricant for Artificial Joints. *ACS Applied Materials and Interfaces*, **11**(46): 43500–43508. https://doi.org/10.1021/acsami.9b14904

Shrestha, S., Choi, W. C., Song, W., Kwon, Y. T., Shrestha, S. P., & Park, C. Y. (2010). Preparation and Field Emission Properties of Er-Decorated Multiwalled Carbon Nanotubes. *Carbon*, **48**(1): 54–59. https://doi.org/10.1016/j.carbon.2009.08.029

Singh, B., & Mohanty, A. (2020). Study of the Mechanical, Dielectric, and Thermal Properties of Annealed Modified Nanodiamond/Epoxy Composites. *Materials Research Express*, **6**(12). https://doi.org/10.1088/2053-1591/ab58d7

Singh, N. P., Gupta, V. K. & Singh, A. P. (2019). Graphene and Carbon Nanotube Reinforced Epoxy Nanocomposites: A Review. *Polymer*, **180**: 121724.

Sinnott, S. B. (2002). Chemical Functionalization of Carbon Nanotubes. *Journal of Nanoscience and Nanotechnology*, **2**(2): 113–123. https://doi.org/10.1166/jnn.2002.107

Smart, S. K., Cassady, A. I., Lu, G. Q., & Martin, D. J. (2006). The Biocompatibility of Carbon Nanotubes. *Carbon*, **44**(6): 1034–1047. https://doi.org/10.1016/j.carbon.2005.10.011

Smoleń, P., Czujko, T., Komorek, Z., Grochala, D., Rutkowska, A., & Osiewicz-

Powęzka, M. (2021). Mechanical and Electrical Properties of Epoxy Composites Modified by Functionalized Multiwalled Carbon Nanotubes. *Materials*, **14**(12). https://doi.org/10.3390/ma14123325

Špitalský, Z., Kromka, A., Matějka, L., Černoch, P., Kováová, J., Kotek, J., & Šlouf, M. (2008). Effect of Nanodiamond Particles on Properties of Epoxy Composites. *Advanced Composites Letters*, **17**(1): 29–34. https://doi.org/10.1177/096369350801700104

Špitalský, Z., Krontiras, C. A., Georga, S. N., & Galiotis, C. (2009). Effect of Oxidation Treatment of Multiwalled Carbon Nanotubes on the Mechanical and Electrical Properties of Their Epoxy Composites. *Composites Part A: Applied Science and Manufacturing*, **40**(6–7): 778–783. https://doi.org/10.1016/j.compositesa.2009.03.008

Stehlik, S., Varga, M., Ledinsky, M., Jirasek, V., Artemenko, A., Kozak, H., Ondic, L., Skakalova, V., Argentero, G., Pennycook, T., Meyer, J. C., Fejfar, A., Kromka, A., & Rezek, B. (2015). Size and Purity Control of HPHT Nanodiamonds down to 1 Nm. *Journal of Physical Chemistry C*, **119**(49): 27708–27720. https://doi.org/10.1021/acs.jpcc.5b05259

Subedi, D. P. (2011). Contact Angle Measurement for The Surface Characterization of Solids. *Himalayan Physics*, **2**(1): 1–4. https://doi.org/10.3126/hj.v2i2.5201

Suherman, H., Dweiri, R., Sulong, A. B., Zakaria, M. Y., & Mahyoedin, Y. (2022). Improvement of the Electrical-Mechanical Performance of Epoxy/Graphite Composites Based on the Effects of Particle Size and Curing Conditions. *Polymers*, **14**(3). https://doi.org/10.3390/polym14030502

Suherman, H., Mahyoedin, Y., Septe, E., & Rizade, R. (2019). Properties of Graphite/Epoxy Composites: The in-Plane Conductivity, Tensile Strength and Shore Hardness. *AIMS Materials Science*, **6**(2): 165–173. https://doi.org/10.3934/MATERSCI.2019.2.165

Suherman, H., Sahari, J., & Sulong, A. B. (2010). Electrical Conductivity and Micro Hardness of Synthetic and Natural Graphite Epoxy Composite. *Key Engineering*

Materials, **447**: 614–618. https://doi.org/10.4028/www.scientific.net/KEM.447-448.614

Sulong, A. B., Muhamad, N., Sahari, J., Ramli, R., Deros, B. M., & Park, J. (2009). Electrical Conductivity Behaviour of Chemical Functionalized MWCNTs Epoxy Nanocomposites. *European Journal of Scientific Research*, **29**(1): 13–21.

Sun, Y. & Chen, Q. (2009). Diameter Dependent Strength of Carbon Nanotube Reinforced Composite. *Applied Physics Letters*, **95**(2): 2007–2010. https://doi.org/10.1063/1.3168520.

Syrgiannis, Z., Melchionna, M., & Prato, M. (2020). Encyclopedia of Polymeric Nanomaterials. *Encyclopedia of Polymeric Nanomaterials*, ***1***: 1–8. https://doi.org/10.1007/978-3-642-36199-9

Tang, J., Zhou, H., Liang, Y., Shi, X., Yang, X., & Zhang, J. (2014). Properties of Graphene Oxide/Epoxy Resin Composites. *Journal of Nanomaterials*, **2014:** 175-175 https://doi.org/10.1155/2014/696859

Torelli, M. D., Nunn, N. A., & Shenderova, O. A. (2019). A Perspective on Fluorescent Nanodiamond Bioimaging. *Small*, **15**(48): 1–20. https://doi.org/10.1002/smll.201902151

Tucker, S. J., Fu, B., Kar, S., Heinz, S., & Wiggins, J. S. (2010). Ambient Cure POSS-Epoxy Matrices for Marine Composites. *Composites Part A: Applied Science and Manufacturing*, **41**(10): 1441–1446. https://doi.org/10.1016/j.compositesa.2010.06.005

Vajaiac, E., Palade, S., Pantazi, A., Stefan, A., Pelin, G., Baran, D., Ban, C., Purica, M., Meltzer, V., Pincu, E., Berbecaru, C., & Dragoman, D. (2015). Mechanical Properties of Multiwall Carbon Nanotube-Epoxy Composites. *Digest Journal of Nanomaterials and Biostructures*, **10**(2): 359–369.

Viboral, C. De. (2011). *(12) United States Patent US 7927 , 637 B2 Site is*. **2**(12).

Wahab, Z., Foley, E. A., Pellechia, P. J., Anneaux, B. L., & Ploehn, H. J. (2015). Surface Functionalization of Nanodiamond with Phenylphosphonate. *Journal of*

Colloid and Interface Science, **450**: 301–309. https://doi.org/10.1016/j.jcis.2015.03.021

Wahab, Z., Marsh, Z. M., Tessema, A., Kidane, A., Stefik, M., Anneaux, B. L., & Ploehn, H. J. (2017). Effect of Nanodiamond (ND) Surface Functionalization on the Properties of ND/PEEK Composites. *IEEE Transactions on Components, Packaging and Manufacturing Technology*, **7**(2): 165–177. https://doi.org/10.1109/TCPMT.2016.2646671

Wang, H. (2011). *Nanodiamond Particles for Biomacromolecule Immobilization and Dye Contaminant Adsorption* (Doctoral dissertation, University of Saskatchewan).

Wang, H., & Cui, Y. (2019). Nanodiamonds for Energy. *Carbon Energy*, **1**(1): 13–18. https://doi.org/10.1002/cey2.9

Wang, Q., Su, D. S., & Wang, D. Y. (2020). Carbon Nanotube/Epoxy Composites for Improved Fire Safety. *ACS Applied Nano Materials*, **3**(5): 4253–4264. https://doi.org/10.1021/acsanm.0c00423

Wang, W., Bian, W., & Yang, Y. (2016). Incorporation of Nanodiamond into an Epoxy Polymer Network with High Thermal Conductivity for Electrical Insulations. In 2016 *IEEE International Conference on Dielectrics (ICD),* **2**: 868–871. https://doi.org/10.1109/ICD.2016.7547754

Wang, W., Zhu, Y., Liao, S., & Li, J. (2014). Carbon Nanotubes Reinforced Composites for Biomedical Applications. *BioMed Research International*, **2014**: 1–14. https://doi.org/10.1155/2014/518609

Wang, Z., & Zhao, G. L. (2013). Microwave Absorption Properties of Carbon Nanotubes-Epoxy Composites in a Frequency Range of 2 - 20 GHz. *Open Journal of Composite Materials*, **03**(02): 17–23. https://doi.org/10.4236/ojcm.2013.32003

Xu, T., Qi, Z., Tan, Y., Tian, J., & Li, X. (2021). Effect of Multiwalled Carbon Nanotube Diameter on Mechanical Behavior and Fracture Toughness of Epoxy

Nanocomposites. *Materials Research Express*, **8**(1). https://doi.org/10.1088/2053-1591/abd864

Yadav, S. K., Mahapatra, S. S., Yoo, H. J., & Cho, J. W. (2011). Synthesis of Multi-Walled Carbon Nanotube/ Polyhedral Oligomeric Silsesquioxane Nanohybrid by Utilizing Click Chemistry. *Nanoscale Research Letters*, **6**(1): 2–7. https://doi.org/10.1186/1556-276X-6-122

Yao, S. S., Jiang, D., Zhang, Q. Z., & Wang, X. X. (2020). Preparation and Properties of Graphite/Epoxy Resin Conductive Composites. *IOP Conference Series: Materials Science and Engineering*, **740**(1): 1–6. https://doi.org/10.1088/1757-899X/740/1/012064

Yasmin, A., & Daniel, I. M. (2004). Mechanical and Thermal Properties of Graphite Platelet/Epoxy Composites. *Polymer*, **45**(24): 8211–8219. https://doi.org/10.1016/j.polymer.2004.09.054

Ye, B., Kim, S. I., Lee, M., Ezazi, M., Kim, H. D., Kwon, G., & Lee, D. H. (2020). Synthesis of Oxygen Functionalized Carbon Nanotubes and Their Application for Selective Catalytic Reduction of NO_x with NH3. *RSC Advances*, **10**(28): 16700–16708. https://doi.org/10.1039/d0ra01665a

Yudianti, R., Onggo, H., Saito, Y., Iwata, T., & Azuma, J. (2011). Analysis of Functional Group Sited on Multi-Wall Carbon Nanotube Surface. *The Open Materials Science Journal*, **5**(1). https://doi.org/https://doi.org/10.2174/1874088x0110501

Yuen, S. M., Ma, C. C. M., Wu, H. H., Kuan, H. C., Chen, W. J., Liao, S. H., Hsu, C. W., & Wu, H. L. (2007). Preparation and Thermal, Electrical, and Morphological Properties of Multiwalled Carbon Nanotube and Epoxy Composites. *Journal of Applied Polymer Science*, **103**(2): 1272–1278. https://doi.org/10.1002/app.25140

Zaheer, U., Zulfiqar, U., Khurram, A. A., & Subhani, T. (2018). Improving the Performance of Conventional Glass Fiber Epoxy Matrix Composites by Incorporating Nanodiamonds. *Composite Interfaces*, **25**(11): 1005–1018. https://doi.org/10.1080/09276440.2018.1454145

Zehua, Q., & Guojian, N. (2012). A Comparative Study on the Properties of the Different Amino-Functionalized Multiwall Carbon Nanotubes Reinforced Epoxy Resin Composites. *Journal of Applied Polymer Science*, **124**: 403–411. https://doi.org/0.1002/app.35105

Zhan, Y., Meng, F., Yang, X., Lei, Y., Zhao, R., & Liu, X. (2011). Synthesis, Characterization and Properties of Multifunctional Poly(Arylene Ether Nitriles) (PEN)/CNTs/Fe_3O_4 Nanocomposites. *Journal of Polymer Science, Part B: Polymer Physics*, **49**(8): 611–619. https://doi.org/10.1002/polb.22229

Zhang, Q., Zhao, X., Sui, G., & Yang, X. (2018). Surface Sizing Treated MWCNTs and Its Effect on the Wettability, Interfacial Interaction and Flexural Properties of MWCNT/Epoxy Nanocomposites. *Nanomaterials*, **8**(9). https://doi.org/10.3390/nano8090680

Zhang, Y., Rhee, K. Y., Hui, D., & Park, S. J. (2018). A Critical Review of Nanodiamond Based Nanocomposites: Synthesis, Properties and Applications. *Composites Part B: Engineering* **143**: 19-27. https://doi.org/10.1016/j.compositesb.2018.01.028

Zhao, M., Meng, L., Ma, L., Ma, L., Yang, X., Huang, Y., Ryu, J. E., Shankar, A., Li, T., Yan, C., & Guo, Z. (2018). Layer-by-Layer Grafting CNTs onto Carbon Fibers Surface for Enhancing the Interfacial Properties of Epoxy Resin Composites. *Composites Science and Technology*, **154**: 28–36. https://doi.org/10.1016/j.compscitech.2017.11.002

Zhao, S., & Abu-Omar, M. M. (2017). Synthesis of Renewable Thermoset Polymers through Successive Lignin Modification Using Lignin-Derived Phenols. *ACS Sustainable Chemistry and Engineering*, **5**(6): 5059–5066. https://doi.org/10.1021/acssuschemeng.7b00440

Zhou, C., Li, Z., Li, J., Yuan, T., Chen, B., Ma, X., Jiang, D., Luo, X., Chen, D., & Liu, Y. (2020). Epoxy Composite Coating with Excellent Anticorrosion and Self-Healing Performances Based on Multifunctional Zeolitic Imidazolate Framework Derived Nanocontainers. *Chemical Engineering Journal*, **385**: 123835. https://doi.org/10.1016/j.cej.2019.123835

Zhou, L., Zhang, H., Guo, X., Sun, H., Liu, S., Tade, M. O., & Wang, S. (2017). Metal-Free Hybrids of Graphitic Carbon Nitride and Nanodiamonds for Photoelectrochemical and Photocatalytic Applications. *Journal of Colloid and Interface Science*, **493**: 275–280. https://doi.org/10.1016/j.jcis.2017.01.038

Zhu, Y., Murali, S., Cai, W., Li, X., Suk, J. W., Potts, J. R., & Ruoff, R. S. (2010). Graphene and Graphene Oxide: Synthesis, Properties, and Applications. *Advanced Materials*, **22**(35): 3906–3924. https://doi.org/10.1002/adma.201001068

APPENDIX

List of Publications

Tamang, S., Wutzler, A., Lach, R., Grellmann, W., Hai, L. H., Adhikari, R., & Shrestha, S. (2022). Effect of Surface Modification on Structural and Thermal Properties of Nanocarbons of Different Dimensionalities. *Chemistry & Chemical Technology*, **16**(4): 573–580. https://doi.org/10.23939/chcht16.04.573

Tamang, S., Surendran, A., Sharma, K. P., Giri, J., Thomas, S., Maruyama, T., Shrestha, S., & Adhikari, R. (2023). Structural, thermal, and surface wetting properties of epoxy resin/multiwalled carbon nanotubes composites. *Spectrum of Emerging Sciences*, **3**(1): 9–16. https://doi.org/10.55878/SES2023-3-1-2

List of scientific conference and participation

- Poster presentation: Functionalization of nanocarbons of different dimensionalities; KaSAM-2016, October 17-20, 2016, Pokhara, NEPAL.

- Oral presentation: Functionalization of multiwalled carbon nanotubes; KaSAM-2018, October 26-29, 2018, Kathmandu, NEPAL.

- Oral presentation: Functionalization of nanocarbons of different dimensionalities; International Conference on Exploration in Physics (ICEP-2018), May 29-31, 2018, Kathmandu, NEPAL.

- Poster presentation: Functionalization of multiwalled carbon nanotubes for using as fillers with epoxy resin; 8th Asian Conference on Colloid Interface Science (ACCIS-2019), September 24-27, 2019, Kathmandu, NEPAL.

- Participation: Seed NanoTech International Inc. Conference Series, May 25-28, 2021 (Online).

Participation Certificates

3rd International Conference on
KATHMANDU SYMPOSIA ON ADVANCED MATERIALS - 2016
(KASAM-2016), OCTOBER 17-20, 2016

Certificate

It is herewith certified that

Prof. / Dr. / Mr. / Mrs. Sonam Tamang

participated/contributed a paper as keynote/invited/
oral lecture/poster .....

.....

in
3rd International Conference on
Kathmandu Symposia on Advanced Materials – 2016
(KaSAM - 2016)
held in Pokhara, Nepal.

Prof. Dr. Rameshwar Adhikari
Convener

4th International Conference
Kathmandu Symposia on Advanced Materials-2018
(KaSAM-2018), October 26-29, 2018

Certificate

This is herewith certified that
Prof./Dr./Mr./Ms. *Sonam Tamang*
delivered a paper as invited/oral lecture entitled

Mechanical and Thermal Behavior of Epoxy/MWCNTs Nanocomposites

in
4th International Conference
Kathmandu Symposia on Advanced Materials-2018
(KaSAM-2018)
held in Kathmandu, Nepal.

Prof. Dr. Rameshwar Adhikari
Chairman

Supported by

The 8th Asian Conference on Colloid & Interface Science (ACCIS 2019)
Sept. 24-27, Kathmandu, Nepal
ASCASS

Certificate of Participation

This is to certify that

Sonam Tamang

has participated and contributed **Poster Presentation** in

The 8th Asian Conference on Colloid & Interface Science (ACCIS 2019) organized by the Asian Society for Colloid and Surface Science (ASCASS) held in Pulchowk Campus, Institute of Engineering, Tribhuvan University, Lalitpur, Kathmandu, Nepal.

Dr. Lok Kumar Shrestha
Chairperson (ACCIS 2019)

September 27, 2019

Prof. Dr. Toyoko Imae
President (ASCASS)

INSTITUT FÜR
POLYMERWERKSTOFFE e.V.
An-Institut an der Hochschule Merseburg

IPW e.V. Eberhard-Leibnitz-Straße 2, 06217 Merseburg

Sonam Tamang
Ph.D. Scholar

Central Department of Chemistry
Tribhuvan University, Nepal

Abteilung „Kunststoffprüfung und Kunststoffdiagnostik"

Dr. Ralf Lach (IPW-Geschäftsführer)

Tel.-Nr.: +49 (0)3461 30889-67
Fax-Nr.: +49 (0)3461 30889-50
E-Mail: ralf.lach@ipw-merseburg.de

Ihre Zeichen: Ihre Nachricht: unsere Zeichen: unser Schreiben: Durchwahl: Merseburg, den
04/03/2024

PARTICIPATION CERTIFICATE

Confirming the participation of

Sonam Tamang

at the International conference "Polymertec 16"
(June 15-17, 2016; Merseburg / Germany)

Herewith I confirm the participation of Sonam Tamang at the International conference "Polymertec 16" (June 15-17, 2016; Merseburg / Germany) and to present the following contribution as an oral lecture:

"Electrical and mechanical properties of epoxy-resin-MWCNT nanocomposites"

as well as to present a poster entitled:

"Functionalization of nanocarbons for using as fillers with epoxy resin"

With kind regards

Dr. Ralf Lach
CEO of the Institute of Polymer Materials (IPW), Merseburg (GERMANY) and
Head of the Department „Polymer Testing and Polymer Diagnostics" of IPW

Hausanschrift:
Institut für Polymerwerkstoffe
Eberhard-Leibnitz-Straße 2
06217 Merseburg

Bankverbindung:
Saalesparkasse Merseburg
Konto-Nr.: 385321190
BLZ: 80053762
BIC/SWIFT:NOLADE21HAL
IBAN: DE54 8005 3762 0385 3211 90

USt.-IdNr.: DE 158863239
St.-Nr.: 112/143/03428

Vorstandsvorsitzender:
Prof. Dr. Thomas Rödel

Geschäftsführer:
Dr.-Ing. Ralf Lach

INSTITUT FÜR
POLYMERWERKSTOFFE e.V.
An-Institut an der Hochschule Merseburg

IPW e.V. Eberhard-Leibnitz-Straße 2, 06217 Merseburg

Sonam Tamang
Ph.D. Scholar

Central Department of Chemistry
Tribhuvan University, Nepal

Abteilung „Kunststoffprüfung und Kunststoffdiagnostik"

Dr. Ralf Lach (IPW-Geschäftsführer)

Tel.-Nr.: +49 (0)3461 30889-67
Fax-Nr.: +49 (0)3461 30889-50
E-Mail: ralf.lach@ipw-merseburg.de

Ihre Zeichen: Ihre Nachricht: unsere Zeichen: unser Schreiben: Durchwahl: Merseburg, den
04/03/2024

PARTICIPATION CERTIFICATE

Confirming the participation of

Sonam Tamang

at the International conference "Polymertec 18"
(June 13-15, 2018; Merseburg / Germany)

Herewith I confirm the participation of Sonam Tamang at the International conference "Polymertec 18" (June 13-15, 2018; Merseburg / Germany) and to present the following contribution as an oral lecture:

"Epoxy resin/MWCNT composites"

With kind regards

Dr. Ralf Lach
CEO of the Institute of Polymer Materials (IPW), Merseburg (GERMANY) and
Head of the Department „Polymer Testing and Polymer Diagnostics" of IPW

Hausanschrift:
Institut für Polymerwerkstoffe
Eberhard-Leibnitz-Straße 2
06217 Merseburg

Bankverbindung:
Saalesparkasse Merseburg
Konto-Nr.: 385321190
BLZ: 80053762
BIC/SWIFT:NOLADE21HAL
IBAN: DE54 8005 3762 0385 3211 90

USt.-IdNr.: DE 158863239
St.-Nr.: 112/143/03428

Vorstandsvorsitzender:
Prof. Dr. Thomas Rödel

Geschäftsführer:
Dr.-Ing. Ralf Lach


SEED NANOTECH
International Inc.
Seed NanoTech International Inc.
Conference Series
May 24-28, 2021.
CERTIFICATE OF ATTENDANCE AS A PARTICIPANT
This certificate is presented to
Sonam Tamang
for actively attendingh the Conference held on
May 25-28, 2021.
Given this May 28, 2021
Conrad Rizal
Conrad Rizal, PhD SMIEEE CEng.
Session Chair and CEO, Seed NanoTech
Interatioanl Inc. Conference Series